Modulation of East African Precipitation by the Indian Ocean Dipole (IOD) and ENSO

By

Ahmed A. Shaaban

A Thesis

Submitted to the University at Albany, State University of New York

In partial fulfillment of the requirements for

the Degree of

Master of Science

College of Arts and Sciences

Department of Atmospheric and Environmental Sciences

May, 2015

Contents

List of Figures

List of Tables

Acronyms

CMAP	**C**PC **M**erged **A**nalysis of **P**recipitation
SWIO	**S**outhern **W**estern **I**ndian **O**cean
DMI	**D**ipole **M**ode **I**ndex
ENSO	**E**l Ñino **S**outhern **O**scillation
EIO	**E**astern **I**ndian **O**cean
GPCC	**G**lobal **P**recipitation **C**limatology **C**enter
GPCP	**G**lobal **P**recipitation **C**limatology **P**roject
IOD	**I**ndian **O**cean **D**ipole
IO	**I**ndian **O**cean
PNA	**P**acific **N**orht **A**merican pattern
PSA	**P**acific **S**outh **A**merican pattern
PI	**P**recipitation **I**ndex
SOI	**S**outhern **O**scillation **I**ndex
SST	**S**ea **S**urface **T**emperature
SSTA	**S**ea **S**urface **T**emperature **A**nomaly
SEIO	**S**outhern **E**astern **I**ndian **O**cean
SWIO	**S**outhern **W**estern **I**ndian **O**cean
WNP	**W**estern **N**orth **P**acific
WIO	**W**estern **I**ndian **O**cean

Acknowledgments

I would like to thank my advisor Professor Dr.Paul E. Roundy. His advises and encourage have been priceless. His ideas, comments and advises have been extremely helpful. He inspired me with many ideas that opened a new world for me. The way that I am able to look at scientific research points have been completely changed. He encouraged me a lot during my study and research. I faced many hard times due to my late arrival to university, he always give me hope to come over all this. Dr. Paul is a gregarious kind person. His attitude is source of a flourishing interaction with life.

I would like to express my special warm thanks to my father, mother, sister and brother. However, they are in Egypt, their hearts and prays were always with me. They share me my happiness, and hard time. I couldn't feel happy without sharing it with them, and also my hard time moments passed quickly by their support. My mother used to remember me about caring of my life, and health, as if I was in home. No words can express my gratitude to my mother. My father used to support me with all what I need for a happy life. He was the reason of making me love science. When I was a kid, I was fascinated by the mathematical equations that he used to write. He used to offer me a life suitable to enjoy with science. My brother opinions shine with a nice life. My sister, her husband, and their kids were always a continues source of life merriment.

I would also like to thank Dr.Mathias Vuille for his valuable comments on the thesis. I would also like to thank my colleague and managers in Egyptian Meteorological Authority for choosing and supporting me for the scholarship. I would also like to thank Egyptian Cultural and Educational Bureau and USAID

for their funding and support during my stay in US. I would also like to thank UAlbany community for their calm excellent support and help during my study and research. I would also like to thank my colleague Hesham. He was more than brother for me. He was the first person who offer me a help during my stay here.

Abstract

Tropical East Africa is influenced by two main rainy seasons, during autumn and spring. During autumn, tropical East African precipitation is clearly influenced by Indian Ocean Dipole (IOD) and/or ENSO. During spring, there is no clear SST pattern in the Indian Ocean. The association between El Niño and positive IOD phases is much stronger than the association between La Niña and negative IOD during October and November. During October, the association between El Niño and wet condition over tropical eastern Africa is stronger than association between La Niña and dry conditions. During November, the association between positive IOD and eastern African precipitation is stronger than the association between La Niña and dry conditions.

During short wet phases (such as autumn) over eastern Africa, two anticyclones form in the lower troposphere with upper baroclinic structure. These anticyclones decay rapidly by December. These anticyclones are responsible for supplying East Africa with increased moisture.

Most strong positive IOD events are associated with wet outcomes over eastern Africa. Not all strong El Niño events lead to wet outcomes.

It is well known that during northern spring, precipitation over eastern Africa is not connected to any inter-annual SST modes of variability. During northern spring, SST in Indian Ocean is nearly always sufficiently high to sustain convection, however, convection is not always active. We found that precipitation over eastern Africa during spring is associated with a dipole pattern of outgoing longwave radiation anomaly (OLRA) not associated with SST variability.

Chapter 1

East African precipitation and Indian Ocean Dipole

1.1 Review of Studies of Africa precipitation

East Africa (Somali, Kenya, and Tanzania) is characterized by two main rainy seasons:long rain season and short rain season. The long rain season occurs in March, April, and May, during which the Intertropical Convergence Zone (ITCZ) moves pole-ward. During the short rainy season, the ITCZ moves quickly toward the south. The short rainy season occurs from October to December. Ethiopia has one rainy season, which occurs in summer. Several works have been done to understand the variability of precipitation over several parts of Africa. Some authors concentrate on eastern tropical Africa in which precipitation has bi-modal peaks. Others groups concentrate on Ethiopia where precipitation is unimodal. Other groups concentrate on the western African (Sahal) precipitation. Ogallo [1989b] studied the spatial and temporal pattern of precipitation over Kenya, Uganda, and, Tanzania. He found that the first empirical orthogonal function (EOF) pattern dominates over many parts of the domain except at the coast and in the highlands, where the second and third EOFs dominate. The first EOF of rainfall calculated during northern fall includes its greatest loadings at the coast. In summer, the first few EOFs dominate near Lake Victoria and west part region in which Congo basin is a great source of moisture. Such patterns indicate that many factors can affect east Africa precipitation. Locality and topography

have dominant roles on precipitation variability. Indeje *et al.* [2000] used rotated EOF analysis to classify east African precipitation into homogeneous regions based on the correlation of first principle component (PC) with each station point as indicated by Dyer [1975]

Indeje *et al.* [2000] analyzed the seasonal cycle of precipitation during El Niño events and the years following. He found that in most regions, there is a positive anomaly of rainfall during El Niño and a negative anomaly during the next year. Ogallo [1988b] found that there is a strong negative correlation between the Southern Oscillation Index (SOI) and east African rainfall, especially at the eastern coast which peaks in October-November. Low correlation was found during spring. The highest lag correlation has been found to exist between October SOI and November rainfall. Schreck and Semazzi [2004b] show that EOF1 of the rainfall anomaly during autumn for the Greater Horn of Africa (GHA)—that includes Burundi, Djibouti, Eritrea, Ethiopia, Kenya , Rwanda, Somali, Sudan, Uganda, and Tanzania— is correlated with El Niño with positive anomaly over all the domain except Sudan. Projection of the first EOF on wind indicates easterly flow from the Indian ocean and weaker flow form Congo basin. The second EOF represents a trend which may be associated with global warming.

Black *et al.* [2003] showed that the relationship between the rainfall over eastern Africa and the DMI is nonlinear. He showed that only extreme IOD events are associated with positive precipitation anomalies over East Africa. Black *et al.* [2003] showed that for DMI larger than 0.5, the rainfall over east of Africa is above average. Black *et al.* [2003] postulated that the strong El Niño can modulates–weaken– the Hadley circulation over Indonesia by strengthening the descending motion over maritime continent, so causing south easterly winds which trigger the upwelling near Java island—southern eastern Indian ocean— and hence the IOD.

[Latif and Dommenget, 1999] performed a response model experiment using EHCAM3 to diagnose the relative effect of Pacific ocean and Indian ocean during winter 97/98. [Latif and Dommenget, 1999] found that, forcing an SST anomaly in Pacific ocean while forcing with climatological SST in IO leads to precipitation failing. However, the opposite situation leads to succession of precipitation. Mutai and Ward [2000] studied the correlation between the ENSO and several parts in

the east of Africa, he found that most of regions correlate homogeneously with ENSO except some regions in which topography has more important role. Mutai and Ward [2000] found that in Autumn, the OLR pattern looks like horseshoe pattern, and in spring the relationship of East African rainfall with ENSO is weak due to the transient nature of ENSO.

Precipitation anomalies over eastern Africa and Australia are correlated. Positive IOD is connected with positive precipitation anomaly over eastern Africa and negative precipitation anomaly over western Australia. [England, 2006] showed that dry years over southwestern Australia are linked to positive IOD, which enhance moisture fluxes toward Africa. Also, England [2006] showed that during those dry years, the westerlies shifts to south which means southward shift the subpolar front and hence precipitation. However, England [2006] showed that SST at eastern tropical IO is altered by Ekamn layer dynamics, SST in the south central of subtropical IO is altered by air-sea flux, with warming during wet years and cooling during dry years(see Fig 5)

1.2 Indian Ocean Dipole

1.2.1 Indian Ocean Dipole Theory

In 1999, [Saji *et al.*, 1999] reported a climate mode in the Indian ocean, and evaluated connection between that mode and drought and flood events over East Africa and Australia. [Saji *et al.*, 1999] reported that East African flood at 1961 was associated with this dipole. The positive phase of the dipole manifests warming in western equatorial IO and cooling in the southeastern IO. Saji *et al.* [1999] used the difference between the anomaly of the average SST in the western($50°E - 70°E, 10°S - 10°N$) and eastern ($90°E - 110°E, 10°S - 0°$) IO as index for the mode. In summer, the IO SST climatology features cooling in the western IO and warming in the eastern IO. Cooling in the western Indian ocean (IO) is due to the monsoon—strong wind during summer enhances the surface latent heat fluxes thus reducing the SST, and upwelling occurs with the summer monsoon north of equator and with the winter monsoon south of equator. During Autumn, warming in the eastern IO is due to the accumulation of warm water—

via westerly wind through triggering equatorial oceanic downwelling Kelvin waves, and coastal Kelvin waves which aid in deepening the thermocline thereby warming the eastern IO. During IOD events, the southeasterly wind causes upwelling of cold water at Java island so aiding in decreasing the SST. The IOD can occur with or without ENSO—based on ONI3.4 index. In 1961,1967 IOD events occurred without ENSO events during northern fall. However, in 1972,1982,1994,1997 IOD was coincident with warm phase ENSO. There is large debate about whether 1994 in El Niño or not, Many IOD literature follow Meyers *et al.* [2007] classification for IOD, in this classification 1994 is positive IOD and neutral ENSO event. The biggest IOD event was 1997, the second biggest event was 1961.Saji *et al.* [1999] reported two important features of the IOD. The first feature is the powerful phase locking of the IOD. IOD begins in summer, peaks in October, and quickly terminates in December. The second feature, is the biennial tendency (Fig.3. Saji *et al.* [1999])of the IOD. The biennial tendency might depend on the response of the IOD to monsoon circulation. ENSO, monsoon, other tropical modes also have biennial tendencies due to the tropical Quasi-biennial oscillation. Webster *et al.* [1999] proposed a theory of a self coupled ocean-atmosphere in the Indian basin. Webster *et al.* [1999] built his analysis on the 1997-1998 event— A lot of extremes appeared everywhere during 1997-98, it presented good opportunity to discover new modes. Webster *et al.* [1999] argued that ocean-atmosphere coupling in 1997-1998 was not associated with big 1997-1998 El Niño, as drought in Indonesia and flood over East Africa was larger than what was anticipated for ENSO event. Such argument may not be enough to indicate that the precipitation was due to the IOD because response of the precipitation to El Niño is not linear, also several other factors can influence precipitation. Also the analysis used by Webster *et al.* [1999] doesn't show whether the IOD is part of the broader pattern associated with ENSO or independent of ENSO. Webster *et al.* [1999] showed that during Nov 1997 between $5°S$ and $5°N$, eastern IO exceeded $1°C$ and western IO exceeds $-2°$, The wind anomalies exceeded $-5ms^{-1}$ over the central IO. The SSH anomaly exceeded 17 cm.

Strong debate has been raised about whether the IOD mode is part of the ENSO, or has its own dynamics. Baquero-Bernal *et al.* [2002] showed that there

is no correlation between the east and west box of the DMI defined by Saji *et al.* [1999] if all seasons are considered, and a significant negative correlation exists only during the northern fall. Baquero-Bernal *et al.* [2002] removed the ENSO signal from pacific using statistical and physical methods. Removing ENSO statistically was done using Principle Oscillation Pattern (POP) by removing the fist component of Pacific SST POP from the SSTA. Removing ENSO physically was done by using Global Climate Model (GCM) with using climatological SST instead of SSTA in the Pacific ocean. After removing ENSO, Baquero-Bernal *et al.* [2002] found that the IOD signal still exist, but with weaker amplitude from the control run and the raw SST data. Baquero-Bernal *et al.* [2002] conducted GCM–ECHAM4–simulation with mixed layer ocean model with fixed depth of 50 m–nearly half the climatological thermocline depth in IO– to understand whether the weak IOD signal in the no-ENSO run is due to ocean dynamics in IO or just atmospheric condition. They found that the IOD still exits without including internal ocean dynamics. This result indicates that atmospheric forcing may be primary in forcing the IOD. Fischer *et al.* [2005] studied the triggering mechanism for the IOD using model simulation with and without ENSO signals—removal of the ENSO signal was achieved by using only climatological wind stress. He found that the IOD can be triggered with or without ENSO events. During non-ENSO events, a nomalous Hadley circulation over eastern IO causes anomalous southeasterly wind over Java island, leading to upwelling cold SST, and triggering of upwelling Kelvin wave—via the easterly component of the southern-easterly wind—(Fischer *et al.* [2005] fig 10,11) which after colliding with east Summatra propagates to north and south, with signal reaching the Bay of Bengal. Cooling on the east of the IO leads to loses of the climatological heating due to convection, thereby triggering anticyclone on southwest of the anomalous heat sink Gill [1980]. Such anticyclone intensifies the southeasterly wind, and the process continues. The second mechanics for triggering the IOD, is by the shift of walker circulation during the El Niño phase. El Niño weakens the walker circulation by shifting the warm pool to east, leading to loses of the climatological heating over the Maritime-continent triggering the Matsuno-Gill Rossby wave Gill [1980], Matsuno [1966] on south west of the heating source. Such mechanics occurred in

1997—the greatest El Niño year ever observed. Fischer *et al.* [2005] noted that IOD during 1961 was not associated with anomalous Hadly circulation, also 1961 was not El Niño year ,so it seems that there is still other mechanisms for triggering IOD. Li and Wang [2003] has illustrated four differences between the Pacific and Indian ocean air-sea interaction. The first difference is that the negative cloud-radiation-SST feedback is much stronger in the IO than in the Pacific ocean. This is because in the IO the warm/cold SST is coincident with negative/positive net short wave radiation. So strong convection leads to strong reduction of insolation (because of increases of cloud) leading to cooling SST. The same scenario occurs in the eastern IO in which cooling SST leads to convection suppression which leads to cloud free conditions which increases insolation, thus increasing the SST anomaly. In Pacific, the maximum SST is located in eastern basin, however the minimum of the net short wave radiation is in the center of the Pacific, so SST in the eastern Pacific can still warm without being affected by similar negative feedback. The reason for the occurrence of convection in the center of the Pacific ,however the maximum anomaly in the east pacific is that in center pacific the SST exceeds 27° which is enough for triggering convection. The second difference is that, in the Pacific, the climatological wind is easterly, however, in the IO it is westerly. The background westerly wind leads to deeper thermocline in the eastern IO and western Pacific, also it leads to different impacts on oceanic waves. In the pacific, westerly wind leads to downwelling Rossby waves, which move westward until they hit the western boundary, thereby convert to an upwelling kelvin wave which may then subsequently shutdown the EL Niño. It was believed that due to the deep thermocline in IO, the atmosphere cannot force oceanic wave similar to those in the Pacific, however, observations show that Kelvin and Rossby wave in IO that impact the developing IOD. Fischer *et al.* [2005] has shown that not only locally upwelling Kelvin wave at Sumatra or downwelling Rossby wave in the western IO impacts the IO, but also travelling Rossby and Kelvin waves can impact the IO (fig.1.1). The impact of traveling Kelvin and Rossby wave positively feedback on the growth of the IOD in-spite of difference in basic state from the Pacific. Easterly wind in tropical IO trigger upwelling Kelvin wave which propagates to east, upon hitting Sumatra island, it propagates north and south along the shore

and causes cooling. The strong anticyclone south of Sumatra island could be strengthened by the influence of southeasterly wind at Java as the eastern side of the anticyclone is close to Java island. Also easterly wind in the tropical IO can transfer momentum to the southern tropical IO forcing downwelling Rossby wave which moves westward, deepening the thermocline leading, to warming in the western IO so strengthening the IOD Xie *et al.* [2002], Rao and Behera [2005]. Vinayachandran *et al.* [2009] showed that Empirical Orthogonal Function (EOF) of sea level anomalies are consistent with the Kelvin wave trapped at the eastern shore of the IO , and downwelling Rossby wave in the western IO (fig.1.1).

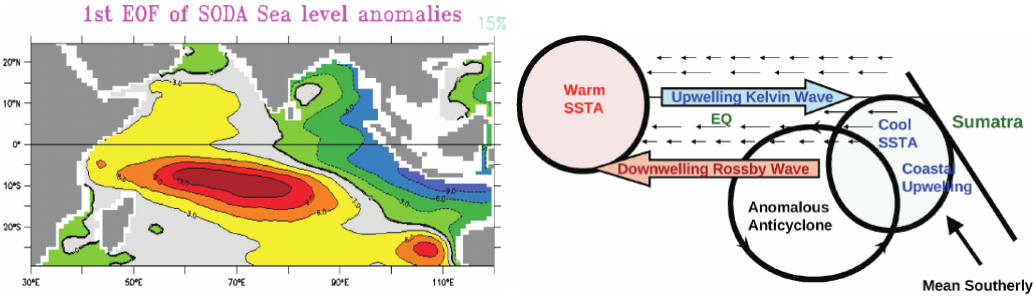

(a) (b)

Figure 1.1: (a) EOF1 for SSH from Vinayachandran *et al.* [2009],(b) propagating kelvin and Rossby wave Vinayachandran *et al.* [2009]

Three rare consecutive IOD events occurred during 2006, 2007, and 2008. The interesting thing about these three events is that they were all positive, which broke the IOD biennial property Behera *et al.* [2008], Du *et al.* [2012], Iskandar *et al.* [2013]. Also the 2007 event was associated with La Niña, when IOD events are usually negative. The short lived IOD events during 2007-2008 were due to the triggering of downwelling kelvin waves by the MJO Rao *et al.* [2008], Yan *et al.* [2012]. The downwelling kelvin wave moves eastward toward the coast deepening the thermocline, so ending the IOD event.

1.2.2 Indian Ocean Dipole - ENSO Interaction

The Indian ocean basin warming (cooling) tends to be preceded by EL Niño (La Niña) phases with lag between 3-6 months. Such warming/cooling in the IO occurs due to changing atmospheric heat flux(short wave radiation and latent heat) via the Walker circulation Alexander and Bladé [2002].

Chambers [1999] used TOPEX/POSEIDON altimetery data to study the warming in the IO during two El Niño events including 1994 and 1997. Meyers *et al.* [2007] and Fischer *et al.* [2005] considered the 1994 event as neutral ENSO, however, ONI3.4 was above 1° for 5 consecutive overlapping 3 months average. Chambers [1999] found that sea level height rises associated with oceanic downwelling Rossby waves during 1994 and 1997. El Niño induces easterly winds over the IO associated with a modified Walker circulation. Such easterly and southeasterly winds are associated with an anticyclone over the south eastern IO, which triggers downwelling Rossby waves, which move westward, causing warming in south western IO.

Besides the warming in the SWIO by oceanic Rossby waves, Du and Xie [2008] investigated the mechanism behind persistence of the the warming in the northern IO(NIO) during summer following El Niño, he found that warming in the SWIO induced by a downwelling Rossby wave induced an asymmetric pattern in the IO with northeasterly wind in north and north westerly wind in the south, giving the wind pattern a C-shape.

Singh *et al.* [2013] studied two long lived La Niña events 1973-1976 and 1998-2001. He found that cooling in the IO after La Niña cannot be explained just by heat flux to the atmosphere. Instead he found that curl of wind stress induced by La Niña causes a local upwelling Rossby wave, which induces cooling centered in the south western IO.

Not all types of El Niño events aid in triggering positive IOD. Wang and Wang [2013] found that although normal El Niño and El Niño Modoki 1– which imply asymmetric SSTA distribution around equator – force positive IOD, whereas the El Niño Modoki 2– which implies an asymmetric SSTA distribution around equator – leads to triggering negative IOD.

Most authors have concentrated on the impact of the Pacific event on IO basin warming/cooling and IOD. Luo *et al.* [2012] studied the influence of the IO SST on Pacific SST. They found that Indian ocean basin warming can strengthen the trade wind over the Pacific, thus leading to more La Niña-like states (strengthening walker circulation).

Luo *et al.* [2010] used the Scale Interaction Experiment-Frontier (SINTEX-F),

a global model provided by the research center for global change in Japan, to examine the impact of extreme IOD events on the different structured El Niño events during 1994 and 2006. He found that extreme IOD event during 1994 suppressed the growing La Niña by inducing anomalous westerlies over the central Pacific due to the cooling in eastern IO. As the IOD matured during Autumn, the IOD induced westerlies in central Pacific aid in rapidly growing El Niño, which begin to decay in January, so leading to rapid El Niño formation and decay (see Fig.2 Luo *et al.* [2012]).

Chen *et al.* [2012] studied the relative roles of SST in the IO and Pacific Ocean, and also the role of air-sea coupling on the seasonal mean precipitation in IO. They found that prescribing monthly SST in the IO is essential for skillful precipitation prediction IO. During boreal winter, SST in Pacific is the most important factor. During Boreal spring, largest skill is found when the air-sea coupling is active. Du *et al.* [2013] discovered new type of IOD that is only observed after mid-1970 climate shift. He found that this unseasonal IOD mode starts in spring, matures in summer, and decays in autumn. Such unseasonal mode is not associated with El Niño events. He also discovered another IOD mode which starts during spring, matures during autumn, and decays during the following winter. This mode is usually associated with El Niño events. These newly documented IOD modes are observed to be terminated by MJO induced doweling Kelvin waves, or anomalous westerly wind over western IO that induces downwelling kelvin waves.

1.2.3 Indian Ocean Dipole, and Northern Summer East African Monsoon

Relationships between the monsoon and the IOD are still under investigation. It is well known that the monsoon often fail during ENSO warm phases (Ju and Slingo [1995], Wang [2006], Webster and Yang [1987], Webster and Magana [1998]). On the other hand, results of Ashok *et al.* [2001], Meehl [1997] indicate that warming in the western Indian ocean enhances the summer monsoon by supplying moisture flux. However, a strong summer monsoon causes cooling of the western IO via upwelling and evaporation. Several feedbacks control the relationship between the monsoon and the IOD. The SST-cloud-radiation negative feedback tends to

warm the eastern IO, and the thermodynamical air-sea feedback tends to cool it. Southeasterly wind anomalies during northern summer over Sumatra and Java islands tend to cause upwelling, leading to decreases in the heat source generated by condensation. Anomalously low latent heat release generates an anomalous anticyclone Gill [1980], Matsuno [1966]. The anticyclone associated with southeasterly wind enhances the upwelling again, leading to positive feedback.

1.2.4 IOD predictability

As precipitation in east Africa and Australia are greatly impacted by the IOD, several authors have studied the predictive skill of the IOD. Shi *et al.* [2012] studied the predictive skill of the IOD using four global models, including Predictive Ocean-Atmosphere Model for Australia (POAMA), NCEP Climate Forecast System (CFS), European Center for Medium-Range Weather Forecast (ECMWF), and Frontier Research Center for Global Change System SINTEX-F. They found that in general, the forecast skill for the IOD is smaller than for the ENSO. They found that the lead time for skillful prediction of WIO SST is 5-6 months, like the lead time for skillful prediction for ENSO. However, the lead time for skillful prediction in the EIO is 3-4 months. So for IOD the lead time for skillful prediction is one season because of the limitation in EIO. Skillful prediction of SST in the EIO for September extends only 3 months, implying that there is a stronger predictability barrier during spring, so prediction starts to work during June. Liu *et al.* [2011] evaluated the performance of prediction of IOD severity using 23 models from Coupled Model Intercomparison Project (CMIP3) phase 3. The IOD severity index is the product of the DMI defined by Saji *et al.* [1999] with the anomaly of equatorial wind averaged over $(5°S - 5°N, 70° - 90°E)$. This index reflects the strength of the atmosphere-ocean feedback. Three feedbacks control the IOD evolution: One is the dynamical feedback—also called Bjerknes feedback, the second one is thermodynamical feedback—also called wind-evaporation-SST positive feedback, and one is the negative cloud-radiation-SST feedback.

The Bjerkens feedback occurs during the ENSO, and it occurs during IOD. Initially, the zonal gradient of the SSTA in the western IO induces strong easterlies, which lift the thermocline in the WIO due to accumulation of warm water. at the

same time, it leads to a shoaling thermocline in the EIO due to intrusion of cold water. This change in the thermocline enhances the SST gradient again, leading to positive dynamical feedback.

In the wind-evaporation-SST feedback, cooling near Java island leads to suppressed convection, leading to loss of climatological heating associated with rainfall in that region, generating an anticycolonic Rossby wave at the western portion of the resulting anomalously negative heat source Gill [1980]. Since the mean wind is southeasterly, this anticyclone will enhance the background wind, leading to reduced SST and the feedback continues.

In the cloud-radiation-SST negative feedback, initially warming in the WIO and cooling in the EIO leads to increases of cloud over the WIO and reducing over the EIO. Due to such change in cloud cover, short wave flux decreases in the WIO and increases in the EIO, thus leading to cooling in the WIO and warming in the EIO, thus contradicting the initial condition of the SST. Liu *et al.* [2011] constructed three scatter plots to study the Bjerknes feedback. The first relation is between low-level wind and SSTA. The second relationship is between thermocline depth and low level wind. The third one is between ocean subsurface temperature and thermocline depth. The three scatters plot suggest a chain interaction from atmosphere to ocean. Comparison between the composites of strong IOD events and weak IOD events shows large biases in thermocline depth. A composite of strong IOD events has a mean thermocline depth of 110 m, while a composite of weak IOD events has thermocline depth of 200m which leads to break in the Bjerknes feedback because the wind can have a little impact on the thermocline that is so deep. Some model didn't capture the positive wind-evaporation-SST feedback due to biases in latent heat flux which caused by large biases in surface wind speed and specific humidity gradient.

A relative inability to predict upcoming ENSO states in model forecasts initialized in May or sooner has become known as the spring predictability barrier. In the IO, things are much more interesting as we have two poles, EIO and WIO, each with different physics. Ding and Li [2012] studied the persistence of the SSTA in the IO during El Niño events. He found that there is a weak spring persistence barrier of SSTA in the WIO, and strong winter persistence barrier in the

EIO. The SSTA persistence barrier means that the SSTA tends to change rapidly at the time. This behavior is detected by using auto-correlation to identify the month with minimum lagged auto-correlation. Weak Spring persistence barrier is due to the sesonal change in WIO SSTA from cold to warm. Such change could be explained as the following. In the spring before the El Niño developes, usually the IO basin is cold due to the influence of previous La Niña. During October, two anticyclones south and north of equator begin to develop at the EIO because of loses the climatological diabatic heat source over Martime-Continent. The easterly flow associated with these two anti-cyclones would oppose the climatolgical wind over the WIO thus leading to warming in the WIO Wang [2002]. So this change from cooling to warming during spring induced by EL Niño yields the predictability barrier.

With respect to the predictability barrier during winter for the south Eastern Indian Ocean (SEIO), an anticyclone formed as a Rossby wave response to the loss of climatological heating. This anticyclone strengthens the climatological southeasterly wind near Java island, thus reducing the SST by evaporation. In winter, the climatolgical monsoon wind opposes the southeasterly wind anomaly associated with this ridge, thus leading to calmer winds and to warming in the WEIO. Thus during winter there is predictability barrier due to changes in the SSTA.

1.2.5 Skewness of the IOD and EL Niño modes

The thermocline in the IO is relatively flat and deep in comparison to the thermocline in the the Pacific ocean. In the IO, the mean climatology of the thermocline is ranges from 110 m in the WIO to 120 m in the EIO. This relatively flat deep thermocline delayed the attention of scientific community to study air-sea interaction modes in the IO. Climatolgical westerly wind leads to accumulation of warm water over the eastern IO during transition season leads to a relatively deep thermocline in the EIO comparable to the WIO. During IOD events, the zonal wind is reversed, and upwelling occurs in the EIO.

Skewness is a measure of asymmetry in a distribution. Skewness tells us how frequently data depart from a normal Gaussian distribution. Positive skewness

of the data means that there is right tail in the frequency distribution. Negative skewness means that there is left tail in the frequency distribution. Zero skewness of the data implies a normal distribution.

Eastern Pacific ocean SST has positive skewness. The SEIO exhibits negative skewness, and as the IOD is represented as the difference between the west and east IO SSTA, the IOD is positively skewed. Hong *et al.* [2008a,b] found that nonlinear advection tends to cool the SEIO in both positive and negative events. During a positive event, cold advection occurs $-u'\frac{\partial T'}{\partial x} < 0$, as we have anomalously easterlies $u' < 0$, and the gradient of the SST is inclined towards west $\frac{\partial T'}{\partial x} < 0$. On the other hand, during negative IOD events, cold advection also occurs $(-u'\frac{\partial T'}{\partial x} < 0)$ as there are anomalous westerlies $u' > 0$ and the SST gradient is inclined to east $\frac{\partial T'}{\partial x} > 0$.

Hong *et al.* [2008a,b] also found that a break of the negative SST-Cloud-Radiation feedback generates skewness in the IOD. Warming in the WIO leads to cloud formation that opposes the SST warming, and cooling in the SEIO leads to cloud suppression that opposes the SST cooling. After suppression of cloud in SEIO, further cooling–by any external forces like nonlinear advection— cannot be damped by more heat flux—short wave— as there is no more cloud to suppress, so cooling grows, and the feedback breaks. A similar break of the SST-Cloud-Radiation feedback does not occur in the WIO.

Hong and Li [2010] argued that the SST skewness is independent of the thermocline feedback, as the subsurface SSH-SST relationship is symmetric, so the asymmetric SSH-SST may be conducted by the asymmetric atmospheric bridge. He also emphasized on the importance of the break of the cloud-raditon-SST feedback. Cai *et al.* [2012] refuted Hong and Li [2010] assumptions about the break of the cloud-Radtition-SST feedback. Cai *et al.* [2012] argued that biases in SODA SST data with false trend in the ERA-40 led to incorrect conclusion by Hong and Li [2010]. Also Cai *et al.* [2012] observed that days of clear sky do not occur in the SEIO, thus breakdown of the SST-Cloud-Radiation does not occur at all.

Ogata *et al.* [2013] studied the role of ocean dynamics in causing negative skewness in the SEIO. They found that the SST in the SEIO is more sensitive to shoaling of the thermocline than to deepening of the thermocline. This nonlinear

relationship between the SST and the thermocline is due to the climatological depth of the thermocline in the SEIO.

Chapter 2

Analysis and Results

2.1 Data

As this research is mainly about precipitation, we compared different precipitation reanalysis datasets to increase confidence in results. We used reanalysis data to avoid the problem of missing data from stations at different parts of eastern Africa. The lack of continuous data is due to several wars and destroyed infrastructure in Africa. We classify observed African rainfall into data that starts before and after 1979. The main difference between those two periods are the way that the data is produced. Before 1979, precipitation data are mainly based on gauge measurement. Precipitation data after 1979 are modified extensively by satellite infrared measurements. The advantages of using satellite data is the high temporal and spatial resolution, providing precipitation data over desert, ocean, etc. There are other differences between different precipitation data sources, like whether numerical models are used in producing the data, mathematical algorithms that used in regriding, etc.

Two issues add to the complexity of station data over Africa. First, heterogeneous distribution of stations, second, the number of reported observations (SYNOP) decreases with time, not only in Africa, but also in many other countries. The number of the Global Telecommunication System (GTS) reported precipitation observations over eastern Africa in 2000 is fewer than in 1990—The Global Precipitation Climatology Center (GPCC) data provides the number of observations per grid.

We used the Global Precipitation Climatology Center (GPCC) data that are constructed by the DWD (Deuthch WetterDienst). This dataset is mainly based on GTS gauge data and it is only available on Land. GPCC data are from 1901-2010 with spatial resolution of $0.5° \times 0.5°$, the data are available at http://www.esrl.noaa.gov/psd/data/gridded/data.gpcc.html. There is also a lower resolution version of these data. These data come in different types, including GPCC full analysis data,which we used. These data are used primarily in trend analysis, model verification, telconnection analysis, etc. The GPCC Monitoring Product is used for satellite data calibration and early annual reporting because this product is available in near real-time before the other GPCC products. The GPCC First Guess Product is used for drought monitoring. Also, number of observations per grid is available.

We also used monthly CPC Merged Analysis of Precipitation (CMAP) [Xie and Arkin, 1997] with spatial resolution of 2.5x2.5. There are two types of these data: standard and enhanced. The standard data, version 1201, are based only on guage and satellite data, from 1979-2011. The enhanced data, version V0809, are based on guage, satellite data ,and model output, it is from 1979-2008. It is available at http://www.esrl.noaa.gov/psd/data/gridded/data.cmap.html. The CMAP data units are mm/day.

We also used Global Precipitation Climatology Project (GPCPv2.2) described by Adler and Huffman [2003], with spatial resolution $2.5° \times 2.5°$. This data is from 1979 to present. The data are available at http://www.esrl.noaa.gov/psd/data/gridded/data.gpcp.html

For improved understanding of precipitation data over Africa, two main projects have been conducted by USAID and Reading university(UK) to support a system for early monitoring of drought and flood. The dataset constructed by the USAID is called the Africa Rainfall Climatology (ARC) http://www.cpc.ncep.noaa.gov/products/fews/AFR_CLIM/afr_clim.shtml . ARC data are daily with high spatial resolution at 0.1°. Both gauge and satellite data are used to generate these data. The data produced by Reading University is called Tropical Applications of Meteorology using SATellite (TAMSAT), both gauge and satellite are used to generate these data. This dataset is basically monthly but it is available daily data

from 2013. The spatial resolution of these data is 0.0375°. More information about this dataset is available at http://www.met.reading.ac.uk/tamsat/about/. We used ARC and TAMSAT to monitor rainfall over different parts of Africa. This dataset hasn't yet been used in the research literature according to author's knowledge.

Several authors postulated that in $2.5°X2.5°$, 5 stations are needed to guarantee accuracy within 10% of the mean rainfall in that cell. Ali and Amani [2005] showed that 5 stations in not enough in Africa. They showed that in western Africa, 5 stations lead to an error from $5 - 30\%$ depending on the month and region. They suggested that 20 gauges station are needed to keep accuracy within 10%. That condition is not available in Africa. Using precipitation data that is based primarily the satellite observations is the only way for accurate precipitation data over Africa. However, one important drawback is that such data begin from 1979, also the algorithms that are used to generate the rainfall are always under-development and also prone to errors especially over large Lakes.

To show the topography of Africa, we used Gridded Global Relief Data (ETOPO2v2) which has 2-minute spatial resolution, the data are available from http://www.ngdc.noaa.gov/mgg/fliers/06mgg01.html

For atmospheric variables, ECMWF Re-Analysis Interim(ERA-I)Dee *et al.* [2011] were used. This dataset is state of the art in atmospheric reanalysis data. Accoding to the Climate data guide https://climatedataguide.ucar.edu/climate-data/atmospheric-reanalysis-overview-comparison-tables., ERA-I is third generation reanalysis data. These data incorporate station data, satellite data, and model output. Sophisticated data assimilation(4DVar) is used in producing these data. ERA-I is $0.75°X0.75°$, and it is available in monthly and sub-daily time scales. ERA-I covers period from 1979 to present, and it will replace the ERA-40 data. ERA-I has solved several problems, like representation of the hydrological cycle, and stratospheric circulation. NCEP1, 2 doesnot assimilate the Special Sensor Microwave Imager (SSM/I)—which started 1987—in their analysis, so there is no information about lower tropospheric humidity. Most data about lower tropospheric humidity over ocean is actually model output Trenberth *et al.* [2011]. Some new reanalysis products assimilate the satellite

data such as the: CFSR(Climate Forecast System Reanalysis) , which is an extension of NCEP data and it is from 1979-2010, and MERRA(MODERN-ERA RETROSPECTIVE ANALYSIS FOR RESEARCH AND APPLICATIONS) is a NASA project and it is from 1979-present. To calculate the streamfunction for long period, we used wind data from NCEP R1 data, we use the monthly data from 1984-present, the spatial resolution of these data is $2.5°X2.5°$.

For Sea Surface Temperature (SST), we used Hadley Ice Sea Surface Temperature (HadISST)Rayner [2003] , these data are $1°X1°$ resolution, it extends from 1870 to present. This dataset is mainly based on observations from the Comprehensive Ocean-Atmosphere Data Set (ICOADS) and Met Office Marine Data Bank (MDB). For comparison purposes, we used the NOAA Extended Reconstructed Sea Surface Temperature (ERSST) V3b dataset Smith *et al.* [2008]. These data cover the period 1854 to present, on a $2°X2°$ degree grid.

For outgoing long wave radiation(OLR), the NOAA interpolated OLR were used, in monthly form from 1974-2013 with $2.5°X2.5°$ spatial resolution. There are some missing months in 1978, missing dates can be found at `http://www.esrl.noaa.gov/psd/data/gridded/data.interp_OLR.html`

2.2 Analysis methods

As this research is mainly about understanding patterns of precipitation and atmospheric conditions during ENSO and IOD events, we depend extensively on composites, correlation, partial correlation, regression, and partial regression methods.

Partial correlation Yule [1907] is calculated from the following formula

$$R_{xy,z} = \frac{r_{xy} - r_{xz}r_{yz}}{\sqrt{((1 - r_{xz}^2)(1 - r_{yz}^2))}} \tag{2.1}$$

where $R_{xy,z}$ is correlation between x and y keeping z constant. r is the normal correlation. The t-value is calculated as the following

$$t = r\sqrt{(\frac{n-3}{1-r^2})} \tag{2.2}$$

where n is the sample length.

If we need to regress variable $Y1$ on $X1$ keeping $X2$ constant, then we regress $Y1$ on $X1$ and keep the residual R_Y

$$\begin{aligned} Y1 &= C1X2 \\ C1 &= (X2^T * X2)^{-1} * X2^T * Y2 \\ R_y &= Y1 - C1 * X2 \end{aligned}$$

After that, we regress also $X1$ on $X2$ and keep the residual R_X.

$$\begin{aligned} X1 &= C2X2; \\ C2 &= (X2^T * X2)^{-1} * X2^T * X1; \\ R_x &= X1 - C2 * X2; \end{aligned}$$

the final step is to regress the residual from the first step on the residual from step 2.

$$R_y = C3 * R_x; \tag{2.3}$$

$$C3 = (R_x^T * R_x)^{-1} * R_x^T * R_y; \tag{2.4}$$

As ENSO and IOD are strongly correlated in Autumn, it is important to isolate each pattern separately to understand the effect of each one on the atmospheric circulation and precipitation. There are several methods to extract climate modes(patterns) from the data: using the Fourier transform to remove frequencies associated with the time band of the mode, using partial regression to extract an index expressing the mode, or utilizing Empirical Orthogonal Function (EOF) and Principle Oscillation Pattern (POP) Baquero-Bernal *et al.* [2002]. Both partial correlation and partial regression were used here to separate the linear covariance of the IOD mode from the ENSO mode. Several authors used this method to study the teleconnection between the IOD and ENSO Cai *et al.* [2011],Behera *et al.* [2005]. Also utilizing composites of pure ENSO events—years in which no IOD event occurred, and vise verse aid in identifying the nonlinear patterns associated with that event which are not recognized by regression analysis, however, years of pure IOD and pure ENSO is still strongly debated. We want

to emphasize that debate still going strong on the relationship between IOD and ENSO, and about how to isolate IOD from ENSO. As strong relationship between the IOD and ENSO and nonexistence of a unified index for ENSO and the IOD complicates the separation of those modes.

Anomalies were calculated by removing the mean and the first four harmonics of the seasonal cycle from the data of the whole period. This method is more general than just subtracting the monthly, daily, or annual climatology of the data for the whole period. The choice of a base period for calculating the anomalies—whatever the method we use— can influence the results. There are no specific rules for choosing a base period, thus choosing different base period can lead—sometimes—to different results.

The trend of the SST in Indian ocean is remarkable and might be associated with global warming. However, the trend is stronger for SST and Sea Surface Height (SSH) than in any other variables. We detrended the data to ensure that regression and correlation analysis was not impacted by strong trends in the data. Detrending data was performed by regressing the data against time. There are several other methods to do that, such as the first finite difference of the time series. One concern of removing the trend by using the projection of a time index on the data is the length of time or the period of time over which to apply such projection. Some authors apply it on the whole time series, but usually trends in the data fluctuate from year to year, thus sometimes it is better to divide the data into segments and apply the detrending algorithm on each segment. Detrending by segments can remove some interannual or decadal variability.

2.3 Indexes used in the analysis

The domain of study, eastern Africa, has suffered from several destructive drought episodes. Besides that, several wars destroyed the weak infrastructure there. These problems have led to insufficient weather data over that region, thus few studies have been conducted on that area. Also, the Indian Ocean has not received enough attention. Most buoy measurements have been made in the Pacific due to the investment to improve understanding of the well known El Niño

phenomenon, because of its pronounced impacts on the entire world. Lack of investment in buoys in the Indian Ocean implies that there is no long record of observation from moored buoys in there. A new project called Research Moored Array for African-Asian-Australian Monsoon Analysis and Prediction (RAMA) is intended to deploy buoys in the IO, beginning in 2005 (more information is available at http://www.pmel.noaa.gov/tao/rama/RAMA_BAMS.pdf). However, there are more ship observations of SST in Indian Ocean than in the Pacific due to ship tracks from India and Australia to England. Also the relatively deep theremocline in the IO gives false impression of non existence of air-sea interactions. All these reasons have reduced our knowledge about the IO.

We used the ETOPO—2 minute data that integrates land topography and ocean bathymetry available at http://www.ngdc.noaa.gov/mgg/global/global.html—to show the terrain height of Africa (Fig.2.1). The highest terrain in Africa is located in Ethiopia, it is called the Roof of Africa.

Variation of precipitation in tropical Africa is associated with the ITCZ movements, so most precipitation is associated with the transition seasons (Autumn and Spring). Panel 2.2 shows the mean of precipitation for every month calculated from 1950-2010. The selected domain is marked with red circles as shown in (Fig.2.1) which shows the location of the GPCP data used in this analysis. Half of these station is in the south Somali, north east Kenya, and southern eastern Ethiopia. The reason behind selecting this domain is that correlation map of El Niño and IOD is high in there. The correlation map between El Niño and precipitation over eastern Africa shows that around Tana Lake, precipitation often occurs in association with La Niña. That is why we did not include central and northern Ethiopia in the domain. Another reason is that over central and northern Ethiopia precipitation occurs mainly during summer. However, the impact of El Niño and the IOD extends far south of the Equator, the selected domain starts north of the equator to avoid overlapping the opposite transition seasons south and north of equator. Precipitation over east Africa is less than precipitation in west of Africa. Also precipitation over Somali and Kenya is less than precipitation over northern Ethiopia, and over lake Victoria. One problem of the location of the domain is the spatial inhomogeneity of the precipitation. Total annual precipitation for the

grid points shown in (Fig.2.1) ranges from 189mm/year to 1800 mm/years. Climatology of each grid point is shown in (Fig.2.3), the bold red line is the average of all these grid points. Results show two seasonal peaks, one during April(long rain season), the other is during October(short rain season).

The next few paragraphs discuss four indexes that we used in the analysis, for precipitation, El Niño, the Indian Ocean Dipole, and Equatorial wind in IO.

The Precipitation Index (PI) is the mean of detrended anomaly of precipitation specified by the red circles (Fig.2.1) using GPCP data. This index was used to composite the circulation pattern associated with extreme rainfall events over eastern Africa. As that domain has a strong correlation of precipitation with positive Indian ocean dipole and El Niño in Autumn, then we expect that PI is good index to study the inter-annual variability between the Indian Ocean Dipole, ENSO, and East African precipitation.

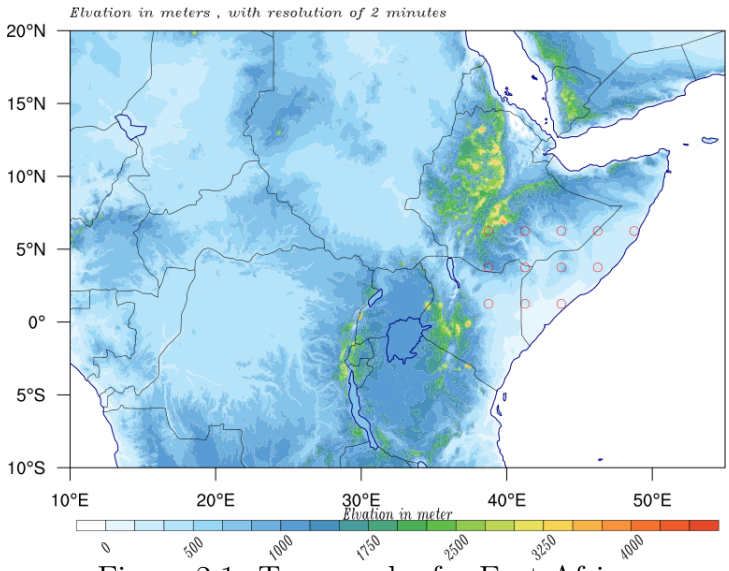

Figure 2.1: Topography for East Africa

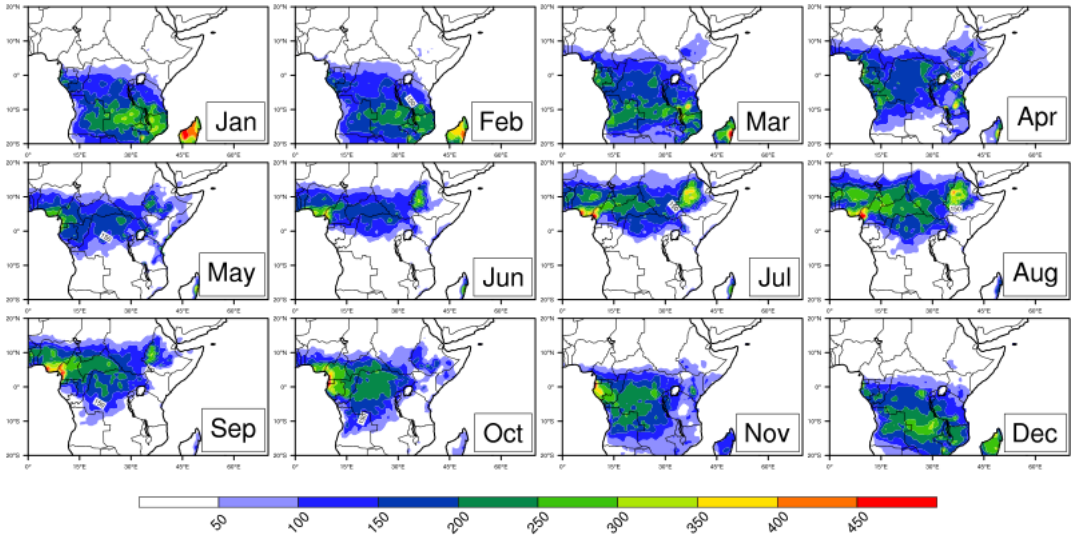

Figure 2.2: climatological precipitation at tropical Africa

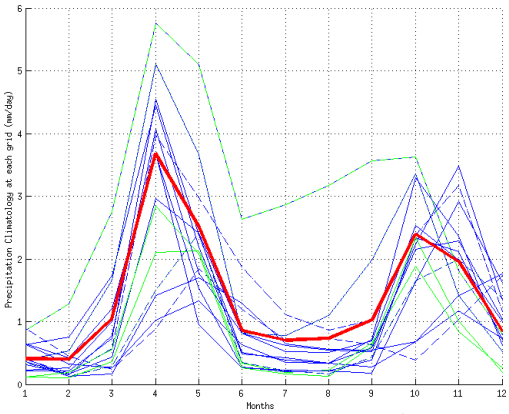

Figure 2.3: thin lines are precipitation at each grid points, bold red curve is the average of all grid point

We calculated the same index again using the GPCP and CMAP data, and found that the correlation between the index that we used in this study (calculated by GPCC) and the index calculated by CMAP (from 1979-2007) is 0.9, statistically significant at the 99% confidence level, and also the correlation between the index calculated by GPCP and GPCC (1997-2012) is 0.96 statistically significant at the 99% level. Analysis of the precipitation index (PI) show that precipitation occurs in two seasons: short rain season, during Autumn, in which the ITCZ moves quickly to south, and long rain season(Spring) in which the ITCZ moves slowly to north. However, the precipitation over eastern Africa follows the ITCZ, and the Walker circulation. Existence of ascending and descending branches in Tropics indicates that the Walker circulation is stronger locally than the Hadley circulation Tanaka *et al.* [2004]. Also, that explains the importance of studying zonal

flow (Walker circulation) variability over the meridional flow variability. However, interannual changes in meridional flow (Hadley circulation) are rare, but they can be catastrophic.

Seasonal Precipitation amplitude in Spring is larger than in Autumn. Precipitation peaks in April during spring and in November during Autumn. Although our region is in the tropics, it is relatively dry. Seasonal dry episodes occasional repeat consecutively for up to 4 years, especially in November (fig.2.4f). Wet events are associated with tropical events, like flood in 1961 was associated with strong positive IOD and changes in the summer monsoon in India, the floods of 1994 and 1997 were associated with both El Niño and IOD events. The Median, first quartile, and inner fences(1.5 Inter Quartile Range (IQR)) of PI in April is higher than in March and May (fig.2.4e). Two outliers—above Q3+1.5IQR which is the far tail of the Gaussian distribution of events if the events are normally distributed, in this case IQR = 1.35 — during April are noted: 1948, and 1961. In Autumn, the median and outliers in October are larger than in November. However, the number of the outliers in November is larger than in October. All months have outliers. Precipitation in the domain is characterized by consecutive extreme dry episodes associated with ENSO and IOD.

The climate community defines several indices for El Niño, some of these indices are based on SST, others are based on atmospheric variables, and others depend on both SST and atmospheric variables. The most used indices are Niño 1+2 , Niño 4, Niño 3.4, and multi-variate El Niño. Chiodi and Harrison [2010] constructed an ENSO index based on OLR data. ONI 3.4(Oceanic Niño index) is defined as 3 months running average of SST anomaly in the Niño 3.4 region $(5°N - 5°S, 120° - 170°W)$. El Niño/La Niña episodes are identified when five consecutive months are above/below $\pm 0.5C$ from the long term mean Trenberth [1997]. Weak El Niño is suggested when ONI3.4 is from 0.5-0.9, moderate El Niño is suggested when ONI3_4 is from 1-1.4 and from 1.5 the El Niño is considered strong. ONI3.4 for SON 1997 was 2.3. Understanding variability of the ENSO would enhance our understanding of precipitation variability in East Africa. ENSO occurs every 2-6 years with events being roughly phase locked to the seasonal cycle in winter (fig.2.4b). El Niño events including

1957/58,1965/66,1987/88,1972/73,1982/83,1991/92,1997/98,2009/10 based on ONI3.4 can be easily found in (fig.2.4b). Mature El Niño events frequently decay and new events occasionally grow during northern spring. The seasonal evolution of El Niño events apparent in (fig.2.4a) confirms the tendency for El Niño events to evolve with the seasonal cycle, however, it is not perfect. The IQR of ONI3.4 increases from spring to winter and decreases from winter to spring. However, El Niño tends to peak in late autumn of developing year and early winter of decaying year, there are no outliers in autumn and winter. Strong El Niño events like 1997,1982 are considered long lived as they lived till the end of spring of decaying year. Dynamical and statistical models tend to have little skill in predicting ENSO SST anomalies months in advance when the models are initialized in the spring. This minimum in prediction skill is known as the spring predictability barrier. We think that this might be because a positive or negative SST anomaly during spring is not an indicator of a positive or negative phase of inter-annual modes. Random processes my trigger a feedback mechanisms (like Bjerknes, wind-evaporation-SST), such feedbacks cause a positive and/or negative anomalies in certain variables, till some threshold is reached which stop the feedback. Discovery of ENSO and IOD was encouraged by the existence of feedback algorithms like Bjerknes feedback that enable us to define some processes that may help to understand and predict such modes. During Spring, there is no clear feedback, which means that process that controls the interaction between the ocean and atmosphere is random, or the climatology during that time of year does not encourage growth of a feedback, or we do not yet discovered the physics of the feedback during that time of year.

The third index is the IOD index, called Dipole Mode Index (DMI), introduced by Saji *et al.* [1999]. DMI is defined as the difference between the average of SSTA of western IO $(50^\circ - 70^\circ E, 10^\circ S - 10^\circ N)$ and average of SSTA of south eastern IO$(90^\circ - 110^\circ E, 10^\circ S - 0^\circ)$. We run 3-months moving average filter over the DMI to remove the intra-seasonal variability to be consistent with the common definition of IOD. As the definition of the DMI requires averaging the data from $10^\circ S - 10^\circ N, 10^\circ S - 0^\circ$, and as the HadISST ranges from $89.5^\circ S - 89.5^\circ N$ spaced

by 1.0°, we interpolated the data to be $89°S - 89°N$, thus we lose the 0.5° from latitude. DMI is normalized by dividing by its standard deviation of the whole period. Saji and Yamagata [2003] used multivariate criteria to define IOD events. In this index DMI, and U_{eq} need to exceed 0.5σ for at least 3 months. U_{eq} is defined as the average of the zonal wind anomaly in $50° - 70°E, 5°S - 5°N$. Also the WIO and EIO SSTA must be of opposite sign. According to this criterion, the climatology includes 9 positive IOD events:1961,1963,1967,1972,1977,1982,1983,1994,1997, and 10 negative events:1958,1960,1964,1971,1974,1975,1989,1992,1993,1996 between 1958-1997. These events are shown in (fig.2.4d).

The seasonality of DMI (fig.2.4c) is complicated. Usually IOD events mature in Autumn with a peak in October. However, although many events mature in Autumn, some events mature in summer. Some events start in spring and mature in summer, then decay in autumn, but the majority of events start in summer, and peak in autumn. Du *et al.* [2013] classify the IOD events that occurred after 1970 into three main categories. The first category is the seasonal (normal) group in which IOD events mature in autumn, the second group is called the nonseasonal, in which IOD peaks in summer (fig.2.4d), The last category is long IOD events which start during spring and mature in autumn. The largest IQR and inner fences of the DMI occur during August and September, then IOD tend to begin to decay. IOD events tend to peak between August and October. We plotted the IOD index year by year from 1950 to 2010, and we found that IOD events from 1980 to 2010 tended to peak during September, but after 2000, more IOD events reached their maxima during October. Before 1980, events are tended to maximize during September.

Zonal equatorial wind over Indian basin is the manifestation of atmospheric zonal circulation over the Indian basin, but zonal wind and zonal circulation are the same thing. We took the average of the detrended zonal wind anomaly at 850mb over IO $(2.25°S - 2.25°N, 70°E - 90°E)$ as index for zonal equatorial wind in the IO U_{eq}. We multiply the zonal wind with -1, thus the correlation is positive with precipitation over eastern Africa. We applied a 3-month centered moving average to remove high frequency variability. Easterly wind anomalies over the Indian ocean transfer moisture to east of Africa. Table 2.1 shows correlation

between PI and U_{eq} from 1950-2010. The precipitation index is highly correlated with equatorial wind over the Indian ocean only during boreal autumn.

Months	1	2	3	4	5	6	7	8	9	10	11	12
R	**0.37**	0.2	0.07	0.15	0	0	**0.32**	*0.29*	0.2	**0.69**	**0.65**	**0.62**

Table 2.1: correlation between equatorial wind in IO and PI from 1950-2010, bold number indicates significance at 99% level, italic number indicate significance at the 95% level

The maximum monthly correlation between the PI and zonal wind is 0.69 (significant at the 99% level) during October, which is the highest known correlation between zonal wind and precipitation on planet Hastenrath and Polzin [2004]. The correlation then slightly decreases in November and December with the normal decaying of the IOD and beginning of the winter monsoon in which the merdional pressure gradient over the IO is stronger than for the zonal wind.

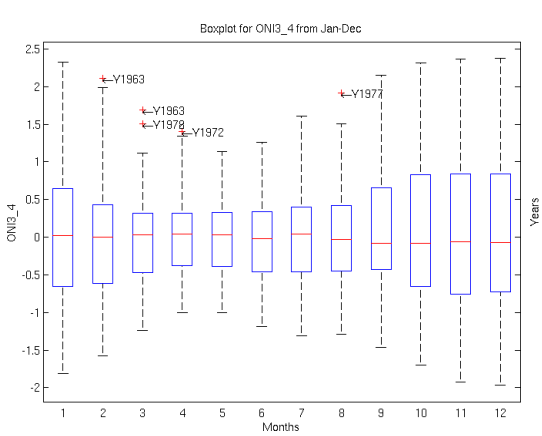

(a) Boxplot for ONI3.4

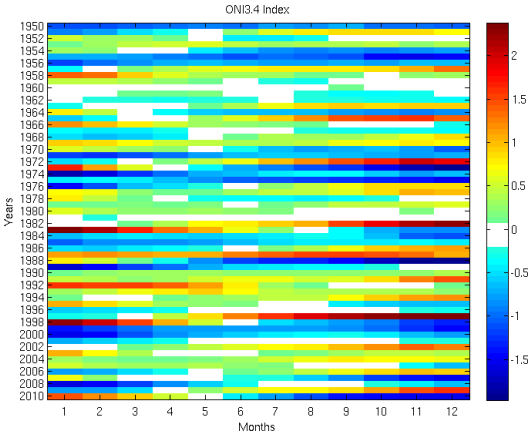

(b) contour for ONI3.4

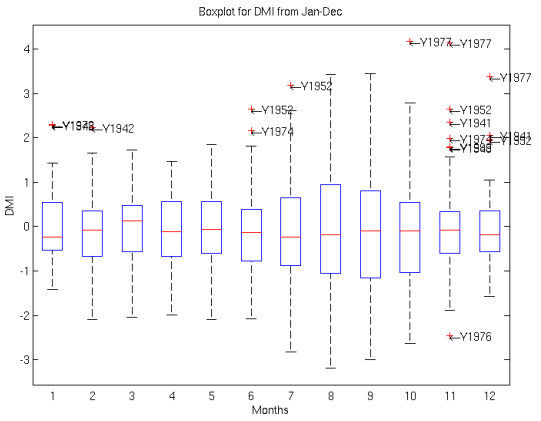

(c) Boxplot for DMI

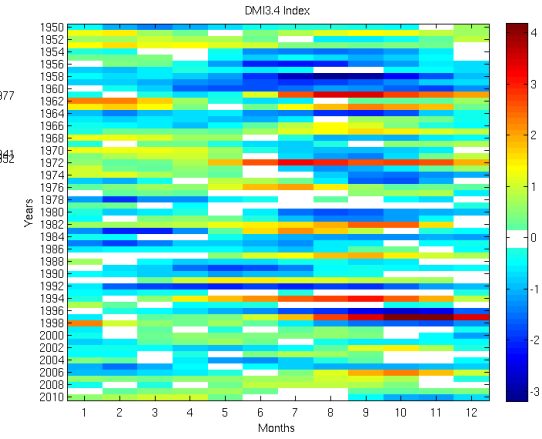

(d) contour for DMI

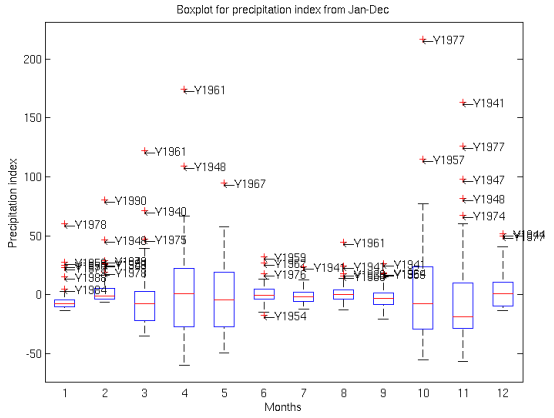

(e) contour for precipitation index

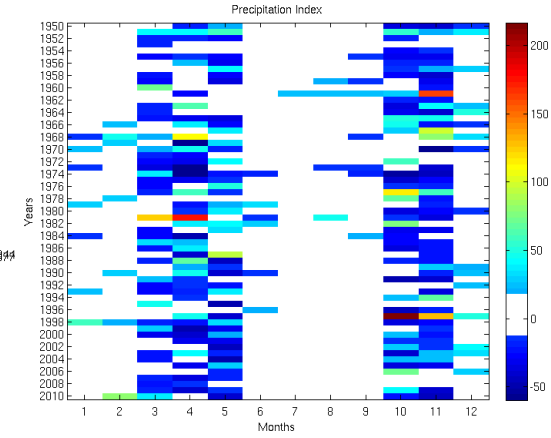

(f) contour for precipitation index

Figure 2.4: First column on the left is contour for ONI3.4 , DMI, and PI. Second column from left is contour for ONI3.4, DMI, and PI.

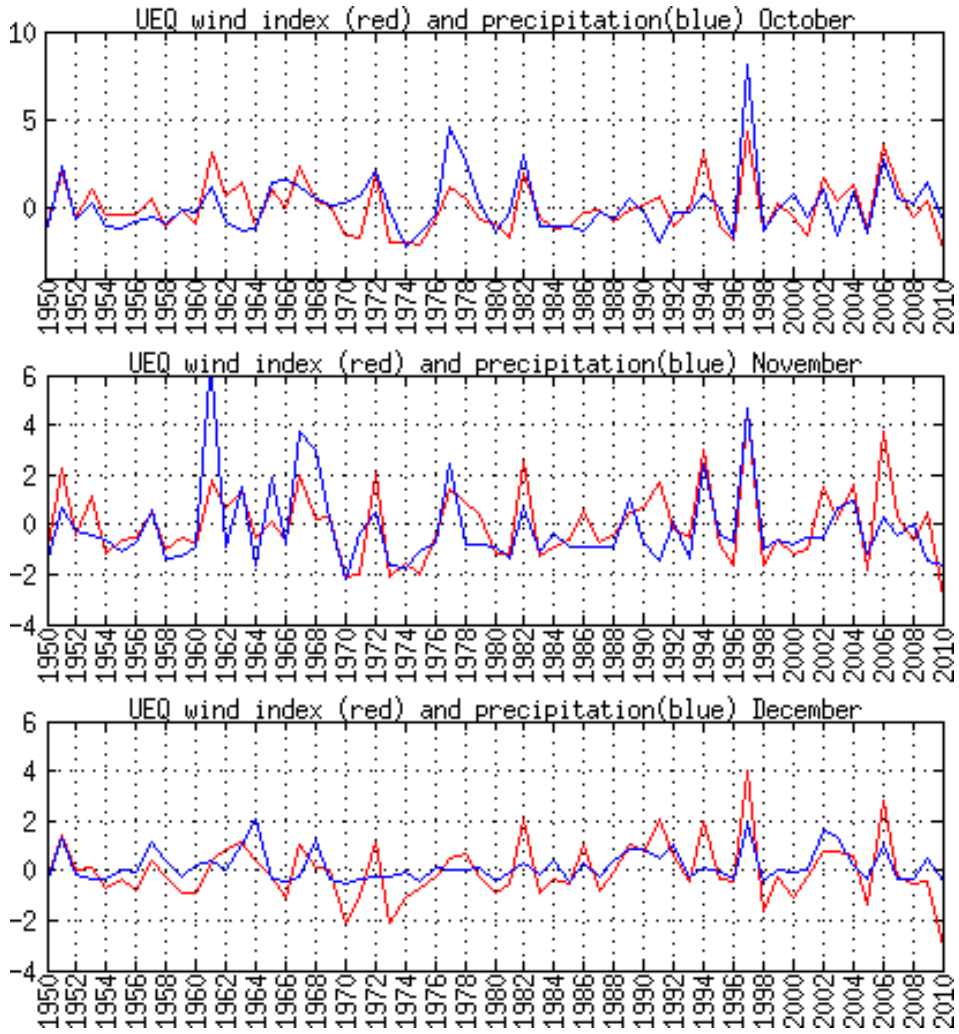

(a) UEQ and precipitation Autumn

Figure 2.5: Equatorial wind index in IO and standardized PI during Oct, Nov,and Dec

Figure(2.5) shows the standardized PI and U_{eq} for October, November, and December. Wind and precipitation decreases from October to December. During 1997, the wind anomaly exceeded $4ms^{-1}$, and the precipitation was 7σ. 1997 was both strongest EL Niño and second strongest IOD since 1950.

2.4 General Circulation associated with precipitation in boreal Autumn and Spring

We show here the circulation patterns associated with precipitation in eastern Africa in boreal Autumn(SON), and spring(MAM). Due to the tendency for rapid growth and decay of the IOD, and the co-occurrence of both ENSO and IOD, we

studied the circulation on monthly basis. Due to the high association between the IOD and ENSO, it is informative to construct statistical models in which we hold one of them constant while allowing the other to vary. For each month, we explain the circulation pattern associated with: pure PI, Pure PI at constant El Niño $PI|_{ONI3.4}$, and Pure Pi at constant DMI $PI|_{DMI}$. We show here SST, OLR, wind, geopotential height and specific humidity pattern associated with PI. HadISST, NOAA OLR, and ERA-I data were used for these projections. Moisture flux was calculated by multiplying the wind component with specific humidity, and anomalies were calculated after that. NCL build-in functions were used to calculate the divergence of moisture flux. To be consistent with the period covered by NOAA OLR and GPCP data, all regressions were calculated from 1979-2010.

Month	ONI3_4	DMI	ONI3_4_DMI	DMI_ONI3_4
3	-0.10	0.12	0	0.14
4	0	0	0	0
5	0.22	*0.32*	0	0.26
10	**0.54**	**0.67**	0.31	**0.51**
11	**0.40**	**0.63**	0	**0.55**
12	**0.41**	0.2	**0.3**	0.1

Table 2.2: Correlation between the precipitation index and ONI3.4 and DMI for 1950-2010. Bold values are statistically significant for p-value of t-test larger than 99% level, italic number are significant at 95% level

Before discussing the circulation patterns associated with precipitation, we present in Table 2.2 the correlation of the precipitation index with the ONI3.4 and DMI for Spring and Autumn. This quantity might help diagnoses the associated circulation pattern for ENSO and IOD. Table.2.2 shows that the correlation of PI with ONI3.4 and DMI is zero in Spring. Such zero correlation is expected because these tropical modes tend to have transient states in that time of year. During Autumn, PI is significantly correlated with ONI 3.4 and DMI. The correlation with DMI is stronger than with ONI3.4, however, correlation between the PI and DMI decay rapidly during December as the IOD mode tends to decay strongly during this month. As both ONI 3.4 and DMI are related to each other, it is important to know the correlation of precipitation with one of those modes keeping the other fixed. Table.2.2 shows that there is no relationship between precipitation and ONI 3.4 when IOD is fixed, but there is relationship between PI and IOD when

keeping ONI 3.4 constant, this suggests that the IOD is more directly relevant for precipitation variability over eastern Africa.

2.4.1 SST and OLR in Autumn

During October, regression of SST on PI (Figure.(2.6a)) features warming in the east Pacific manifesting normal El Niño. The warming and cooling in the western and eastern IO manifest IOD mode. Figure (2.6b) shows the same as Figure(2.6a) but after holding ENSO signal constant—partial regression of SST on PI at constant ENSO. When the ONI 3.4 signal is held constant, a small warming appears in the eastern Pacific, consistent with the notion that ONI 3.4 does not describe all signal in ENSO. Also, a negative SST anomaly intensifies over the north Pacific. The IOD weakens in this result because many IOD events are associated with El Niño events. So removing El Niño implicitly weakens the IOD. The IOD variance associated with ENSO is larger than IOD variance linearly independent of ENSO. The second strongest IOD event occured in the same year as the strongest El Niño event 1997/98. Figure(2.6c) shows the same as Figure(2.6a) but after holding IOD constant, negative and positive anomaly—which manifests the IOD—at eastern and western IO disappears. A substantial part of El Niño remains present in the eastern Pacific Ocean after regressing out the IOD, indicating that a considerable part of El Niño occurs independent of the IOD.

During November, the SST Pattern shown in Figure.(2.6d,e,f) is similar to that in October.

During December, the first thing to note is that the amplitude of SST is stronger than during October and November. The dilemma here is that the El Niño signal tends to strengthen gradually until it peaks during December. However, precipitation tends to peak in October and decay rapidly during December(from 2.5 mm/day per month to 1 mm/day per month). As shown in Figure(2.6g), a tail of positive SST anomaly extended from the north western IO to the south eastern IO near the coast of the west Australia. The positive SST anomaly tail peaks over the south eastern IO. Negative SST anomaly appears at the west coast of Java-Sumatra due to upwelling. However, the area covered by a positive SST anomaly in IO is much larger than the area covered by negative SST

anomaly, the amplitude of the negative anomaly is stronger than the amplitude of the positive anomaly.

However, regressions shown in Figures.(2.6a,e,h) are calculated at constant El Niño, those regressions retain El Niño1+2 patterns. This signal is expected because the El Niño signal was approximately removed based on El Niño 3.4 which is located around the dateline, but Niño 3.4 does not include all signal associated with ENSO. Another point worth mentioning is that fixing the IOD removes El Niño signal during November, but conserves it during December. As IOD decays in December, then removing or conserving it will not alter El Niño signal as shown in Figures.(2.6i).

To the extent that SST modulates convection, OLRA patterns are correlated with SST anomaly patterns. Most literature indicates that SST above $27° - 28°c$ facilitates convection Graham and Barnett [1987], Sabin *et al.* [2013]. Other factors can control convection process, such as large-scale atmospheric subsidence, which can suppress convection even if SST is around $30°C$.

During October, Fig.(2.7a) shows the pattern of the OLR associated with SSTA pattern. The OLR pattern features El Niño in Pacific ,and IOD in Indian Ocean. Fixing El Niño as shown in Fig.(2.7b) decreases the amplitude of the convection. Retention of a negative OLR anomaly after removing the El Niño SST signal indicates that either ONI3.4 is not a complete index of El Niño or that sometimes El Niño-like convective signals emerge without the associated SST anomalies. In Indian ocean, as expected, the IOD mode weakens a little as the half of the IOD events are linearly associated with ENSO. However, fig.(2.7c) depicts projection of OLR on PI at constant DMI, a weak IOD pattern still exists. As the relationship between SST and OLR is nonlinear, and as our method of removing IOD or ONI3.4 is based on a linear method, then we expect that our modes will not be completely removed, or only linear part of the relationship will be removed.

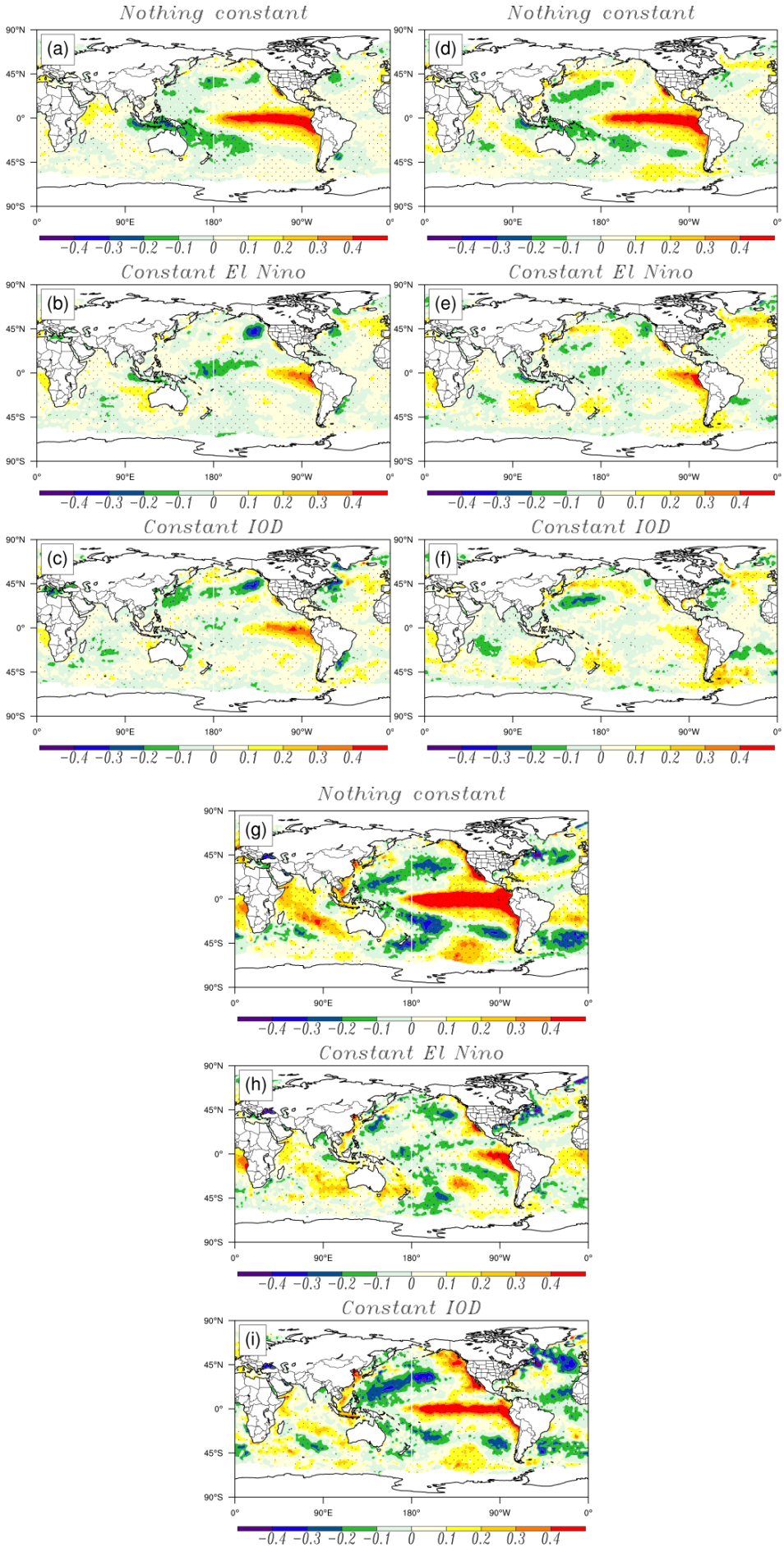
Nothing constant
(a)
Nothing constant
(d)
Constant El Nino
(b)
Constant El Nino
(e)
Constant IOD
(c)
Constant IOD
(f)
Nothing constant
(g)
Constant El Nino
(h)
Constant IOD
(i)
90°N
45°N
0°
45°S
90°S
0°
90°E
180°
90°W
−0.4 −0.3 −0.2 −0.1 0 0.1 0.2 0.3 0.4

Figure 2.6 *(previous page)*: Regression of SST on Precipitation index for October(a,b,c first column),November(e,f,g second column), and December(h,i,j third column). First row is for pure PI, second row is for PI at constant ENSO, Third row, for PI at constant IOD. Points shading indicates statistical significance greater or equal to 95%.

Two sources of non-linearity exist, the first is due to using indexes for El Niño and IOD that are based on SST only, thus the projection of different atmospheric variables on those indexes will only retain the linear part of the association of the index with the predictor. The other source of the non-linearity, is because adoption of a linear regression method to isolate the climate modes.

During November, Figs.(2.7d,e,f) feature the same pattern as during October, but with two main differences: convection in Pacific does not extend far west as during October, instead it decays at dateline, and subsidence spread from tropical dateline to $90°E$. The second main difference beween pattern during October and November is convection at Eastern Africa and western IO intensify, however, the precipitation peaks during October.

During December, Figs.(2.7g,h,i) feature the same pattern as during November, but with two main differences. First, OLR in Eastern African and western IO resembles a horseshoe shape. Consistent with the decay of precipitation during December, the OLR anomaly signal is much stronger than during October and November.

For a complete view about the general circulation associated with precipitation over Eastern Africa, we regressed both wind and geopotential height at the surface and upper air on the PI.

During October, Figs.(2.8a,b,c) show a negative anomaly of geopotential height over northern Europe around 50N, 40E at 850 mb . This negative extra-tropical anomaly intensifies after fixing ONI3.4, and peaks after we remove IOD as shown in Figs.(2.8b,c). It is unclear whether this anomaly is related to changes in meridional circulation at 40E caused by convection over Eastern Africa. The Southern Hemisphere shows a traveling Rossby wave, which radiates from southern Australia.

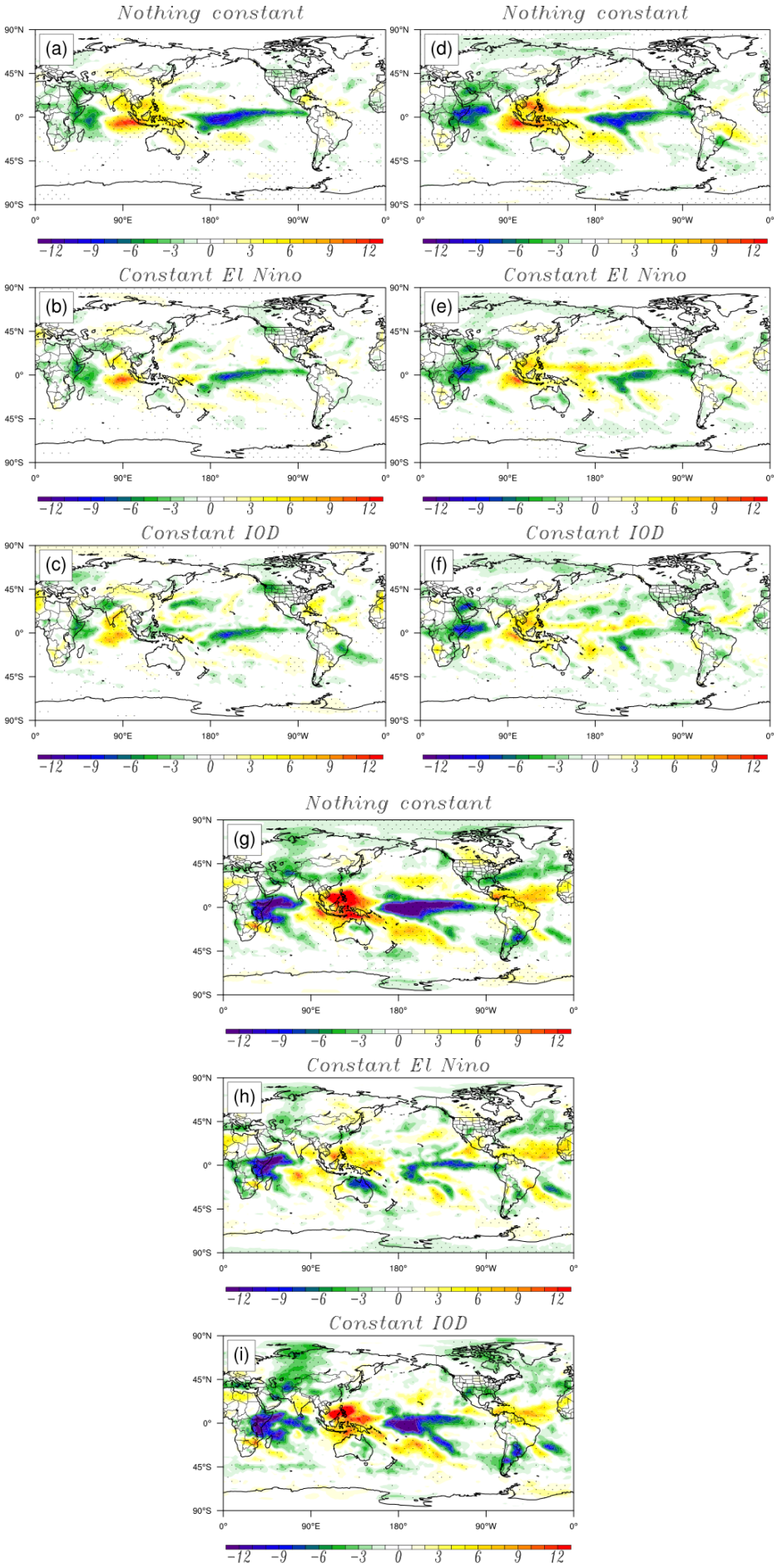
Nothing constant
(a)
Nothing constant
(d)
Constant El Nino
(b)
Constant El Nino
(e)
Constant IOD
(c)
Constant IOD
(f)
Nothing constant
(g)
Constant El Nino
(h)
Constant IOD
(i)
90°N
45°N
0°
45°S
90°S
0°
90°E
180°
90°W
−12 −9 −6 −3 0 3 6 9 12

Figure 2.7 *(previous page)*: Regression of OLR on Precipitation index for October(a,b,c first column),November(e,f,g second column), and December(h,i,j third column). First row is for pure PI, second row is for PI at constant ENSO, Third row, for PI at constant IOD. Points shading indicates statistical significance greater or equal to 95%

During November, as El Niño is growing, two anticyclone straddle the north and south western IO west of the heat source. A traveling Rossby wave is radiated from the Southern Hemisphere over the western IO toward the south pole as is apparent in Figs.(2.8d,e,f).

During December, Figs.(2.8g,h,i) show a traveling Southern Hemisphere Rossby wave radiated from eastern IO. Removing ONI3.4 weakens the pattern, while fixing IOD strengths it, thus the southern Rossby wave radiation from eastern IO is mainly maintained by El Niño.

To get a complete view about the circulation that is generated by baroclinic or baratropic mechanics, we regressed wind and geopotential height at 150 mb on PI, also as before we fixed ONI3.4 and IOD to show the impact of each mode separately. Due to the lose of climatological heating over the eastern IO and western Pacific ocean, anticyclones straddle the equator over the north and south IO in the lower troposphere, these anticyclones are inverted in upper troposphere as troughs as shown in Figs.(2.9a,d,g). The southern cyclone weakens from October to December. Removing ONI3.4 and seasonal weakening of the IOD would yield a pattern shown in Figs.(2.9b,e,h) and Figs.(2.9c,f,i). Over the Pacific, two cyclones are generated west of the heat source at lower levels, which flip into anticyclones in the upper troposphere as shown in Figs.(2.9a,d,g). This pattern strengthens as we move from October to December in spite of the pattern over the IO. Removing ONI3.4 nearlly removes the traveling Rossby pattern over the northern and southern Pacific. Removing IOD just weakens it.

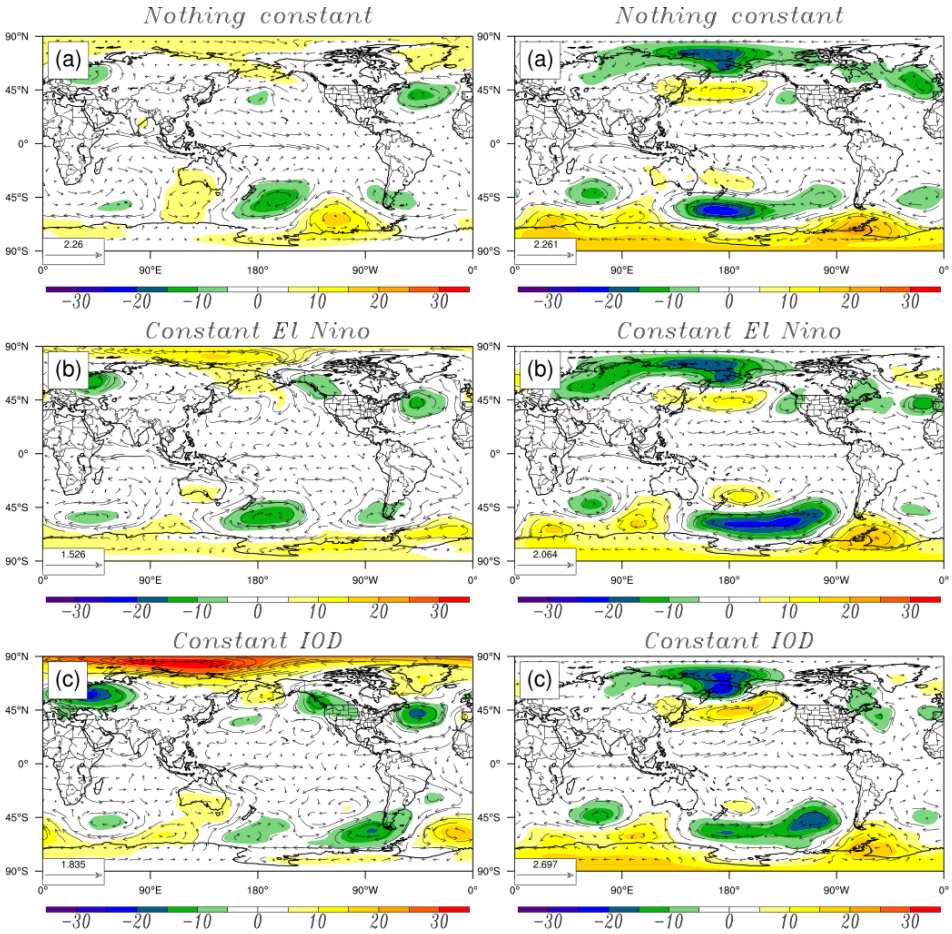
Nothing constant
(a)
2.26
Nothing constant
(a)
2.261
Constant El Nino
(b)
1.526
Constant El Nino
(b)
2.064
Constant IOD
(c)
1.835
Constant IOD
(c)
2.697
90°N
45°N
0°
45°S
90°S
0°
90°E
180°
90°W
−30 −20 −10 0 10 20 30

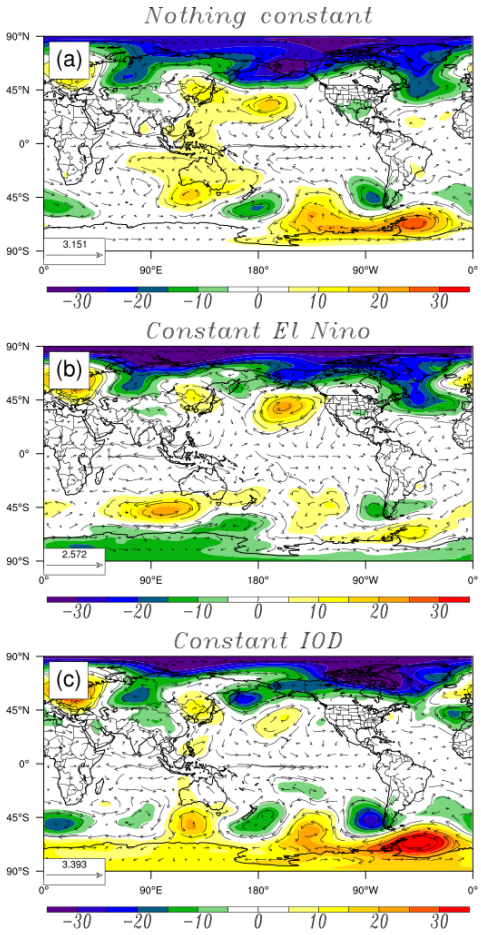
Nothing constant
(a)
3.151
Constant El Nino
(b)
2.572
Constant IOD
(c)
3.393
90°N
45°N
0°
45°S
90°S
0°
90°E
180°
90°W
−30 −20 −10 0 10 20 30

Figure 2.8 *(previous page)*: Regression of wind and geopotential height at 850 mb on Precipitation index for October(a,b,c first column),November(e,f,g second column), and December(h,i,j third column). First row is for pure PI, second row is for PI at constant ENSO, Third row, for PI at constant IOD

Most literature about drought/flood events study the moisture sources, and there are several ways to do that, One method is to back track the moisture source for individual events using models—like FLEXPART model—and determining the moisture contribution from different areas to each wet event. This study focuses more on the teleconnection patterns, and we build regression maps for moisture flux and moisture flux divergence using ERA-I. The first row of fig.(2.10) shows moisture flux and moisture flux divergence at 1000mb, while the second row and third rows show the moisture fluxes at constant El Niño and IOD. Figs.(2.10) shows that our source of moisture is mainly the Eastern IO. Two anticyclones are settled over the northeastern basin (over India) and southeastern IO. During October, fixing IOD as shown in Figs.(2.10c) leads to shifting of two anticyclones westward, the southern anticyclone center shifts from $90°E$ to $70°E$, nearly $15°$ of displacement. Also comparison of Fig.(2.10a) with Fig.(2.10c), shows that the left side of the northern anticyclone bends northward at constant IOD, in contrast to a pure regression map. Fixing IOD implies removing the heating over the western IO thus reducing convergence there. Figs.(2.10a,d,g) shows eastward movement of the northern anticyclone from the central Indian Ocean to western India to the Bay of Bengal.

To get some idea about the level at which maximum convergence of moisture flux accumulates over Eastern Africa, we regressed moisture flux at different levels. Figs.(2.11a,b,c,d) show moisture flux at 1000, 900, 800, and 700 mb respectively. At 800 and 700mb respectively, moisture convergence at the eastern coast and inland Eastern Africa, suggests the presence of a front inclined to the west.

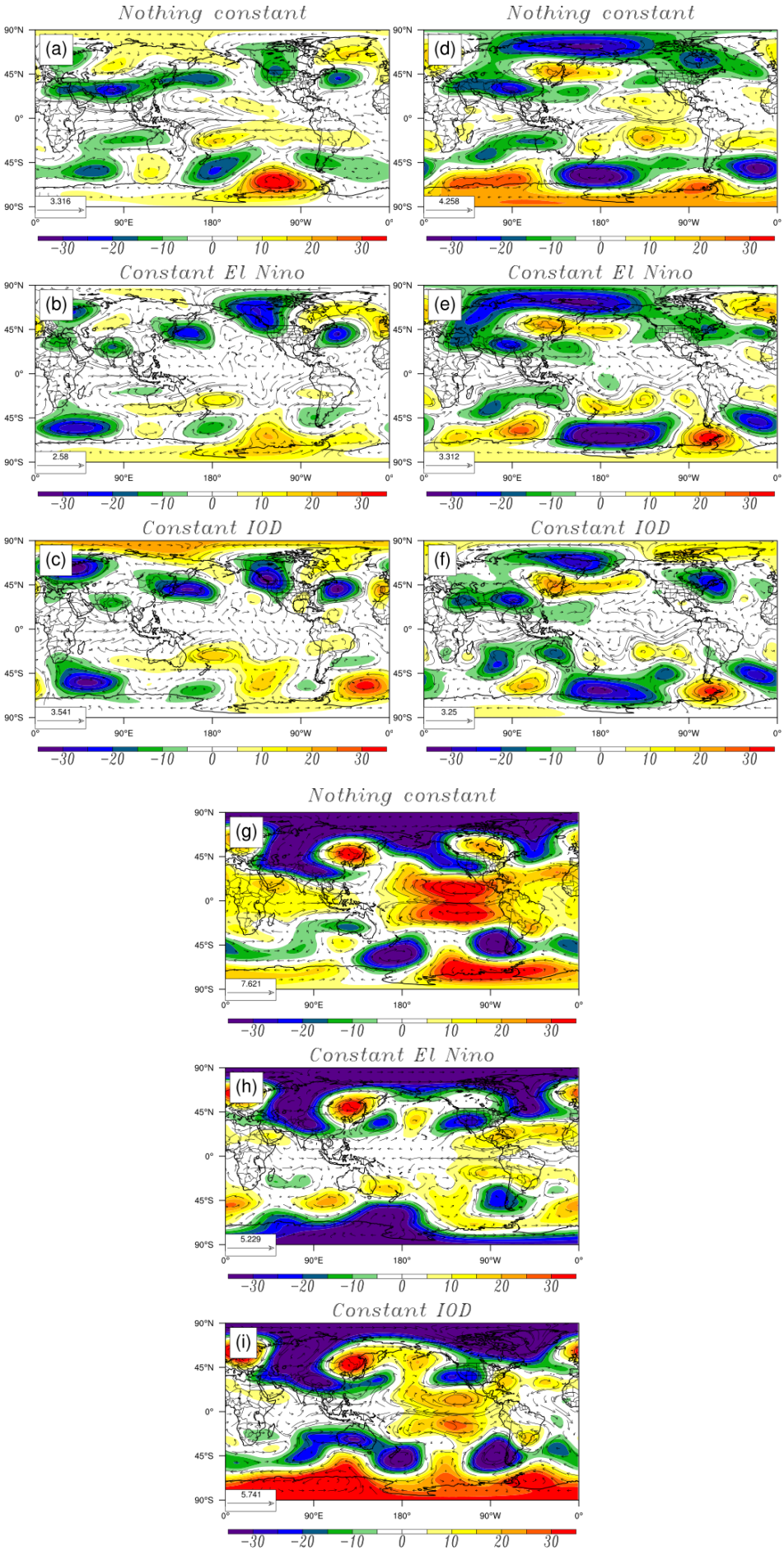
Nothing constant
(a)
3.316
Nothing constant
(d)
4.258
Constant El Nino
(b)
2.58
Constant El Nino
(e)
3.312
Constant IOD
(c)
3.541
Constant IOD
(f)
3.25
Nothing constant
(g)
7.621
Constant El Nino
(h)
5.229
Constant IOD
(i)
5.741
90°N
45°N
0°
45°S
90°S
0°
90°E
180°
90°W
−30 −20 −10 0 10 20 30

Figure 2.9 *(previous page)*: Regression of wind and geopotential height at 150 mb on Precipitation index for October(a,b,c first column),November(e,f,g second column), and December(h,i,j third column). First row is for pure PI, second row is for PI at constant ENSO, third row, for PI at constant IOD

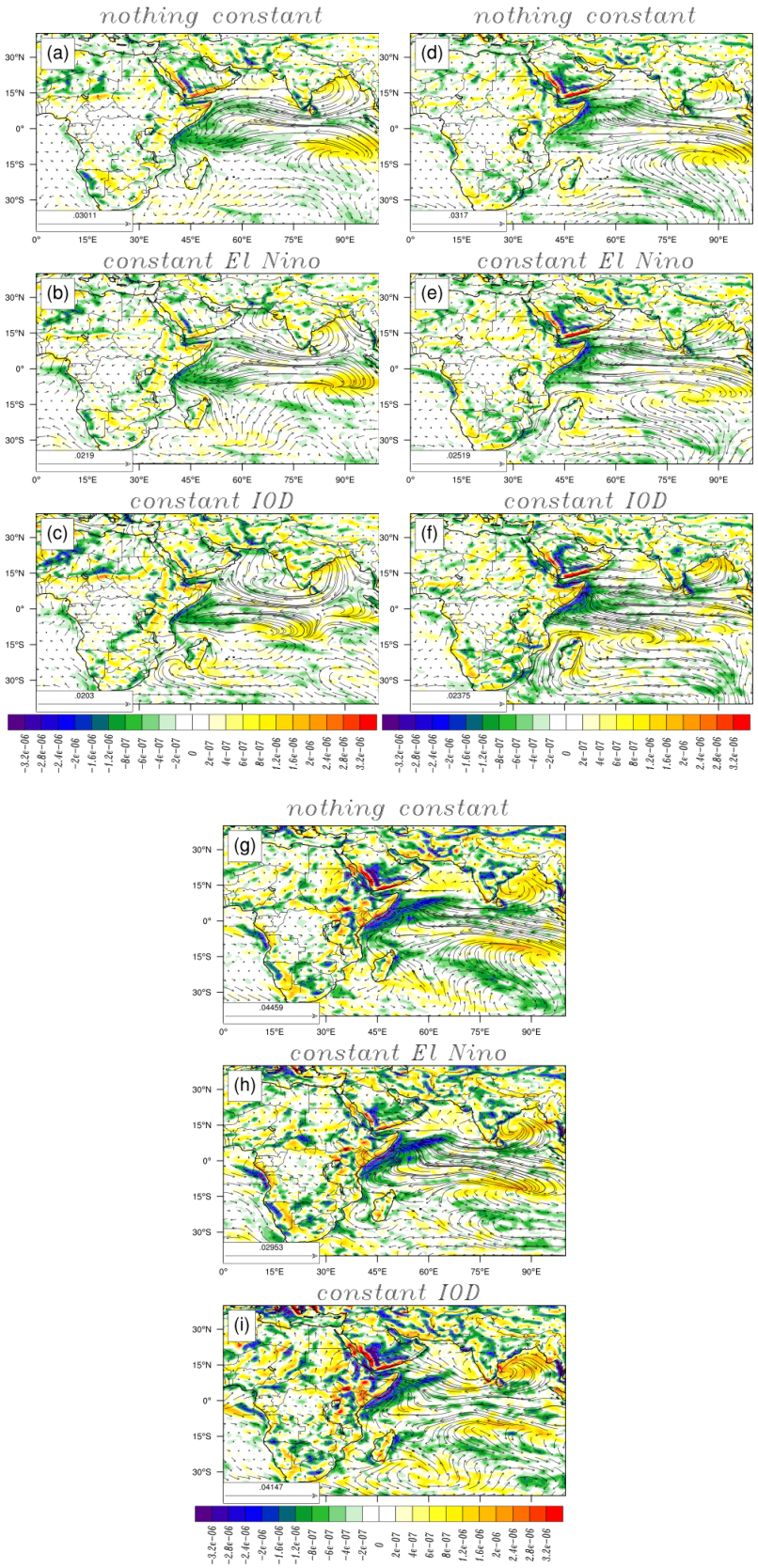

Figure 2.10 *(previous page)*: Regression of moisture flux and moisture flux divergence at 1000mb on PI For October(a,b,c first column), November(e,f,g second column), and December(h,i,j third column). First row is for pure PI, second row is for PI at constant ENSO, third row, for PI at constant IOD.

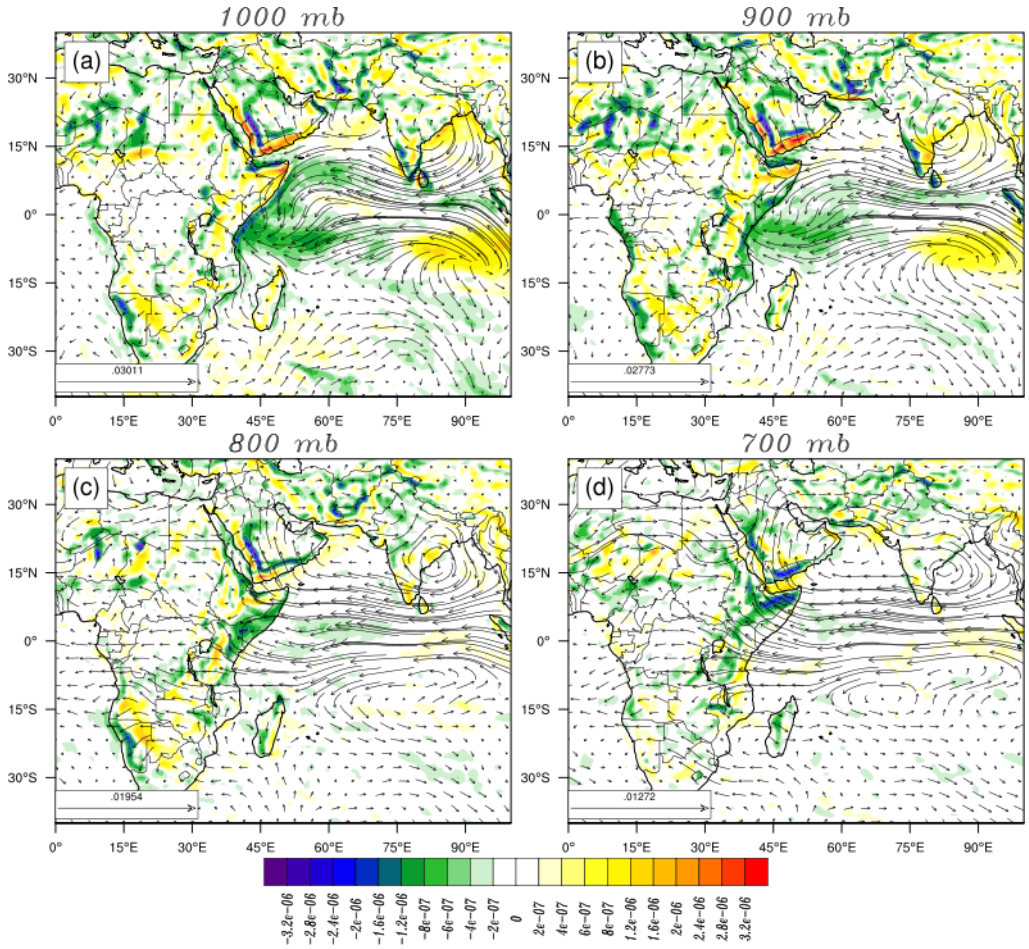

Figure 2.11: Regression of moisture flux and moisture flux divergence on PI in October at (a) 1000 mb , (b) 900 mb ,(c) 800mb, (d) 700mb

2.4.2 SST and OLR in Spring

In essence, the difference between patterns during Autumn and Spring is due to the nature of the climate modes themselves. IOD and ENSO modes mature in Autumn and Winter respectively. During spring, these modes are frequently in transition. It is impossible to judge whether the existent state (positive or negative) during spring will lead to positive or negative outcomes even if we have some clear signal of positive or negative SST anomaly, because we don't know how the atmosphere will respond to such variations, or whether the atmosphere might force a reversal. In other words, equal probability of occurrence of a positive or negative ENSO or IOD events can occur following the same SST state during spring. During spring, the way that atmosphere and ocean interact with each other is poorly understood. Existence of a clear pattern during autumn leads to skillful prediction of precipitation using statistical prediction for winter. The lack of a clear pattern during spring makes prediction of precipitation difficult. Dynamical models could be the best way to forecast precipitation during the spring season.

There is a difference between using regression to predict precipitation during autumn and spring. During spring positive SST may lead to either El Niño or La Niña because the future condition of ENSO following spring is poorly correlated with the condition during spring, also negative SST leads to similar outcomes, however, during autumn positive SST in the Pacific cold tongue region implies El Niño, and also negative SST implies La Niña. The difference between the patterns in the spring when conditions are evolving toward or away from El Niño motivate calculating regression models for these types of events separately in addition to building such models based on the full climatology.

In the first row, Figs.(2.12a,d,g) show regression of the SST on PI during March, April, and May respectively. In the second row, Figs.(2.12b,e,h) shows the same as in Figs.(2.12a,d,g) for the same months but at constant El Niño. Figs.(2.12c,f,i) in the third row is the same as in previous figures but at constant IOD. For sake of accuracy, we do not refer in terms of El Niño/La Niña or $\pm$ IOD here, instead we just use the positive/negative SST anomaly, as in spring we cannot judge about the future of the SST in autumn and winter.

During March, as shown in Figs.(2.12a,b,c), precipitation is associated with

positive SST anomaly at eastern and central Pacific. The IO features a weak negative SST anomaly in the east and positive SST anomaly in the west. In March, during El Niño decay, a positive SST anomaly exists in the central pacific, and negative SST anomaly tends to occur in the south eastern Pacific. In March during periods of La Niña decay, negative SST anomaly exists north and south of pacific. Thus our regression does not resemble periods of El Niño nor La Niña decaying during March. During periods of El Niño development, positive SST anomaly exists at west coast of South America, also in the central Pacific. During periods of La Niña developing, negative SST anomaly exists in the southern Pacific and near the western US proximate to the eastern shores of the Pacific near the Western United States, and positive SST anomaly exists in the Western Pacific. Thus we conclude that the regression pattern is closest to the pattern of La Niña development in March.

During April, as shown in Figs.(2.12a,b,c), negative SST anomaly exists in the eastern and central Pacific, in a pattern that looks similar to periods of La Niña development.

During May, as shown in Figs.(2.12g,h,i), positive SST anomaly exists in the eastern Pacific, in a pattern similar to that which develops during periods of El Niño development. IO SST features positive SST anomaly in the WIO and negative SST anomaly in the EIO. Du *et al.* [2013] showed that some IOD events do not follow the canonical seasonal progression of most events. They labeled these events as "unseasonal" because these events begin during May and decay during the summer. Such signals could be labeled as early IOD events.

Removing El Niño and IOD signals during March and April doesn't actually change SST patterns. This indicates that during March and April the behavior of climate mode is completely transient. During May, the regression technique succeeded in removing positive SST anomalies, this indicate that from May we have some indication of El Niño signal.

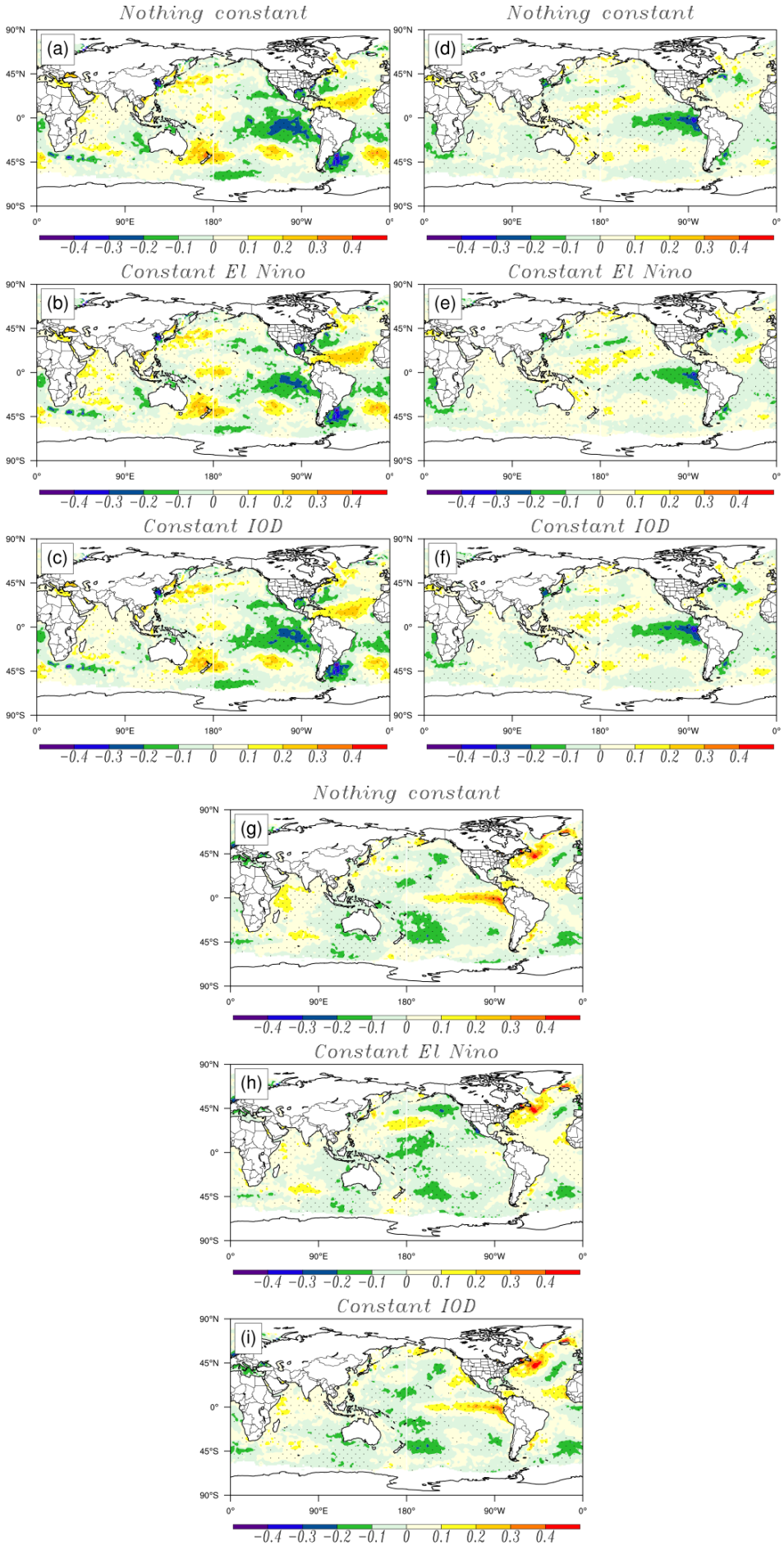
Nothing constant
(a)
Nothing constant
(d)
Constant El Nino
(b)
Constant El Nino
(e)
Constant IOD
(c)
Constant IOD
(f)
Nothing constant
(g)
Constant El Nino
(h)
Constant IOD
(i)
90°N
45°N
0°
45°S
90°S
0°
90°E
180°
90°W
−0.4 −0.3 −0.2 −0.1 0 0.1 0.2 0.3 0.4

Figure 2.12 *(previous page)*: Regression of SST on the East Africa precipitation index for March(a,b,c first column), April(e,f,g second column), and May(h,i,j third column). First row is for pure PI, second row is for PI at constant ENSO, third row, is for PI at constant IOD. Points shading indicates statistical significance at above the 95% level

During March, As shown in Figs.(2.13a,b,c), convection is located at eastern Africa, and at dateline. The convection anomaly over eastern Africa is present by design as an expression of the precipitation index used in building the regression. In the Pacific, convection is centered at the dateline with flanked by suppressed convection extending toward the northeastern and southeastern Pacific. Compared with SST partial regressions, removing El Niño or IOD signals does not change the pattern.

During April, as shown in Fig.(2.13d,e,f), convection cover most Pacific north of the equator, with subsidence located at above the equator. Removing IOD or ONI3.4 does not change the pattern as in the SST regression.

During May, as shown in Fig.(2.13g,h,i), the convection covers the eastern and central tropical pacific. The presence of subsidence anomaly over India is in agreement with most literature that describes failure of monsoon during El Niño development (Ju and Slingo [1995], Webster and Yang [1987], Webster and Magana [1998], and Wang [2006]).A band of convection extends over most of northern Africa and Saudi Arabia. Removing ONI3.4 reduces the convection over the tropical pacific, as with removing the ONI3.4 by regressing against SST.

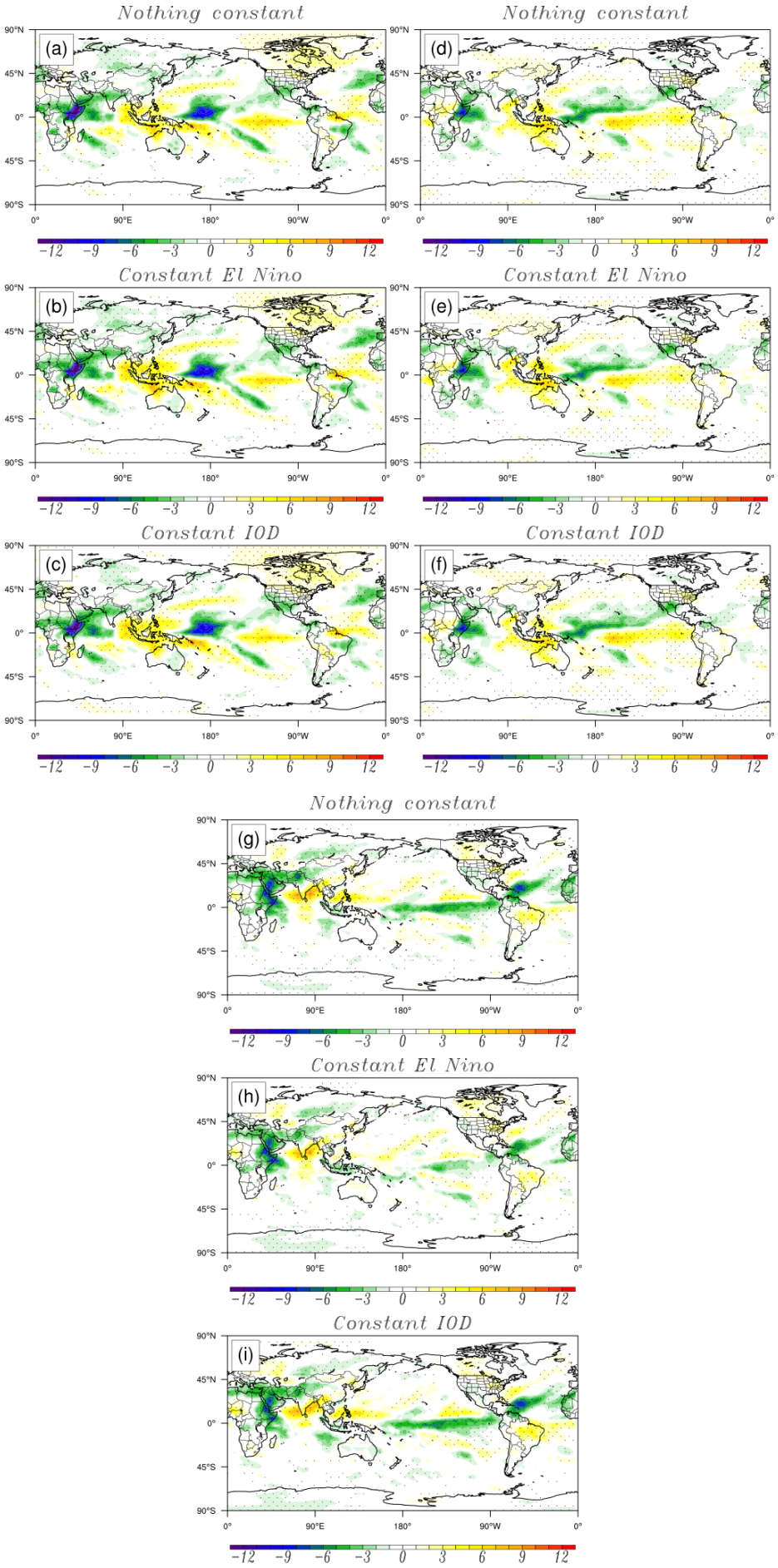
Nothing constant
(a)
Nothing constant
(d)
Constant El Nino
(b)
Constant El Nino
(e)
Constant IOD
(c)
Constant IOD
(f)
Nothing constant
(g)
Constant El Nino
(h)
Constant IOD
(i)
90°N
45°N
0°
45°S
90°S
0°
90°E
180°
90°W
−12 −9 −6 −3 0 3 6 9 12

Figure 2.13: Regression of OLR on the index of east African precipitation for March(a,b,c first column), April(e,f,g second column), and May(h,i,j third column). First row is for pure PI, second row is for PI at constant ENSO, and the third row is for PI at constant IOD. Points shading indicates statistical significance at above the 95% level

To complete the analysis of atmospheric patterns during spring associated with the eastern African wet season, wind and geopotential height were regressed on the PI. Fig.(2.14) shows the pattern of traveling Rossby waves that are radiated from the south eastern IO. During April, there is no clear traveling Rossby wave radiating from the IO. Those patterns are the same with fixed ONI 3.4 and also fixed IOD (not shown).

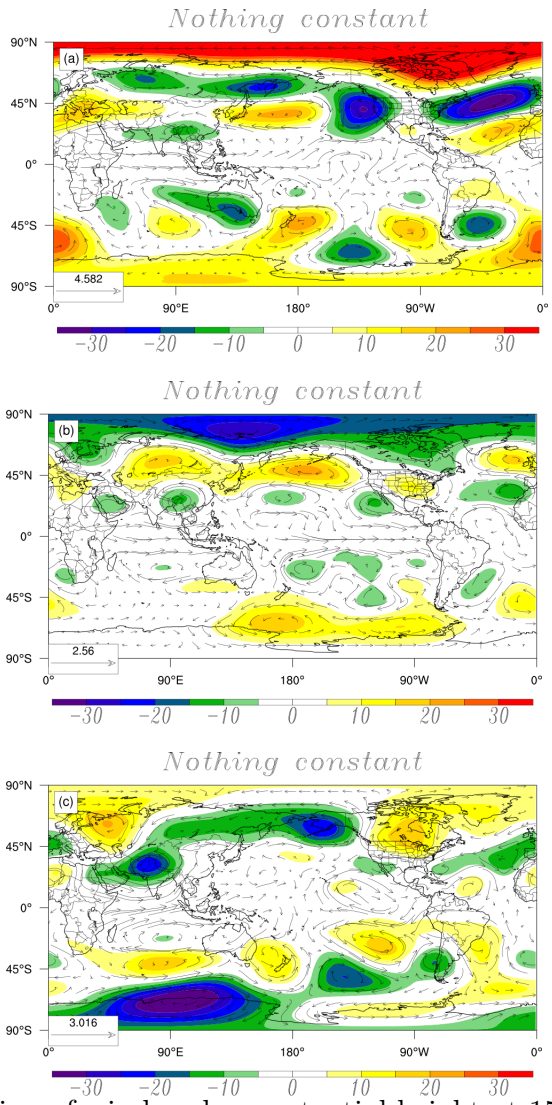

Figure 2.14: Regression of wind and geopotential height at 150 mb on the precipitation index for (a) March, (b) April, and (c) May.

During March, Fig.(2.15a) shows moisture convergence over the western and

central equatorial IO at 1000mb. During April, Fig.(2.15b), the pattern features cyclonic circulation settled on the eastern African coast. During May, Fig.(2.15c) features moisture flux coming from the Indian subcontinent, which is opposite to the base state at that time, in which the Somali jet begins to develop. Thus we can suggest that strong precipitation during May is associated with weakening or delay in the formation of the Somali jet. Fixing El Niño or the IOD, as we noted before does not change the pattern (not shown).

Figure.(2.16) suggests that the level of maximum moisture convergence over eastern Africa is around 700 hPa. One major difference between moisture convergence during autumn and during spring, is during spring inflow from Atlantic/western tropical Africa enhances convergence, such inflow from the Atlantic does not tend to occur during autumn.

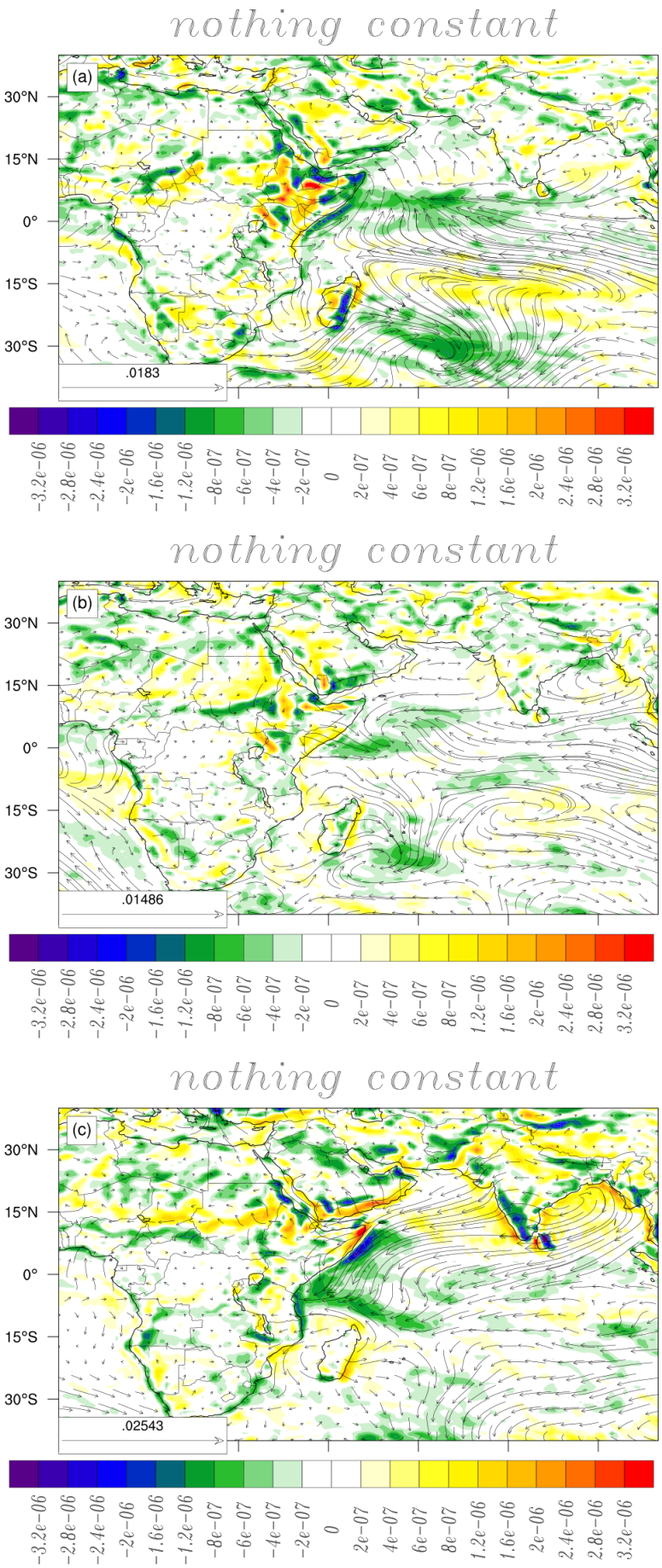

Figure 2.15: Regression of moisture flux and moisture flux divergence at 1000mb on PI during (a) March ,(b) April, and (c) May.

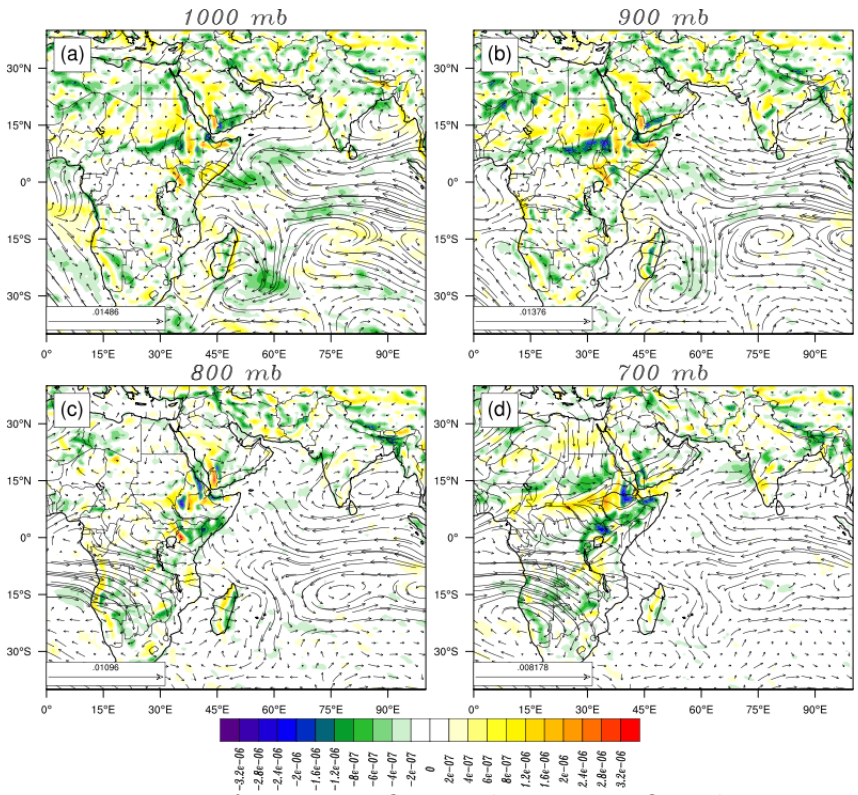

Figure 2.16: Regression of moisture flux and moisture flux divergence on PI in April at (a) 1000 mb , (b) 900 mb ,(c) 800mb, (d) 700mb.

2.5 Defining Indian Ocean Dipole Event and wet/dry event over Eastern Africa

Based on Saji and Yamagata [2003] criteria to define multivariate IOD, we defined the following criteria for categorizing strong, weak, positive moderate, and negative moderate IOD events.

1. For strong positive(negative) IOD events two conditions must be satisfied: First, DMI was required to be larger (smaller) than the sigma of DMI for each of a three consecutive months. Second, U_{equ} was required to be larger (smaller) than the positive (negative) sigma of U_{equ} for each of a three consecutive months.

2. For moderate positive (negative) IOD events, two conditions must be satisfied: First, DMI was required to be larger than positive (negative) 0.5σ for each of a three consecutive months, and at least one month of the three

months was required to be less (large) than positive (negative) σ. Second, U_{equ} were required to be larger (smaller) than positive (negative) $0.5U_{equ}$ for each of a three consecutive months, and at least one month of the three months is required to be smaller (larger) than positive (negative) σ . Thus, three consecutive months with $DMI = U_{equ}$ of values $2, 0.7, 0.9\,\sigma$ are considered as a moderate event. That event is not a strong event as the three consecutive months are not all larger than σ of DMI and U_{equ}.

According to these criteria, events from 1950-2010 were classified into strong and moderate positive and negative events Table (2.3).

Strong Positive #9	Strong negative #7	moderate positive #5	moderate negative #12
Jun-Nov 1961	Aug-Oct 1971	Aug-Oct 1951	Sep-Nov 1958
Aug-Oct 1963	Sep-Nov 1974	Mar-May 1953	Aug-Dec 1960
Sep-dec 1967	Sep-Nov 1975	Sep-Dec 1972	Jun-Aug 1969
Oct-dec 1972	Aug-Oct 1984	Jun-Aug 2003	Jul-Dec 1970
Sep-Nov 1982	Aug-Nov 1996	Jul-Sep 2007	Aug-Oct 1973
May-Dec 1994	Oct-Dec 1998		Jun-Dec 1980
Jul-Dec 1997	Sep-Nov 2010		Jul-Oct 1981
Sep-Nov 2002			Mar-Aug 1985
Aug-Dec 2006			Apr-Aug 1989
			May-Oct 1992
			May-Jul 2004
			Sep-Dec 2005

Table 2.3: DMI events from 1950-2010

The following criteria were used to define abnormally wet and dry seasons over the selected region Fig.(2.1). These categories are strong wet, moderate wet, strong dry, and moderate dry.

1. Wet short rain season (occurs in Boreal Autumn–from September to October) is defined as two consecutive months above 1σ of the PI for the whole period over all months.

2. Dry short rain season (occurs in Boreal Autumn) is defined the same as the wet short rain season except for months less than $-\sigma$.

3. Moderately wet rainy season is defined as the same as the wet season, but the condition here is PI needed to be above 0.5σ, and at least one month was required to be less than σ. This conditions is motivated because some events have only one month that is above 1σ and the following or previous months are below 1σ like 1951. Also the months are not required to be successive, it may be separated by one month that doesn't satisfy the condition like 2002, 2006 in which only October and December satisfy the condition without November.

4. Moderately dry rainy season is the same as before but with replacing $+1\sigma$ with -1σ.

Table (2.4) shows classifications resulting from these criteria. All wet years are associated with El Niño and/or positive IOD. However, not all El Niño or positive IOD events are associate with abnormally wet seasons over eastern Africa. All dry events are associated with La Niña and/or negative IOD except at 1991 in which a moderate El Niño occurred. Some moderate wet years are associated with strong El Niño or strong positive IOD. The amplitude of El Niño is not always a good indication of the amplitude of the corresponding wet events.

Strong Wet #7	Strong dry #8	moderate wet #11	moderate dry #14
Sep-Nov 1961(N)	Oct-Nov 1950(WL)	Oct-Dec 1951(ME)	Oct-Nov 1954(WL)
Nov-Dec 1963(ME)	Oct-Nov 1955(ML)	Nov-Dec 1957(SE)	Oct-Nov 1956(WL)
Oct-Nov 1965(SE)	Oct-Nov 1964(WL)	Oct-Nov 1972(SE)	Oct-Nov 1958(WE)
Oct-Nov 1967(N)	Oct-Nov 1974(WL)	Sep-Nov 1982(SE)	Oct-Nov 1962(N)
Nov-Dec 1968(ME)	Oct-Nov 1975(SL)	Aug-Sep 1983(WL)	Nov-Dec 1970(ML)
Oct-Nov 1977(WE)	Oct-Nov 1983(WL)	Sep-Dec 1989(N)	A,S,N 1973(SL)
Oct-Dec 1997(SE)	Oct-Nov 1991(ME)	Oct-Nov 1994(ME)	Oct-Nov 1980(N)
	Oct-Nov 2005(WL)	Oct,Dec 2002(ME)	Oct-Nov 1985(N)
		Nov-Dec 2003(N)	Oct-Nov 1986(ME)
		Oct-Nov 2004(WE)	Oct-Nov 1988(SL)
		Oct,Dec 2006(WE)	Oct-Nov 1996(N)
			Oct-Nov 1998(ML)
			Oct-Nov 2001(N)
			Oct-Nov 2010(SL)

Table 2.4: Wet-Dry years classification from 1950-2010.Red marked years indicate strong positive IOD, blue one indicates strong negative IOD, BrickRed indicates moderate positive IOD, Aquamarine indicates moderate NIO. Black one indicates no IOD event. Abbreviations N, SE, ME, WE refer to no event in Pacific ocean, strong El Niño, moderate El Niño, weak El Niño respectively. Also SL, ML, WL refer to strong La Niña, moderate La Niña, weak La Niña.

Table (2.5) shows the number of El Niño, La Nina, ENSO neutral, positive DMI, and negative DMI during abnormally wet and dry years. Half of the dry events are associated with neutral IOD. A pie chart for the Table(2.4) are shown in Fig.(2.17). It is shows that, 72% of wet events are assoicated with El Niño and 61% are associated with +IOD events, all strong +IOD are associated with strong wet seasons, and some of the strong EL Niño events are associated with strong wet events.

ENSO events during wet years	ENSO events during dry years	IOD events during wet years	IOD events during dry years
13/18 El Niño	14/22 La Niña	11/18 +IOD	11/22 -IOD
1/18 La Niña	5/22 No event	5/18 No event	11/22 ± IOD
4/18 No Event	3/22 El Niño	2/18 - IOD	0/22 +IOD

Table 2.5: Number of El Niño/ La Niña and +IOD/-IOD during wet/dry years 1950-2010

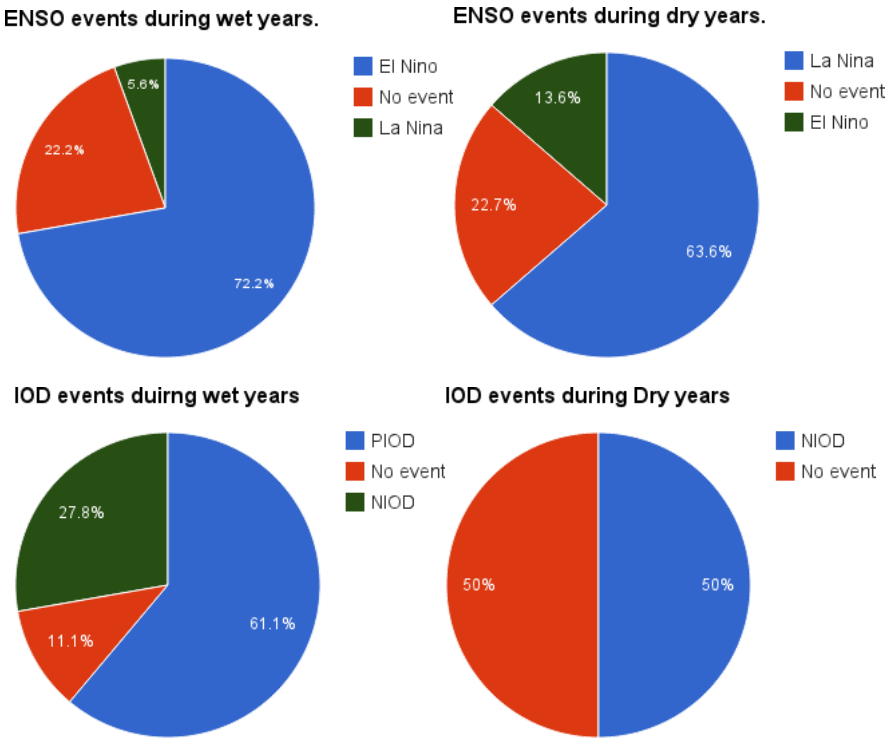

Figure 2.17: Pie chart of the ENSO and IOD event during wet and dry years

2.6 ENSO teleconnection pathway: How does ENSO impact East African Precipitation?

It is well known that precipitation anomalies during the short rain season is associated with El Niño (Ogallo [1988a, 1989a], Schreck and Semazzi [2004a], and Mutai and Ward [2000]). There is association between ENSO and Eastern African precipitation—correlation between the precipitation index and ONI3.4 is r=0.53, 0.41, 0.4 each statistically significantly different from zero at above the at 99% level during October, November, and December respectively, but the mechanism for such teleconnection is not clear. Cai *et al.* [2011] illustrated the teleconnection pathway of ENSO and IOD signal over Australia. Motivated by that study, we investigate here the mechanism of ENSO teleconnection to Eastern African rainfall. One important clue to address the teleconnection of ENSO to east African rainfall is provided by Wang *et al.* [2000] and Wang and Zhang [2002]. They showed that during boreal winter, ENSO can influence the East Asian via triggering anticyclone west of the negative SST anomaly (or negative convective anomaly) in the western Pacific as a Rossby wave response to climatological latent heat release not achieved due to anomalous suppression of convection Gill [1980],and Matsuno [1966]. They called the associated pattern the Western North Pacific (WNP) pattern. This pattern strength the Philippine high so weakening the winter Asian monsoon during periods of El Niño development. Wang *et al.* [2000] and Wang and Zhang [2002] also showed that a positive thermodynamics feedback occurs between this anticyclone and SST. East of the anticyclone, the climatological trade wind supplements the anomlaous wind of anticyclone, thus intensifying total northeasterly wind (Wang *et al.* [2000].Fig.16). Intensification of the northeasterly wind increases the evaporation, thereby decreasing the SST. Decrease of SST enhances the amplitude of the anticycolone as described above according Gill [1980] and Matsuno [1966]. The trade wind west of the anticyclone is opposite to the anomalous wind—so that the total wind intensity decreases, leading to warming on western side of the anticyclone. In this section, we investigated whether such pattern exists during wet events over eastern Africa.

As the region of study is confined in the tropics, we used detrended anomalies

stream-function to construct composites during wet/dry events. As wet months during short rain season shift from year to year, the composites didn't include the same months at each wet year. Figures.(2.18a,b) depict composites of detrended anomalies of streamfunction during short rain season months for wet and dry events respectively defined in Table (2.4). As shown in Fig.(2.18a), two anticyclones cover the northern and southeren IO. Both northern and southern anticyclones work like pumps of moisture flux from the western and central IO to Eastern Africa. Boxes showed in Fig.(2.18a) are boundaries to define an index for those anticyclones. Northern and southern anticyclones represent($R^2 = 57\%, 60\%$) of the equatorial wind variance U_{eq} during October. As composite of dry events—defined in Table (2.4)—as shown in Fig.(2.18b), shows two cyclones. These twin cyclones over the northern and southern IO suppress moisture fluxes to eastern Africa. To manifest such patterns, we plot the composites of wet minus dry events as in Fig.(2.18c). Figure.(2.18) features twin anticyclones over the IO and weak cyclones over the Pacific Ocean which is generated as a Rossby wave response to heating over the Pacific.

To inspect the upper tropospheric structure of these twin anticyclones, we presented in Figs.(2.18d,e,f) stream function at 200mb that match Figs.(2.18a,b,c). It is evident in Fig.(2.18d) that the twin anti-cyclones are reversed at 200mb, the same is also evident in Figs.(2.18e-f). Figure.(2.18c) imply the presence of divergence at the Martime-Continent while convergence occurs over eastern Africa. Figure.(2.18f) show the opposite in the upper troposphere, suggesting that there is an upward branch of the Walker circulation at Eastern Africa and a descending branch over the Maritime-Continent. *These patterns suggest that anomalous eastern Africa precipitation is manifestation of weakening of the Walker circulation in Autumn.*

Figures.(2.18.g,h,i) feature SST for wet, dry and wet minus dry events respectively. It is clear that wet events are associated with El Niño, and dry events are associated with La Niña. Figure.(2.18.g) features negative SST anomalies in the EIO and western Pacific ocean which extend to the south central Pacific. Anomalously low SST responsible for creating the anomalous anticyclone over the IO. On the opposite hand, the cyclones in dry events are created in response to the

positive SST anomalies in the western Pacific as shown in Fig.(2.18.h).

It is difficult to separate the roles of El Niño and the IOD in triggering these anticyclones. It is well known that during IOD events, an anticyclone forms over the SIO due to cooling near Java island, and it persists due to positive wind-SST feedback. As most wet events occur with IOD events, thus we can expect that the anticyclone is just the response of the reduced SST near Java island during IOD events. Correlation of DMI with the southern anticyclone is -0.67, -0.60, -0.28, with these correlations each statistically significant at above the 99% level during October, November, and December.

Is the evolution of the anti-cyclone patterns associated with precipitation?. We know that precipitation over eastern of Africa peaks during October and decays after that. Figures(2.19a,b,c) feature that the pattern weakens and shifts to the east from October to December. Correlation between the ONI3.4 and the northern IO pattern is 0.62, 0.44, 0.29 all at the 95% significance level for October, November, and December. The correlation between DMI and the southern IO pattern is -0.67, -60, -0.28 all significant at the 95% level for October, November, and December. To complete the picture, we present the detrended anomaly of the SST during October, November, and December in Figure(2.19d,e,f). Figures.(2.19d,e,f) shows that the reduced SST over the eastern IO and over western Pacific also relaxes. Thus we can say that as the negative SST anomalies weaken—which is the source of the Rossby wave, the anticyclone intensity decreases.

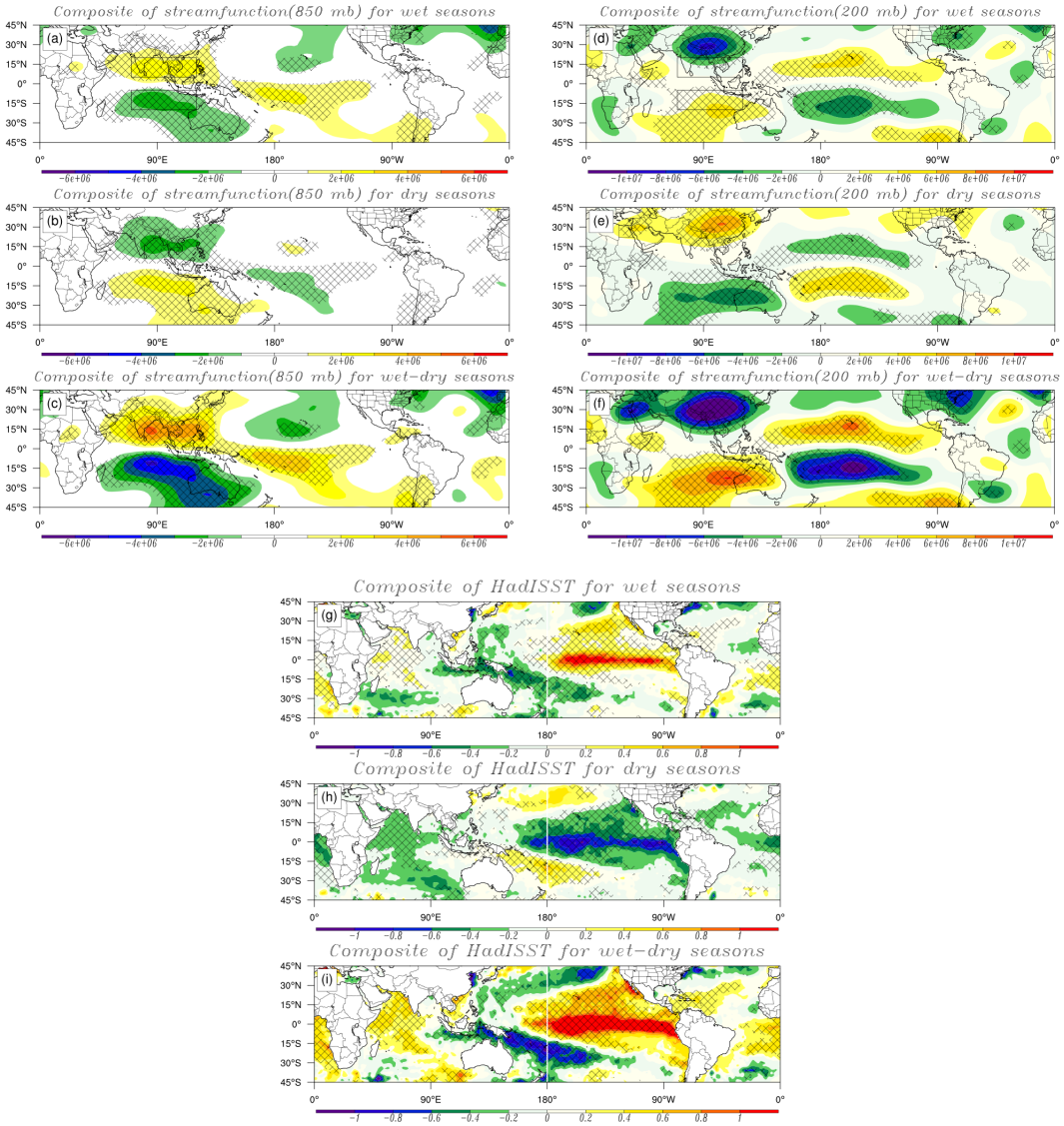

Figure 2.18: Composites of detrended anomlies of NCEP streamfucntion at 850 mb(first column) and at 200mb(second column) and SST(third column). (a) composite of streamfunction at 850mb for wet years (b) composite of streamfunction at 850mb for dry years (c) composites of streamfunction at 850mb for wet-dry years (d) composite of streamfunction at 850mb for wet years (e) composite of streamfunction at 850mb for dry years (f)composites of streamfunction at 850mb for wet-dry years (g) composite of SST for wet years (h) composite of SST for dry years (i)composites of SST for wet-dry years

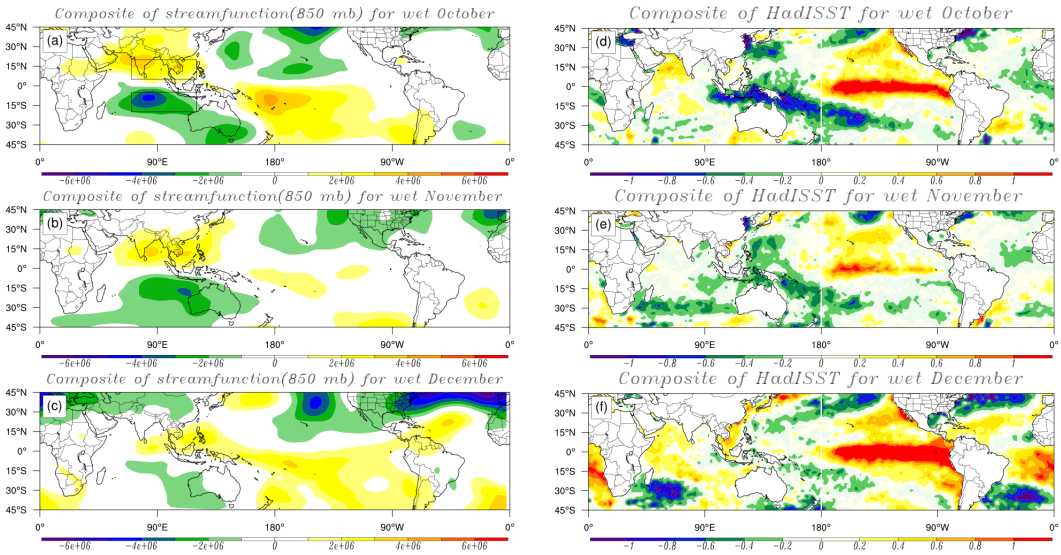

Figure 2.19: First column shows composites of detrended anomlies of streamfucntion at 850 mb calculated from wind components from NCEP1 for wet event in October, November, and December. The second row shows composites of SST for wet events in October, November, and December. (a) composite of streamfunciton in October (b) composite of streamfunction in November (c)composites of streamfunction in December. (d) composite of SST in October, (e) composite of SST in November (f) composite of SST in December.

In the end of this section, we present a schematic shown in Figure.(2.20) to express the teleconnection of both the El Niño and IOD pathways to rainfall over eastern Africa. Blue shaded ellipses indicate negative SSTA and it is represented by letter C, the anticyclones are represented by two ellipses with the letter A in the middle.

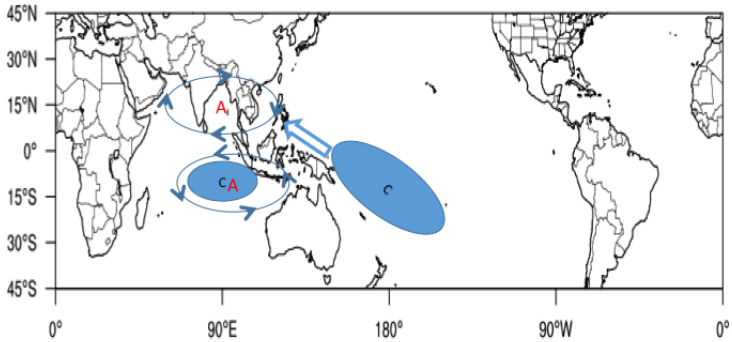

Figure 2.20: Schematic for Teleconnection of ENSO and IOD on East African Precipitation, blue shaded ellipse indicate negative SSTA and it is represent by letter C, the anticyclones are represented by two ellipses with the letter A in the middle.

We defined an index for the intensity of the anti-cyclones over the northern and southern IO. We took the average for the area enclosed by boxes in the

northern $(5-20^{\circ}N, 70-120^{\circ}E)$ and southern $(5-20^{\circ}S, 70-120^{\circ}E)$ IO as shown in Fig.(2.18a). We defined the Northern Indian Ocean Pattern (NIOP) as the spatial average of the anomaly of the streamfuncion over the northern IO. The same also for the Southern Indian Ocean Pattern (SIOP). To get a comprehensive summary about the circulation over the IO and precipitation in eastern Africa, we calculated the correlation between the precipitation over eastern Africa with ONI3.4, DMI, equatorial wind, NIOP, SIOP, WIO SST, and EIO SST Table (2.6). the main conclusions of these correlations are itemized in the following list.

- El Niño is strongly correlated with northern and southern Indian ocean anti-cyclones (NIOP, and SIOP) in October. Correlation of El Niño with NIOP weakens after that. However, correlation of ONI3.4 with SIOP strengthens at the same time.

- DMI is strongly correlated with NIOP and SIOP in October, and after that the correlation weakens for both patterns.

- The correlation between equatorial zonal wind U_{eq} and IOD peaks in October and decreases after that. However, the correlation between U_{eq} and ONI3.4 peaks in November and decreases after that.

- Correlation between PI with NIOP and SIOP is persistent during October and November.

- WIO SST is significantly correlated with ONI3.4 during OND. Whereas, EIO SST is negatively correlated during October, and positively correlated during December.

NIOP	SIOP	ONI3.4	DMI	U_{eq}	Pre	Ebox	Wbox
a.October							
NIOP	**-0.77**	**0.62**	**0.68**	**0.73**	**0.61**	**-0.41**	**0.58**
SIOP		**-0.65**	**-0.70**	**-0.76**	**-0.64**	**0.56**	**-0.53**
ONI3.4			**0.63**	**0.62**	**0.53**	**-0.32**	**0.60**
DMI				**0.86**	**0.66**	**-0.74**	**0.73**
U_{eq}					**0.68**	**-0.69**	**0.58**
pre						**-0.47**	**0.49**
Ebox							-0.08
Wbox							
b.November							
NIOP	**-0.79**	**0.58**	**0.57**	**0.69**	**0.64**	-0.17	**0.54**
SIOP		**-0.72**	**-0.60**	**-0.81**	**-0.62**	*0.23*	**-0.52**
ONI3.4			**0.57**	**0.71**	**0.41**	-0.02	**0.68**
DMI				**0.78**	**0.63**	**-0.58**	**0.70**
U_{eq}					**0.65**	**-0.33**	**0.66**
pre						**-0.41**	**0.41**
Ebox							0.15
Wbox							
c.December							
NIOP	**-0.55**	*0.49*	0.39	**0.71**	**0.66**	0.14	*0.51*
SIOP		**-0.61**	-0.32	**-0.79**	**-0.44**	-0.18	**-0.48**
ONI3.4			**0.34**	**0.67**	**0.41**	**0.43**	**0.73**
DMI				**0.51**	0.18	**-0.43**	**0.51**
U_{eq}					**0.62**	0.14	**0.61**
pre						0.19	**0.36**
Ebox							0.53
Wbox							

Table 2.6: Correlation between NIOP, SIOP, ONI3.4, DMI, U_{eq}, PI, Ebox, and Wbox from 1950-2010. Bold values are statistically significant based on a t-test at above the 99% level, italic values are statistically significant at 95%.

2.7 OLR DMI Based Index

Chiodi and Harrison [2010] found that redefining El Niño events based on outgoing longwave radiation (OLR) data instead of SST gives more complete indication of El Niño events. They found that their El Niño OLR based index exceeds 2.5 σ in four events—82/83,86/87,91/92,97/98—that are widely agreed by climate community as El Niño events. These events are not well separated from weak events identified in other indexes that are based on the SST and atmospheric pressure. Motivated by Chiodi and Harrison [2010], we constructed index of the Indian ocean dipole based on OLR instead of SST. We defined the index using the same geographical averaging as for the SST index—by calculating the difference between the western SST and eastern SST box over the IO.

To get some idea about the relationship between the OLR and SST-based indexes, we calculated the correlation between OLR and SST index on a monthly basis in the western box and then did the same for the eastern box.

As shown in Table (2.7), the correlation between OLR based DMI (hereafter referred as DMIO) and SST based DMI ((hereinafter referred as DMIS) increases gradually from April(r=0) to November (r=-0.9) significant at 99% level). Thus the strongest correlation between DMIO and DMIS is during Autumn and the weakest correlation is during spring.

As DMI is based on difference of the western and eastern SST boxes, we investigated the correlation between DMIO and DMIS for each box separately to get a closer look. The western IO SST box features weak correlation between DMIO and DMIS except during November and December, thus atmospheric conditions may control convection there except during November and December. The eastern IO box features a strong correlation between DMIO and DMIS during Summer and Autumn(from May-November), then the correlation converts to a negative during Winter(r=0.51, 0.66, 0.53 for January, February, and March respectively). Eastern IO SSTA may control convection in summer and autumn, and convection may control SSTA in winter.

	1	2	3	4	5	6	7	8	9	10	11	12
wbox OLR and SST	-0.22	0.06	-0.03	-0.25	-0.21	-0.12	-0.22	-0.25	-0.28	*-0.43*	**-0.57**	**-0.54**
Ebox OLR and SST	**0.51**	**0.66**	**0.53**	-0.01	-0.34	**-0.59**	**-0.69**	**-0.77**	**-0.83**	**-0.81**	**-0.69**	-0.11
DMI OLR and SST	*-0.38*	0.20	0.23	0.00	-0.13	-0.44	**-0.66**	**-0.81**	**-0.87**	**-0.89**	**-0.90**	**-0.72**

Table 2.7: correlation between DMI,WIO, and EIO calculated by SST and OLR . Bold values are statistically significant for p-value of t-test larger than 99%, italic values are statistically at 95%

To identify whether DMIO is better than DMIS in representing the variability of the precipitation, we calculated the correlation of the two indexes with precipitation as shown in Table 2.8. DMIS is significantly correlated with precipitation during October, November, December, and January. DMIO shows either the same or better correlation with precipitation in the same mentioned months. Not only this, but also DMIO shows a significant correlation(-0.55) with precipitation during April which in not correlated at all with DMIS. It is well known that precipitation is not correlated with SST due to the transient property of the SST at that time, but with the DOLR, we found significant correlation. This correlation suggests an opportunity to use the DOLR to predict the precipitation using statistical model. It looks like the nature of the OLR signal is not transient. Comparison of each OLR pole with precipitation shows that the western IO is responsible for most of the relationship of East African precipitation with DOLR during April. Another point is that EIO SST is significantly correlated with precipitation only during October and November. However, correlation with the western Indian Ocean with precipitation remains high during December, January, and February.

	1	2	3	4	5	6	7	8	9	10	11	12
DMISST and pre	**0.52**	0.27	0.20	-0.07	0.32	0.13	0.23	-0.08	-0.03	**0.77**	**0.68**	**0.52**
DMIOLR and pre	**-0.59**	-0.18	-0.26	**-0.55**	0.16	-0.18	*-0.35*	-0.11	-0.04	**-0.77**	**-0.71**	**-0.68**
ESST and pre	0.04	0.33	-0.09	0	-0.09	0	-0.18	0.09	0	**-0.66**	**-0.63**	0.06
WSST and pre	*0.42*	**0.52**	0.04	-0.06	0.19	0.13	0.08	0	-0.06	**0.56**	**0.45**	**0.59**
WOLR and pre	-0.33	0.10	-0.01	**-0.54**	0.13	-0.09	*-0.40*	-0.26	-0.20	**-0.67**	**-0.62**	**-0.61**
EOLR and pre	**0.52**	0.25	0.31	*0.35*	-0.14	0.18	0.19	0	-0.02	**0.76**	**0.71**	**0.64**

Table 2.8: Correlation between the precipitation index and the Indian ocean dipole and poles based on SSTA and OLRA . Bold values are statistically significant at above the 99% level, italic values are statisticant at the 95% level.

In the western and eastern IO, base state SST is always higher than $27°C$ Fig.(2.21). The eastern IO SST climatology shows generally higher values than

for the western IO. The minimum EIO SST is $28°C$ during September, and the maximum is close to $29.5°C$ during May. The EIO SST climatology varies by $1.5°C$, and WIO varies by $2.5°C$. However, SST is always above $27°C$, which is considered the threshold temperature to trigger convection (Graham and Barnett [1987], Sabin *et al.* [2013])—SST begins favoring convection at values between $27°C$ and $28.5°C$, the threshold varies geographically and across the seasonal cycle. The western IO climatology lies in the region of relatively low activity in convection ($> 239w/m^2$). The OLR climatology of EIO suggests prevalent convection except from June-August. These relationships between OLR and SST suggest that modulation of convection by SST is nonlinear and that the large-scale atmospheric circulation impacts convective outcomes in addition to SST.

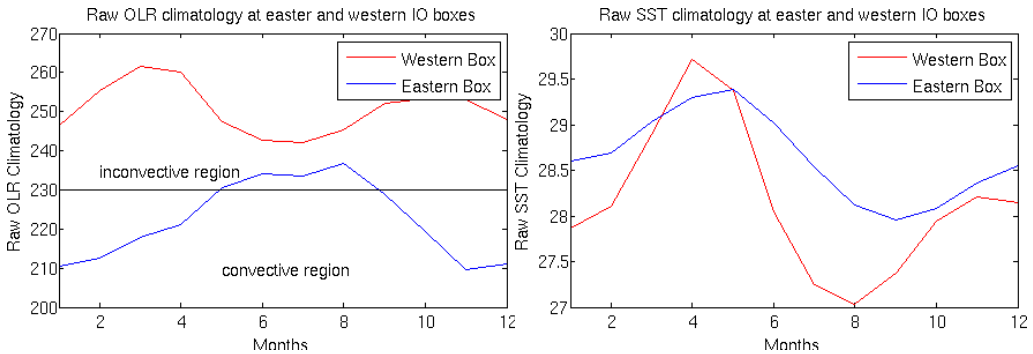

Figure 2.21: Raw OLR and SST climatology at eastern and western IO boxes

Figure (2.22) shows IOD, Ebox, and Wbox calculated using (–)OLR and SST. In the WIO as shown in Fig.(2.22.c), OLR is highly influenced by intraseasonal variability, while SST is highly influenced by inter-annual variation. SST peaks in the WIO occur simultaneously with/or after occurance of strong El Niño. WIO SST peaks strongly at the beginning of 1983, middle of 1987, and 1997-1998, reaches minima with La Niña like cooling in beginning of 1989, 2007-2008. The eastern IO has a more complicated relationship. First, OLR intraseasonal variation is not strong like as in WIO. Secondly, if we look at the signature of El Niño events in the EIO, We find that there are cold anomalies during 1982-1983, 1997-1998, 1994-1995, and 2006-2007. However, the signature of strong El Niño events like 1987-1988 is not apparent at all. Close investigation of the relationship between OLR and SST shows that SST and OLR are evolve together in some events like 1994-1995 and 1997-1998, while opposite signals emerge in some events like 2000-

2001.

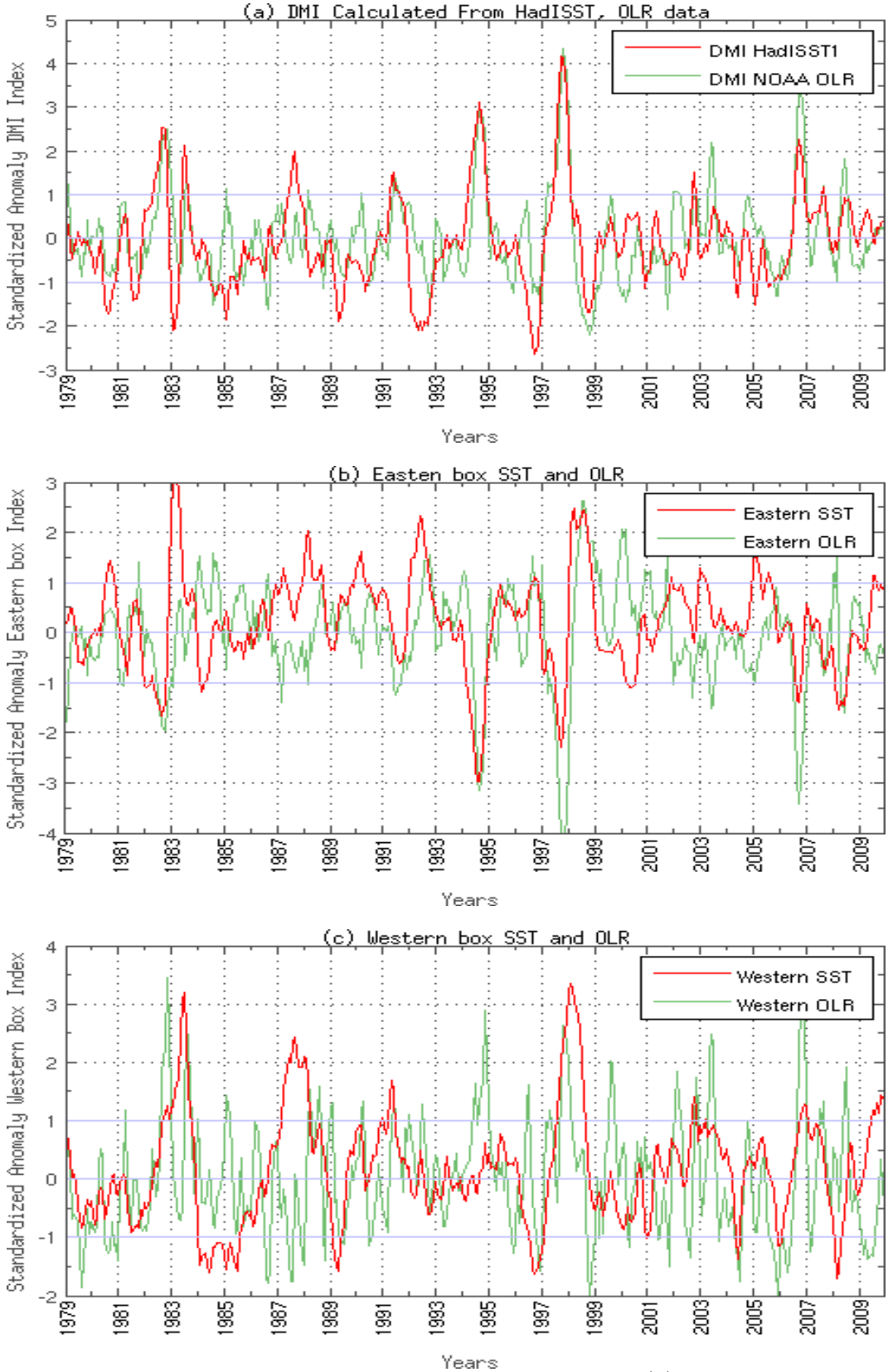

Figure 2.22: Index calculated in IO using -OLR and SST. (a) Indian ocean dipole calculed using -OLR, and SST, (b) Eastern box standarized SST and standarized -OLR, (c) Western box standarized SST and -OLR

2.8 Skewness of SST and OLR fields

Sea surface temperature at some locations deviate from the normal distribution, thus exhibiting skewness to positive or negative temperature. Kang [2002] and An and Jin [2004] reported asymmetric characteristics between El Niño and La Niña events, thus the El Niño amplitude signal tends to be larger than the La Niña signal. Hong *et al.* [2008a,b], Ogata *et al.* [2013] reported of positive skewness in the Indian ocean dipole because of negative skewness in the eastern Indian ocean. Skewness following An and Jin [2004] and Wilks [2006] can be calculated as

$$skewness = \frac{{m_3}^{3/2}}{m_2}$$
$$m_k = \sum_{i=1}^{N} \frac{\left(x_i - \overline{X}\right)^k}{N}$$

where x is variable at certain month for whole period, $\overline{X}$ is the climatolgoy of the SST at given month. N is the number of months.

Figures.(2.23a,b,c) show skewness of detrended SST in September-December from 1979-2013 using HadISST. Zero skewness in SST means a symmetric distribution of positive and negative SST events. Positive skewness means that there is extension of the right tail of the frequency distribution, and the opposite is true for negative skewness. In October, November, and December there is positive skewness in the eastern Pacific, and this skewness decrease with position to the central Pacific, where the SST follows normal distributions indicating that there is skewness toward positive events associated with El Niño1, 2, however, Niño3.4 has a nearly normal distribution (see Trenberth [1997]Fig.2 , Chiodi and Harrison [2010]) in SST field during October. In the western Pacific, there is negative skewness in SST. Although ONI3.4 nearly has a normal distribution, the OLR in the same region has large negative skewness. Positive skewness of SST is mainly concentrated in the Eastern Pacific, whereas OLR skewness is mainly centered east of the date line. Such out of phase–displacement of the OLR skewness relative to SST skewness results from loose dependence of the OLR on the absolute SST.

The south eastern IO SST features a strong negative skewness in October. However, during December, skewness disappears from the IO with the fast decline

of the IOD mode. During Septemper, in the central IO, positive skewness of SST exists, with positive skewness in the OLR.

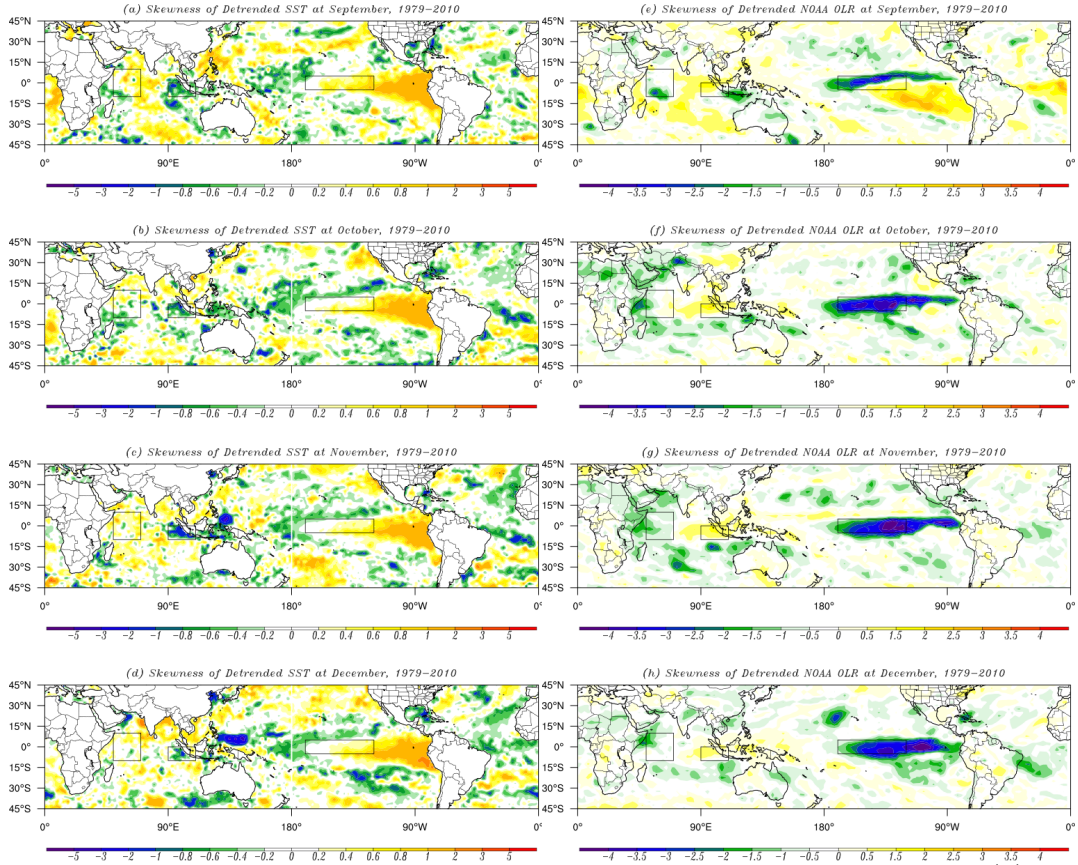

Figure 2.23: Skewness of detrended SST and NOAA OLR 1979-2010 for (a) SST skewness October (b) SST skewness November (c) SST skewness December (d) OLR skewness October (e) OLR skewness November (f) OLR skewness December

2.9 Relationship between El Niño/La Niña and Positive/Negative IOD

Cai *et al.* [2012] studied the effect of the asymmetry of the IOD and ENSO on Australian precipitation. Cai *et al.* [2012] found that positive IOD is associated with a more powerful wave train and convective anomaly than with negative IOD . They found that the impact of El Niño over Australia is conducted via the IO but, during La Niña the impact is conducted via Pacific South American pattern (PSA).

Results of Cai *et al.* [2012] and Weller and Cai [2013] have not verified by a robust statistical method to demonstrate that the coherence between El Niño and PIOD is really different than the coherence between La Niña and NIOD and follows a different pathway. We used a non-parametric significance tests to analyze this suggested difference. The bootstrap method was applied to diagnose whether regression slope coefficients are significantly different). The nonparametric test is based on resampling the observations into new samples that have the same number of data values as in the original data. Tests like Monte Carlo, and bootstrap are nonparametric. Wilks [2006] described the bootstrap as the resampling process equivalent to writing each of the n data values on separate slips of paper and putting all n slips of paper in a hat. To construct one bootstap sample, n slips of paper are drawn from the hat and their data values recorded, but each slip is put back in the hat and mixed (this is the meaning of "with replacement") before the next slip is drawn. Generally some of the original data values will be drawn into a given bootstrap sample multiple times and others will not be drawn at all.

We present how precipitation over Eastern Africa can be modulated by warm/cold phases of ENSO/IOD modes. In this study we examined the asymmetry on a monthly basis instead of over an entire season as suggested by Cai *et al.* [2012], due to the large fluctuations in the IOD signal.

Most previous works about precipitation variability over East Africa did not regard the non linearity of warm and cold asymmetry of ENSO and the DMI Cai *et al.* [2012], Kang [2002], An and Jin [2004], Hong *et al.* [2008a], Hong *et al.* [2008b], and Ogata *et al.* [2013]. Using ONI3.4 and DMI in regression and corre-

lation does not account for such asymmetry of positive and negative events. This result may lead to positive/negative biases. We study the impact of warm and cold phases separately here.

Figure (2.24.a) depicts a scatter plot between ONI3.4 and standardized DMI. The green line results from regression across whole events (both positive and negative). Blue lines indicate the slope of separate positive/negative ONI3.4 with DMI events. Red lines indicate the slopes of positive ONI3.4 without the inclusion of the big El Niño event (1997/98). Scales of ONI3.4 and DMI indicate positive skewness. Coherence between positive ONI3.4 and positive DMI is much stronger than coherence between the negative ONI3.4 and DMI. As positive ONI3.4 gets larger we anticipate much stronger DMI events, but the opposite is not true, so strong events of negative ONI3.4 do not imply stronger negative DMI events. The coherence between La Niña and negative DMI is not as strong as the relation between the El Niño and positive DMI. Several authors prefer to repeat the calculation after removing the biggest El Niño event ever observed 1997/98. Removing the 1997 leads to decreases the slope (coherence) between the El Niño and positive DMI as indicated by the Red Line. Green lines show the regression of all warm/cold ENSO phases, and positive/negative IOD. The slope of the all events is less than the slope if only warm phases of ENSO and DMI are included, but it is larger than the slope during cold phases of ENSO and DMI.

We applied the bootstrap test to assess the difference between the regression slope coefficients calculated based on subsamples of the data for La Niña and NIOD and for El Niño with PIOD. We took 1000 random samples and recalculated the regression slope coefficients for each sample. The histogram of the bootstrap test for October is shown in Fig.(2.24.b). The two histograms, which represent 1000 resampled coefficients result of random draws from events of positive/negative ONI3.4. If 90% of samples of the distribution with larger median are larger than the 90 percentile of the distribution with smaller median, then we can say that the two distributions have a statistically significant different slopes at 90% level.

Results show that the coefficient of both positive and negative ONI3.4 are distinct. However, there is a small intersection for some samples, indicating that they give the same slope. Based on our statistical significance test, both distributions

are statistically significantly different as nearly all of the distribution that has the larger median is larger than the 90 percentile of the distribution with the smaller median. The bootstrap test was repeated again excluding 1997, and the result is shown as the dashed red histogram. Removing 1997 leads to a small shift of the red histogram to the left, indicating that both slope coefficients are more similar than with 1997. A large part of the positive skewness of the ONI3,4 and DMI is due to 1997. The two slopes are still statistically significantly different after removing the 1997. Comparison of the right tail of the bootstrap frequency distribution in Fig. (2.24.c,d) indicates that during November, the slope of both positive and negative ONI3.4 with DMI decreases. During November, results show less asymmetry than in October, and slope decreases more during December. Figure (2.24.e,f) confirms that asymmetry decreases as the intersection between the random slopes increases. Thus we can conclude that the coherence between El Niño and PIOD is maximum during October and decreases during November and December. Shifting of the frequency distribution of the bootstrap test without the 1997 for November and December also indicates that 1997 causes a significant asymmetry between positive/negative ONI3.4 and also positive/negative IOD. During November, the two slopes are statistically significant different even after removing the 1997. During December, almost 75% of the red distribution is larger than the 95 percentile of the blue distribution and after removing the 1997, only half of the distribution is above the 95 percentile of the blue distribution indicating that the two slopes are not statistically significantly different. Table 2.9 shows a summary of the statistical significance test for the slopes.

Months	10	11	12
with 1997	different	different	Not-different
without 1997	different	different	Not-Different

Table 2.9: Summary of the statistical significance test for the slopes with and without the inclusion of 1997.

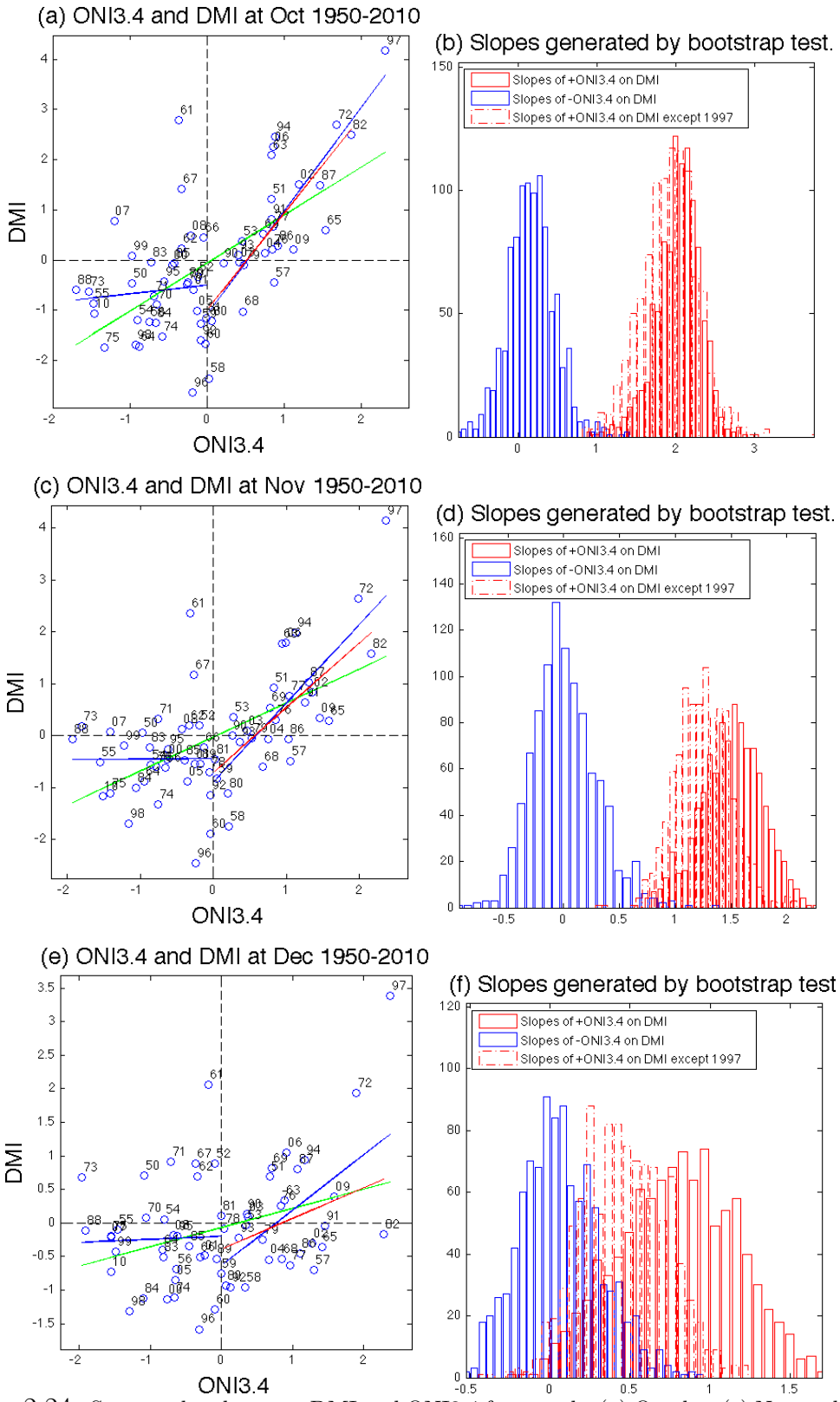

Figure 2.24: Scatter plots between DMI and ONI3.4 for months (a) October (c) Novermber (e) December. Red, blue, and green lines are for linear regression using all events, only positive and negative, and all events except 1997. On the right the associated bootstrap test for difference between the slope of red and blue line based on testing slope for 1000 random sample from events for months (b) October (d) November (f) December. Red and green lines are generated using all available events. Dashed red and green line is the same as red and green line but without 1997.

2.10 Skewness of Precipitation associated with ENSO/IOD

To study how ENSO/IOD asymmetry modulates the precipitation over Eastern Africa, scatter plots have been constructed between the precipitation index and DMI/ONI 3.4. Figure (2.25a,c,e) show scatter plots between PI and ONI3.4 during October, November, and December. Figure (2.25b,d,f) show histograms bootstrap-resampled coefficients for 1000 random draws from the available period. During October, coherence between the PI and positive ONI3.4 is stronger than the coherence between the PI and negative ONI3.4. The big El Niño event of 1997 strengthens the asymmetry between warm/cold ENSO. During November, precipitation coherence with positive ONI 3.4 is more similar to precipitation coherence with negative ONI 3.4. However, positive ONI3.4 events still lead to stronger precipitation than negative ONI3.4. Removing 1997 enhances the similarity of the impact of positive and negative ONI3.4 on PI.

During December, increasing intensity of negative ONI3.4 is not associated with stronger signals in precipitation. Also after excluding 1997, increasing the intensity of positive ONI3.4 is also not associated with increasing precipitation. The bootstrap test after removing 1997 indicates that slopes are not significantly different.

The two slopes are statistically significantly different during October with and without inclusion of 1997. During November, and December, the slopes are not statistically different with and without inclusion of the 1997. Table 2.10 shows a summary of the statistics significance test for the slopes.

Months	10	11	12
with 1997	different	Not-different	Not-different
without 1997	different	Not-different	Not-different

Table 2.10: Summary of the statistical significant test for the slopes with and without the inclusion of 1997.

During December, the non-linear relationship between the ONI3.4 and precipitation indicates that regression and correlation analysis based on the entire record should be used with caution.

Composite analysis may be better than using regression and correlation in this case. Results also suggest two different clusters of wet years are associated with El Niño, one cluster of combined events (1990, 1992, 2003, 2006, 1963, 1957, 1986, 1951, 1997) with more than 20 mm/month (above the standard deviation of the PI), and (1985, 1976, 1977, 1994, 1986, 1982, 2004, 1960) with PI lower than 20 mm/month (lower than the standard deviation of PI). It may be interesting to diagnose the atmospheric pattern associated with these two different clusters (Fig.2.26).

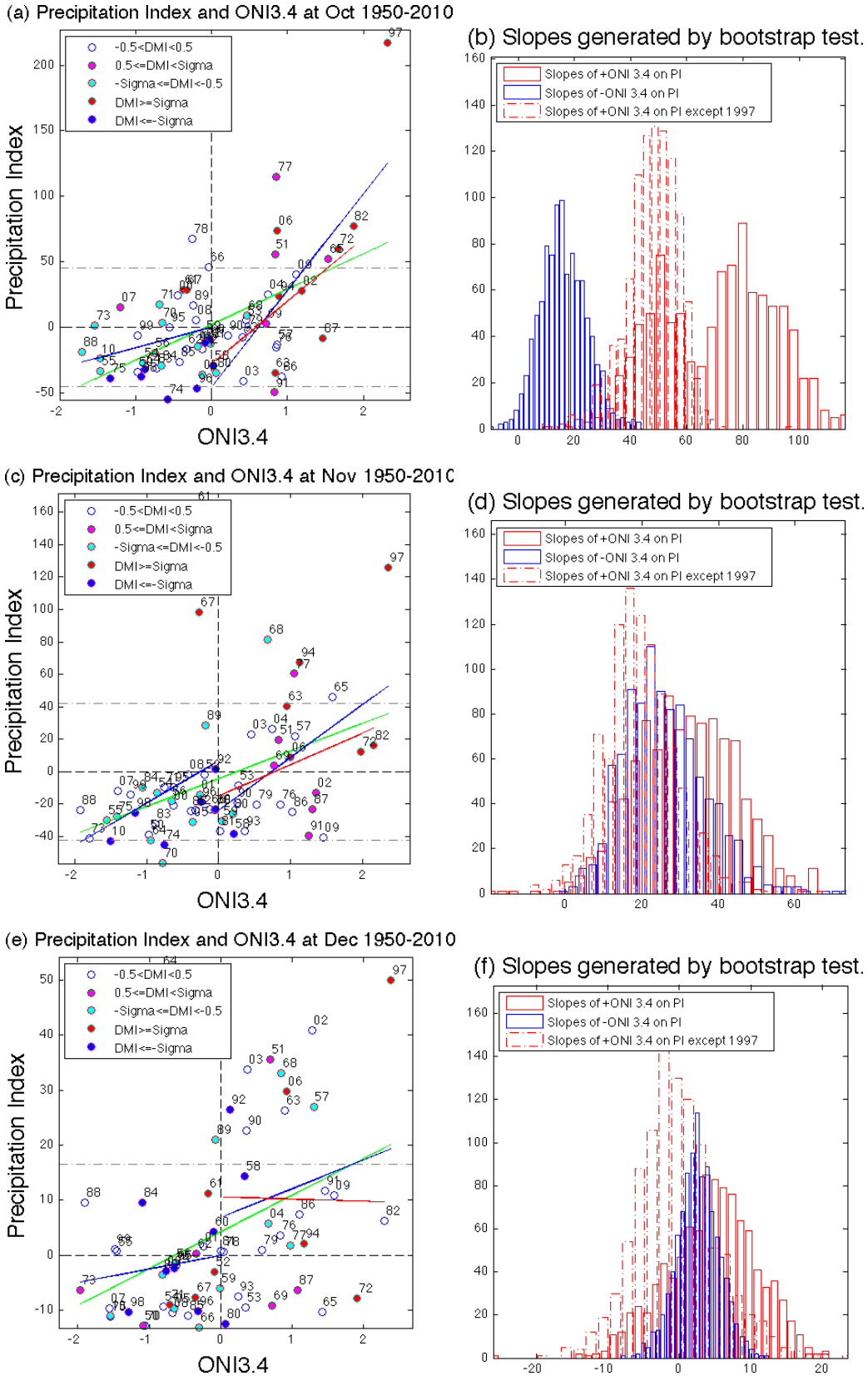

Figure 2.25: The same as Figure.2.24, but for precipitation index with ONI3.4.

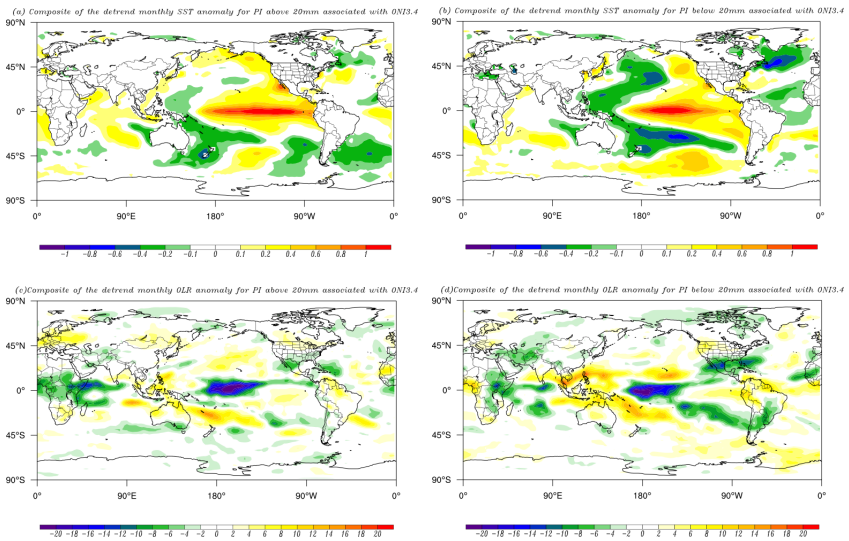

Figure 2.26: SST and OLR associated with wet events during December for (a) SSTA for events above 20mm(nearlly 1σ (b) SSTA for events below 20mm (nearly 1σ (c) OLRA for events above 20mm (nearly 1σ (d) OLRA for events below 20mm (nearlly 1σ)

.

The SSTA composite for the PI events above the standard deviation of PI as depicted in (Fig.2.26.c) features warm anomaly in most of the Pacific Ocean and also whole IO SSTA warming, which may be a result of a strong El Niño event. Strong El Niño events cause IO SST warm anomaly by changing surface flux such as in increases in short wave radiation, which modulates the IO SSTA. OLRA composite for PI events above the standard deviation of PI (Fig. 2.26.c) features convection over the central Pacific Ocean and also convection over most of the west and central IO. The SSTA composite for events associated with below the standard deviation of PI (Fig 2.26.b) features positive SST anomaly in the central Pacific ocean and cooling in western Pacific ocean, in a pattern that is similar to El Niño Modoki, however the only difference is the lack of negative SST anomaly in the eastern Pacific ocean in our composite. The OLRA composite for events associated with below the standard deviation of PI (Fig.(2.26.d)) features anomalous convection over eastern Africa and the equatorial IO.

Figures (2.27a,c,e) show scatter plots of PI with DMI in October, November, and December. Fig.(2.27a) shows that the coherence between the PI and positive DMI is a little stronger than the coherence between the PI and negative DMI. Excluding the year 1997 decreases the slope of the precipitation index with positive DMI. Figure (2.27b) shows that removing 1997 leads to large shift of the slopes

toward smaller values. The bimodality of the frequency distribution of the positive DMI bootstrap test disappears.

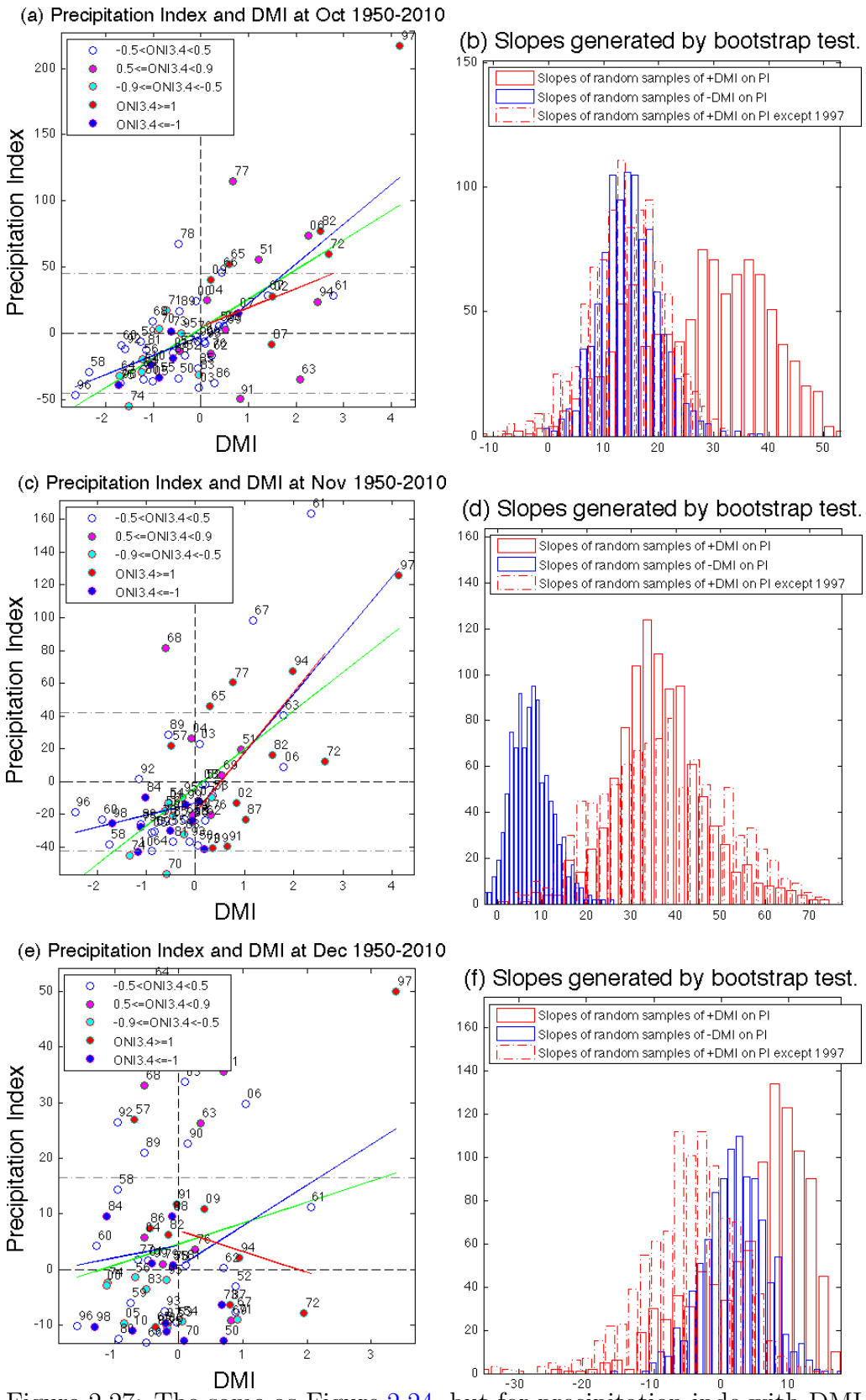

Figure 2.27: The same as Figure.2.24, but for precipitation inde with DMI

During November, strong asymmetry exists between the coherence between the wet or dry PI and positive or negative DMI. Stronger positive DMI is associated with stronger PI, however, stronger negative DMI does not lead to stronger drought. The bootstrap test shown in Fig.(2.27d) confirms that the strong asymmetry of positive or negative DMI with wet or dry PI is statistically significantly different from periods of negative DMI. Even after removing 1997, the asymmetric pattern remains the same. During December, things are more interesting. December includes two groups of events, one cluster is above the standard deviation of precipitation, the other cluster is below the standard deviation of precipitation during December. After removing the year 1997, precipitation does not increases with increases of the IOD for positive events. On the other hand, decreasing of the IOD does not lead to decreases of precipitation, instead precipitation increases. Such behavior is due to wet events above one standard deviation. This behavior might be plausible as IOD decays quickly during December. ENSO appears to impact PI most during December, when both IOD and PI signals tend to decline but ENSO often peaks. The two slopes are statistically different (Table 2.11).

Months	10	11	12
with 1997	Not-different	different	Not-different
without 1997	Not-different	different	Not-different

Table 2.11: Summary of the statistical significant test for the slopes with and without the inclusion of 1997

Month	PONI3.4 DMI	NONI3.4 DMI	PONI3.4 PI	NONI3.4 PI	PDMI PI	NDMI PI
October	**0.81**	0.13	**0.60**	**0.30**	**0.54**	**0.49**
November	**0.76**	0.11	**0.47**	**0.31**	**0.67**	0.08
December	**0.60**	0.15	0.19	0.03	0.28	-0.11

Table 2.12: correlation between positive or negative ONI3.4 (PONI3.4 or NONI3.4), positive or negative DMI (PDMI or NDMI) and PI, Bold numbers are significant over 90%, calculation are based on data from 1950-2010

Table (2.12) shows that during October, November, and December, the correlation between positive ONI3.4 and positive DMI is high, however, the correlation between the negative ONI3.4 and negative DMI is small.

Also the correlation between the positive ONI3.4/DMI and +PI is higher than the correlation between negative ONI3.4/DMI and −PI. So these correlations support our conclusions based on the scatter plot that precipitation is influenced by the skewness of the ONI3.4 and DMI.

Only 7 events during October from 1950-2010 were above 1σ of PI 1977, 1978, 1951, 2006, 1982, 1972, 1997, all those events have positive DMI except one event, 1978, which had slightly negative DMI. Only 2 events from the 60 years were below -1σ, 1991 which had positive DMI, and 1974 which is negative DMI. During November, 7 events were above 1σ of PI 1968,1977,1965,1994,1967,1997,1961 all are positive DMI except 1968 which is negative DMI. During December, 11 events are above 1σ of December PI, 3 of those events were associated with negative DMI, and no events exceed -1σ.

October 1991 was a dry year (PI=-σ), however, DMI=0.5=0.5σ. October 2009 was wet year (PI is around 0.9 σ), however, it had negative DMI. Such behavior needs to be explained to understand what might cause a positive IOD event to be associated with a dry outcome, and also why a negative IOD event could be associated with wet year. Our working hypothesis was that atmospheric convection over the IO did not evolve as it does on average during IOD events, leading to different atmospheric circulation outcomes. To analyze these events, we calculated the IOD again but using NOAA OLR instead of SST.

Figures.(2.28a,c) show that only 3 events are above 1σ of PI during October, and no event exists below the σ. During November, Figs.(2.29a,c) show only two cases 1994 and 1997 are above 1σ in the PI, and 3 events are below 1σ in the PI. During December, 7 events are above the 1σ in the PI, however, there is no event below 1σ in the PI. During December, after removal of 1997, the slope for +DMI is totally different from that before. The bootstrap test suggests that statistically significant assymmetry between +DMI and -DMI with PI occurs only during November.

As shown in table 2.13, slopes during October, November, and December are not statistically different for both DMI calculated with the SST and with the OLR.

Months	10	11	12
with 1997 (OLR DMI)	Not-different	Not-different	Not-different
with 1997 (SST DMI)	Not-different	Not-different	Not-different
without 1997 (OLR DMI)	Not-different	Not-different	Not-different
without 1997 (SST DMI)	Not-different	Not-different	Not-different

Table 2.13: Summary of the statistical significant test for the slopes with and without the inclusion of 1997.

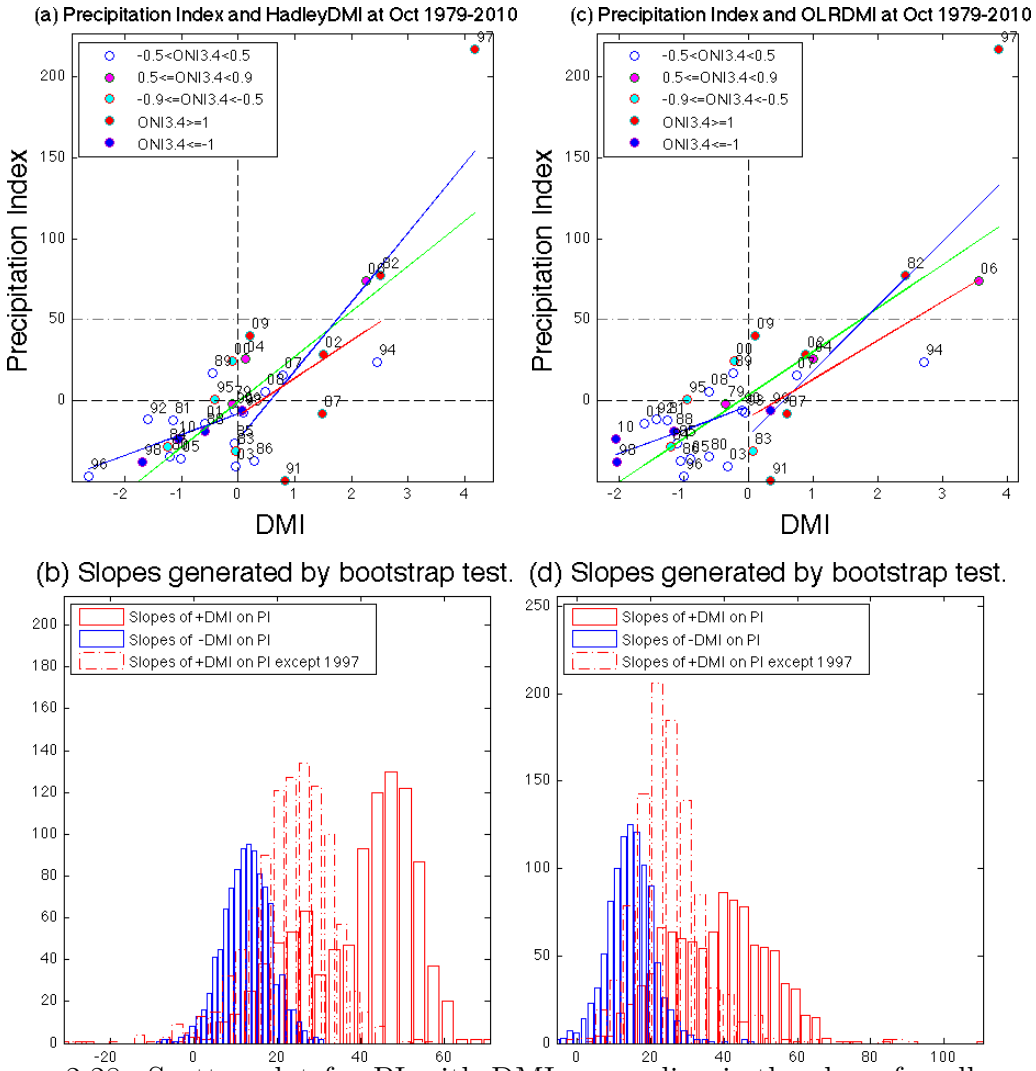

Figure 2.28: Scatter plot for PI with DMI, green line is the slope for all events (positive and negative DMI), blue lines are for positive DMI and negative DMI seperatly. Red line is slope for positive DMI without inclusion of 1997. (a) DMI calculated using SST (c) DMI calculated with OLR, dashed lines indicate $\pm 1\sigma$. A bootstrap test is conducted to check the statitical significance of the difference between the slope of positive and negative DMI. (b) Histogram of the bootstrap test for the slope of positive DMI and negative DMI whih is calculated using SSTA, dashed histogram is the same test without inclusion of the 1997. (b) Histogram of bootstrap test for the slope of positive DMI and negative DMI which is calcualted using OLRA, and the dashed histogram is the same test excluding 1997.

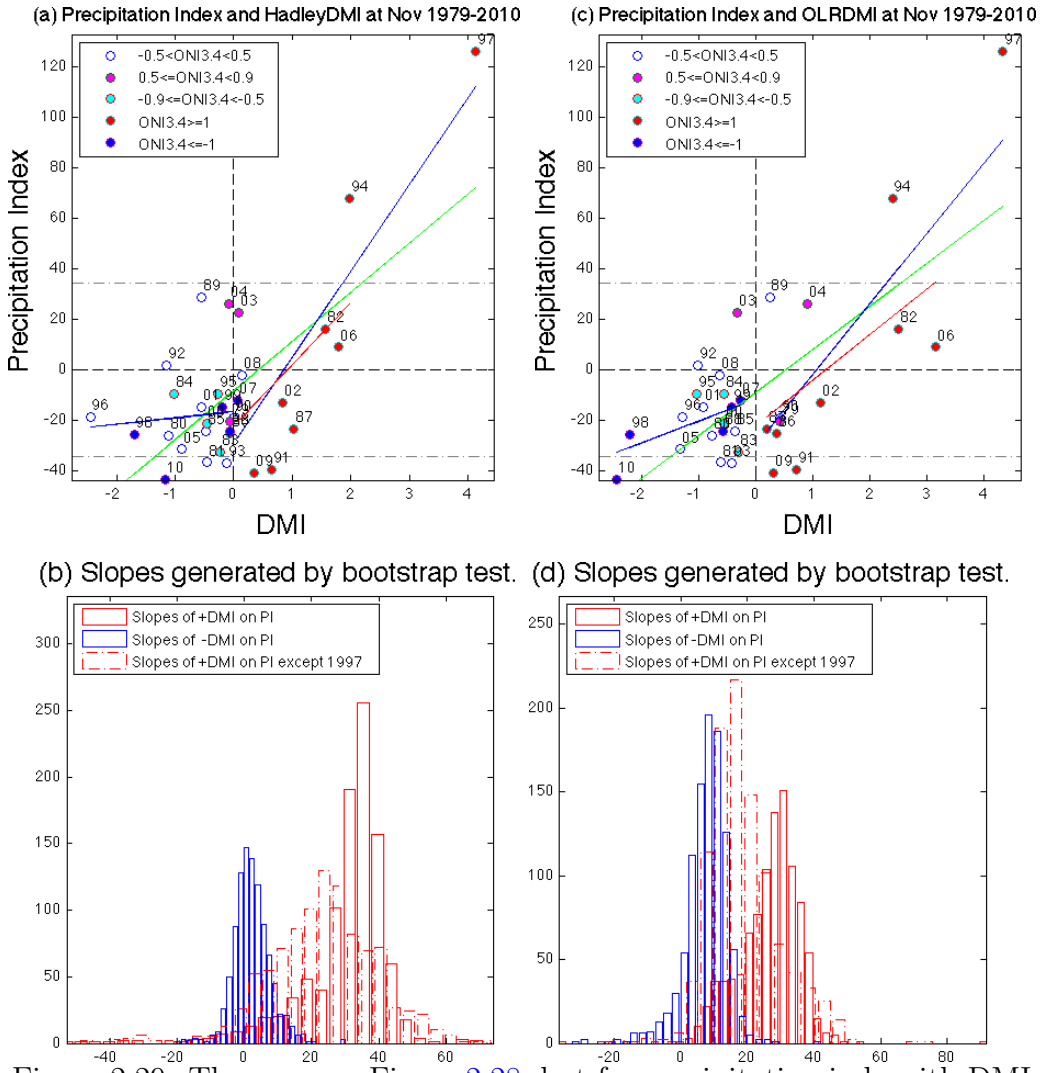

Figure 2.29: The same as Figure.2.28, but for precipitation inde with DMI

The first difference between using the HadISST and NOAA OLR for calculating the DMI is that the DMI OLR based index shows that all events larger than 1σ DMI are wet event and all events that are less than -1σ DMI are dry. Such condition is not satisfied in the DMI SST based index. For example, 1987 was greater than or equal to 1σ DMI, but each of these were anomalously dry over east Africa (PI was negative).

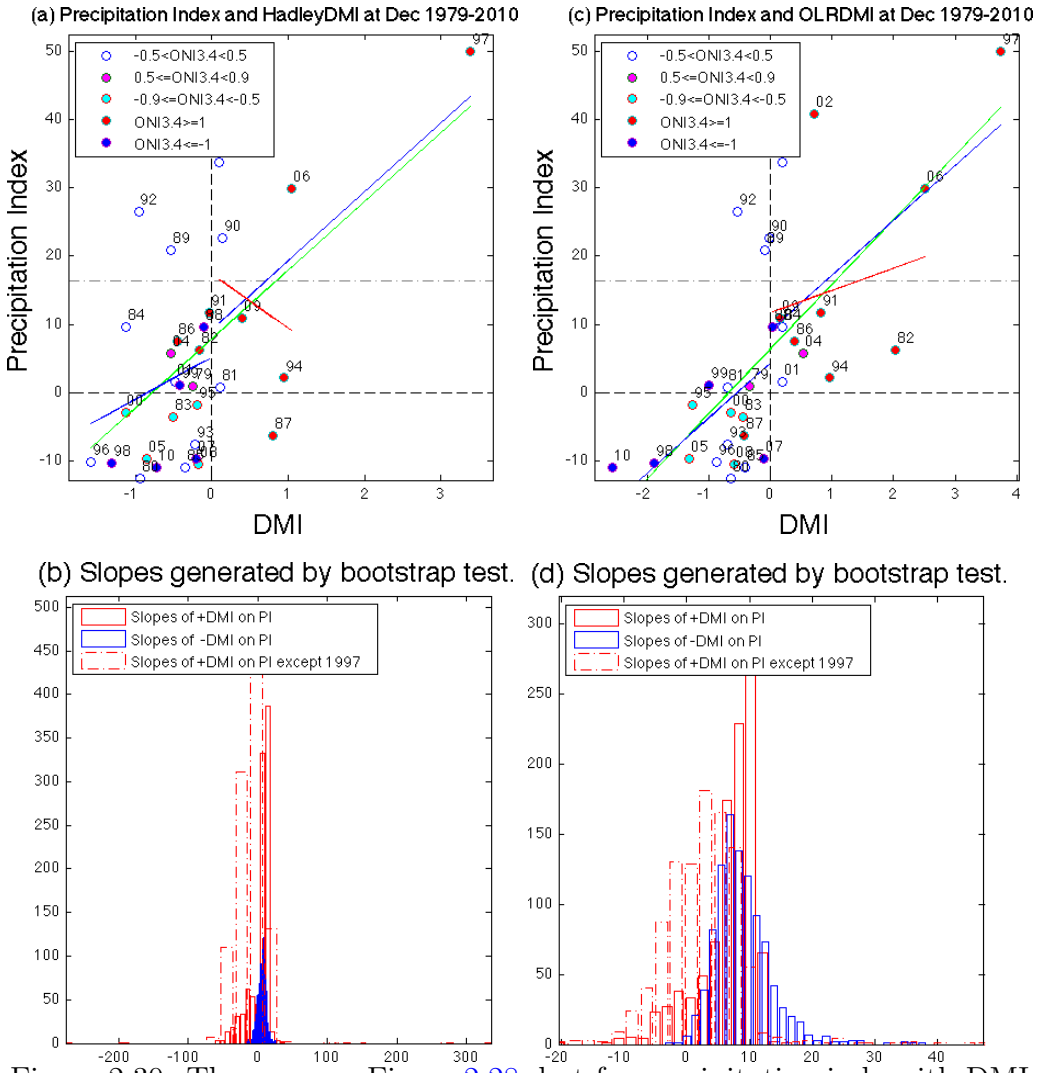

Figure 2.30: The same as Figure.2.28, but for precipitation inde with DMI

Some events have a positive DMI, however, the IO SST distributions does not looks like a dipole. On some occasions, negative SST anomalies occur in both the eastern and western IO, but with stronger negative anomalies to the east, such that taking the difference between the two yields a positive DMI but without a true dipole. Such events occurred in 2004, and 2007 (Fig.2.31a,b). Also, some events have negative DMI SST values, but the opposite expected OLR index signal like October 2009. The 2009 was a wet year over eastern Africa, however, it also had a negative DMI event with the DMI calculated based on the SST. The DMI index calculated using OLR shows a positive event, which better explains the wet outcome over eastern Africa. (Fig.2.31c,d) Two events that are as indicated by both SST and OLR anomalies include positive 1987 and 1991, but these events were dry over eastern Africa, and OLR anomalies averaged over these events show

an eastward shift of the IOD pattern, so the strongest convection was over the middle of the IO (Figs.2.31e,f).

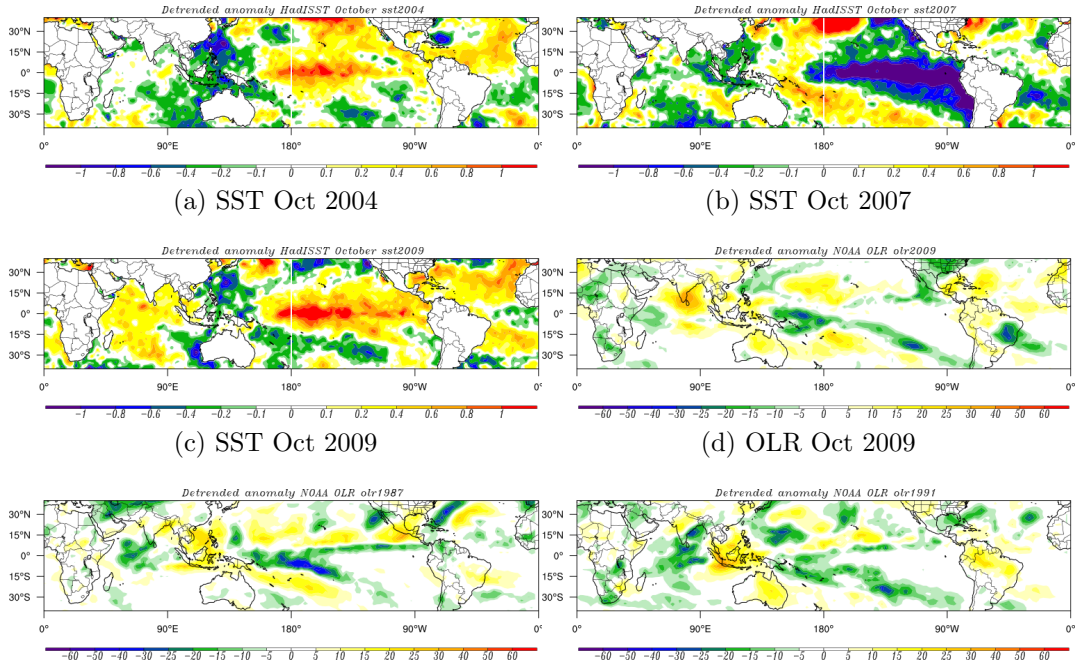

(a) SST Oct 2004 (b) SST Oct 2007

(c) SST Oct 2009 (d) OLR Oct 2009

(e) OLR Oct 1987 (f) OLR Oct 1991

Figure 2.31: Detrended anomaly of SST during (a) October 2004 (b) October 2007, detrended anomlay for 2009 (c)SST (d) Detrended anomalies of NOAA OLR duing (e) 1987 (f)1991.

Chapter 3

Conclusion

There is still debate about the existence/nonexistence of IOD, and also debate about its relationship with ENSO. However, the impact of IOD signal over on East African precipitation during autumn is strong. Regressions of SST and atmospheric variables on a precipitation index over eastern Africa demonstrate the influences of IOD and ENSO during autumn. Although completely isolating IOD from ENSO including nonlinear effects and a clear demonstration of independence is beyond the scope aim of this study, results show the atmospheric patterns associated with precipitation at fixed ENSO and fixed IOD. The partial regression technique linearly isolated ENSO and IOD pattern during wet seasons. This technique has been used to isolate IOD from ENSO in most IOD literature. However, this technique has many drawbacks, which are listed in the following points:

- Fixing IOD or ENSO weakens the amplitude of atmospheric signals associated with IOD or ENSO because half of IOD events are ENSO events.
- Isolating ENSO depends on the index used to define it, thus different indexes may give different patterns. This problem applies to any method used to isolate the ENSO. This problem is related with the essence of the definition of ENSO and IOD themselves.
- Partial regression doesn't remove the lagged effect of ENSO.

Although precipitation declines strongly during December, the strongest circulation pattern appears during this month.

During April, precipitation is correlated with negative SST anomaly over eastern Pacific. Fixing ONI3.4 or IOD did not impact on the strength of the signal over the Pacific.

Maps of moisture flux divergence show that the source of East African moisture is the Indian basin.

The relationship between the positive/negative ENSO and IOD is itemized in the following points:

- During autumn, there is a negative skewness in eastern Indian ocean and positive skewness in the eastern Pacific. There are many theories for explaining the skewnesses. The high SST climatology in the eastern IO and the western Pacific may limit the existence of positive skewness there.

- Based on the skewness over the eastern IO and the eastern Pacific, there is a positive skewness in ONI3.4 and IOD. In other words, maximum of +ONI3.4 is 2.5, and +DMI is larger than 3. However, the minimum of -ONI3.4 is larger than -2 and the minimum of -DMI is larger than -3.

- During October and November, an Increase of +ONI3.4 (El Niño) is associated with increases of +IOD. However, a decrease of the -ONI 3.4 (La Niña) is not strongly associated with decreases of -IOD as in the positive case. During these two months, slope of positive ONI3.4 with positive IOD is statistically significantly different from the slope of negative ONI3.4 with negative IOD at 90% level.

The relationship between the positive/negative ENSO/IOD with precipitation over eastern Africa is itemized in the following point.

- During October, the slope of positive ONI3.4 with positive PI is statistically significantly different from the slope of negative ONI3.4 with negative PI at 90% level. The association between +ONI3.4 and flood is stronger than the association between -ONI3.4 and dry conditions.

- During November, the slope of positive DMI with positive PI is statistically significantly different from the slope of negative DMI with negative PI at

90% level. The associations between DMI and flood is stronger than the association between DMI and dry conditions.

Most negative DMI events are associated with below average precipitation, but not all negative precipitation anomalies are associated with negative DMI. During October and November DMI above 2 is associated with above average precipitation.

Most strong positive IOD events are associated with wet outcomes over eastern Africa. Not all strong El Niño events lead to wet event outcome, for example, during 1986, East Africa suffered from a dry event. During this year, weak easterlies appeared over the eastern IO, with strong subsidence over the eastern IO and strong ascending motion with convection over the central IO. The data suggest that the weak easterlies shrunk the zonal circulation over IO so that the ascending branch didn't touch Eastern Africa, thereby leading to drought conditions over East Africa.

Teleconnection mechanisms are important to understanding how ENSO and the IOD can influence the midlatittude geopotential height and the tropic via stationary Rossby waves. Usually, teleconnections imply interaction between the tropical and extra-tropical wave pattern (imply Baratropic interaction). Although the main focus of this work is the effect of a tropical inter-annual mode on Eastern Africa, which usually is described as associated with a direct structure of the Walker circulation—the location of ascending and descending branches, assessing the associations with other types of teleconnection patterns may be of interest. The Walker circulation is mainly controlled by location of diabatic heating; it could also be modulated by mid-latitude disturbances. Understanding such mechanisms may help us to understand precipitation failures over East Africa during some IOD or El Niño events. During positive phases of ENSO and/or IOD, two anticyclones formed over central IO at 850mb. These anticyclones form because of lose of the climatological release of latent heat Maritime-Continent. These anticyclones are damped quickly with the IOD signal. The southern anticyclone is much more correlated with the cooling near Java island than the northern anticyclone. These anti-cyclones are associated with intensification of the equatorial easterly wind, thus supplying the east African with increased moisture.

There are differences between DMIS and DMIO. The DMIO shows stronger and more consistent relationship with for the atmospheric circulation, as the relationship between the OLR and SST is not linear. DMIO shows a similar but closer relationship with precipitation over eastern Africa during autumn. Correlation of the PI with DMIO and DMIS during October receptively is 0.76, 0.69. During spring, DMIS based index is not correlated with precipitation over eastern Africa, but DMIO shows a significant correlation with precipitation over eastern Africa. Large skewness of the SST in EIO causes aliasing of non DMI events into positive DMIS events like October 2004 and 2007, thus the DMIS needs to be used with caution. Some events that have basin wide-warming behave like positive DMI events with convection over the WIO and subsidence over the EIO like October 2009. Positive DMIO based event which are not associated with wet outcomes over Eastern Africa have eastward shifts of convection from the western IO to the central IO.

Existence of a climate pattern in the IO that has impacts East African precipitation gives us hope that we might be able to predict and understand precipitation variability during autumn. Enhancing the skill of predictability of the IOD pattern will enable east African countries to prepare for severe wet or dry conditions. During spring, there is no clear SST pattern to explain what controls in the inter-annual variability of precipitation. However, DMIO gave a significant correlation with precipitation over eastern Africa. Thus DMIO can be used to study the variability during spring.

Lyon [2014] proposed the following questions regarding the inter-annual precipitation variability over the Greater Horn of Africa:

- Why the Greater Horn Of Africa is semiarid despite its location in the deep tropics?
- Why does the long rainy season during MAM generate more rainfall than the short rain season?
- What controls MAM rainfall?

Bibliography

Adler, R. and Huffman, G. (2003). The version-2 global precipitation climatology project (GPCP) monthly precipitation analysis (1979-present). *Journal of Hydrometeorology*, (January 1997), 1147–1167.

Alexander, M. and Bladé, I. (2002). The atmospheric bridge: The influence of ENSO teleconnections on air-sea interaction over the global oceans. *Journal of Climate*, pages 2205–2231.

Ali, A. and Amani, A. (2005). Rainfall estimation in the Sahel. Part II: Evaluation of rain gauge networks in the CILSS countries and objective intercomparison of rainfall products. *Journal of Applied Meteorology*, pages 1707–1722.

An, S. and Jin, F. (2004). Nonlinearity and Asymmetry of ENSO*. *Journal of Climate*, pages 2399–2412.

Ashok, K., Guan, Z., and Yamagata, T. (2001). Impact of the Indian Ocean dipole on the relationship between the Indian monsoon rainfall and ENSO. *Geophysical Research Letters*, **28**(23), 4499–4502.

Baquero-Bernal, A., Latif, M., and Legutke, S. (2002). On dipolelike variability of sea surface temperature in the tropical Indian Ocean. *Journal of Climate*, pages 1358–1368.

Behera, S., Luo, J., and Masson, S. (2005). Paramount impact of the Indian Ocean dipole on the East African short rains: A CGCM study. *Journal of Climate*, pages 4514–4530.

Behera, S. K., Luo, J.-J., and Yamagata, T. (2008). Unusual IOD event of 2007. *Geophysical Research Letters*, **35**(14), L14S11.

Black, E., Slingo, J., and Sperber, K. (2003). An observational study of the relationship between excessively strong short rains in coastal East Africa and Indian Ocean SST. *Monthly Weather Review*, pages 74–94.

Cai, W., Van Rensch, P., Cowan, T., and Hendon, H. H. (2011). Teleconnection pathways of enso and the iod and the mechanisms for impacts on australian rainfall. *Journal of Climate*, **24**(15), 3910–3923.

Cai, W., van Rensch, P., Cowan, T., and Hendon, H. H. (2012). An Asymmetry in the IOD and ENSO Teleconnection Pathway and Its Impact on Australian Climate. *Journal of Climate*, **25**(18), 6318–6329.

Chambers, D. (1999). Anomalous warming in the Indian Ocean coincident with El Nino. *Journal of Geophysical Research: Oceans (1978-2012*.

Chen, M., Wang, W., and Kumar, A. (2012). Ocean Surface Impacts on the Seasonal-Mean Precipitation over the Tropical Indian Ocean. *Journal of Climate*, (Zhang 1993), 3566–3582.

Chiodi, a. M. and Harrison, D. E. (2010). Characterizing Warm-ENSO Variability in the Equatorial Pacific: An OLR Perspective* , +. *Journal of Climate*, **23**(9), 2428–2439.

Dee, D. P., Uppala, S. M., Simmons, a. J., Berrisford, P., Poli, P., Kobayashi, S., Andrae, U., Balmaseda, M. a., Balsamo, G., Bauer, P., Bechtold, P., Beljaars, a. C. M., van de Berg, L., Bidlot, J., Bormann, N., Delsol, C., Dragani, R., Fuentes, M., Geer, a. J., Haimberger, L., Healy, S. B., Hersbach, H., Hólm, E. V., Isaksen, L., Kå llberg, P., Köhler, M., Matricardi, M., McNally, a. P., Monge-Sanz, B. M., Morcrette, J.-J., Park, B.-K., Peubey, C., de Rosnay, P., Tavolato, C., Thépaut, J.-N., and Vitart, F. (2011). The ERA-Interim reanalysis: configuration and performance of the data assimilation system. *Quarterly Journal of the Royal Meteorological Society*, **137**(656), 553–597.

Ding, R. and Li, J. (2012). Influences of ENSO Teleconnection on the Persistence of Sea Surface Temperature in the Tropical Indian Ocean. *Journal of Climate*, **25**(23), 8177–8195.

Du, Y. and Xie, S.-P. (2008). Role of atmospheric adjustments in the tropical Indian Ocean warming during the 20th century in climate models. *Geophysical Research Letters*, **35**(8), L08712.

Du, Y., Liu, K., and Zhuang, W. (2012). The Kelvin wave processes in the equatorial Indian Ocean during the 20062008 IOD events. *Atmos. Oceanic Sci. Lett*, pages 324–328.

Du, Y., Cai, W., and Wu, Y. (2013). A New Type of the Indian Ocean Dipole since the Mid-1970s. *Journal of Climate*, **26**(3), 959–972.

Dyer, T. (1975). The assignment of rainfall stations into homogeneous groups: an application of principal component analysis. *Quarterly Journal of the Royal Meteorological*.

England, M. (2006). Interannual rainfall extremes over southwest Western Australia linked to Indian Ocean climate variability. *Journal of Climate*, pages 1948–1969.

Fischer, A., Terray, P., and Guilyardi, E. (2005). Two independent triggers for the Indian Ocean dipole/zonal mode in a coupled GCM. *Journal of climate*, pages 3428–3449.

Gill, A. (1980). Some simple solutions for heatinduced tropical circulation. *Quarterly Journal of the Royal Meteorological Society*.

Graham, N. E. and Barnett, T. P. (1987). Sea Surface Temperature, Surface Wind Divergence, and Convection over Tropical Oceans. *Science (New York, N.Y.)*, **238**(4827), 657–9.

Hastenrath, S. and Polzin, D. (2004). Dynamics of the surface wind field over the equatorial Indian Ocean. *Quarterly Journal of the Royal Meteorological Society*, **130**(597), 503–517.

Hong, C.-C. and Li, T. (2010). Independence of SST skewness from thermocline feedback in the eastern equatorial Indian Ocean. *Geophysical Research Letters*, **37**(11), n/a–n/a.

Hong, C.-C., Li, T., and Kug, J.-S. (2008a). Asymmetry of the Indian Ocean Dipole. Part I: Observational Analysis*. *Journal of Climate*, **21**(18), 4834–4848.

Hong, C.-C., Li, T., and Luo, J.-J. (2008b). Asymmetry of the Indian Ocean Dipole. Part II: Model Diagnosis*. *Journal of Climate*, **21**(18), 4849–4858.

Indeje, M., Semazzi, F. H., and Ogallo, L. J. (2000). ENSO signals in East African rainfall seasons. *International Journal of Climatology*, **20**(1), 19–46.

Iskandar, I., Irfan, M., and Saymsuddin, F. (2013). Why was the 2008 Indian Ocean Dipole a short-lived event? *Ocean Science Journal*, **48**(2013), 149–160.

Ju, J. and Slingo, J. (1995). The Asian summer monsoon and ENSO. *Quarterly Journal of the Royal Meteorological*, (December 1994).

Kang, I.-S. (2002). El Niño and La Niña sea surface temperature anomalies: Asymmetry characteristics associated with their wind stress anomalies. *Journal of Geophysical Research*, **107**(D19), 4372.

Latif, M. and Dommenget, D. (1999). The role of Indian Ocean sea surface temperature in forcing East African rainfall anomalies during December-January 1997/98. *Journal of ...*, (January 1997), 3497–3504.

Li, T. and Wang, B. (2003). A Theory for the Indian Ocean Dipole-Zonal Mode*. *Journal of the Atmospheric Science*, pages 2119–2135.

Liu, L., Yu, W., and Li, T. (2011). Dynamic and Thermodynamic AirSea Coupling Associated with the Indian Ocean Dipole Diagnosed from 23 WCRP CMIP3 Models *. *Journal of Climate*, **24**(18), 4941–4958.

Luo, J.-J., Zhang, R., Behera, S. K., Masumoto, Y., Jin, F.-F., Lukas, R., and Yamagata, T. (2010). Interaction between El Niño and Extreme Indian Ocean Dipole. *Journal of Climate*, **23**(3), 726–742.

Luo, J.-J., Sasaki, W., and Masumoto, Y. (2012). Indian Ocean warming modulates Pacific climate change. *Proceedings of the National Academy of Sciences of the United States of America*, **109**(46), 18701–6.

Lyon, B. (2014). Seasonal Drought in the Greater Horn of Africa and Its Recent Increase during the MarchMay Long Rains. *Journal of Climate*, **27**(21), 7953–7975.

Matsuno, T. (1966). Quasi-geostrophic motions in the equatorial area. *J. Meteor. Soc. Japan*.

Meehl, G. (1997). The south Asian monsoon and the tropospheric biennial oscillation. *Journal of Climate*, (1992), 1921–1943.

Meyers, G., McIntosh, P., Pigot, L., and Pook, M. (2007). The years of el niño, la niña, and interactions with the tropical indian ocean. *Journal of Climate*, **20**(13).

Mutai, C. and Ward, M. (2000). East African rainfall and the tropical circulation/convection on intraseasonal to interannual timescales. *Journal of Climate*, pages 3915–3939.

Ogallo, L. (1988a). Relationships between seasonal rainfall in east africa and the southern oscillation. *Journal of Climatology*, **8**(1), 31–43.

Ogallo, L. (1989a). The spatial and temporal patterns of the east african seasonal rainfall derived from principal component analysis. *International Journal of Climatology*, **9**(2), 145–167.

Ogallo, L. (1989b). The spatial and temporal patterns of the East African seasonal rainfall derived from principal component analysis. *International Journal of Climatology*, **30**.

Ogallo, L. J. (1988b). Relationships between seasonal rainfall in east africa and the southern oscillation. *Journal of Climatology*, **8**(1), 31–43.

Ogata, T., Xie, S.-P., Lan, J., and Zheng, X. (2013). Importance of Ocean Dynamics for the Skewness of the Indian Ocean Dipole Mode*. *Journal of Climate*, **26**(7), 2145–2159.

Rao, S. a. and Behera, S. K. (2005). Subsurface influence on SST in the tropical Indian Ocean: structure and interannual variability. *Dynamics of Atmospheres and Oceans*, **39**(1-2), 103–135.

Rao, S. a., Luo, J.-J., Behera, S. K., and Yamagata, T. (2008). Generation and termination of Indian Ocean dipole events in 2003, 2006 and 2007. *Climate Dynamics*, **33**(6), 751–767.

Rayner, N. a. (2003). Global analyses of sea surface temperature, sea ice, and night marine air temperature since the late nineteenth century. *Journal of Geophysical Research*, **108**(D14), 4407.

Sabin, T. P., Babu, C. a., and Joseph, P. V. (2013). SST-convection relation over tropical oceans. *International Journal of Climatology*, **33**(6), 1424–1435.

Saji, N. and Yamagata, T. (2003). Structure of SST and Surface Wind Variability during Indian Ocean Dipole Mode Events: COADS Observations*. *Journal of Climate*, **1997**, 2735–2751.

Saji, N., Goswami, B. N., Vinayachandran, P., and Yamagata, T. (1999). A dipole mode in the tropical indian ocean. *Nature*, **401**(6751), 360–363.

Schreck, C. J. and Semazzi, F. H. (2004a). Variability of the recent climate of eastern africa. *International Journal of Climatology*, **24**(6), 681–701.

Schreck, C. J. and Semazzi, F. H. M. (2004b). Variability of the recent climate of eastern Africa. *International Journal of Climatology*, **24**(6), 681–701.

Shi, L., Hendon, H. H., Alves, O., Luo, J.-J., Balmaseda, M., and Anderson, D. (2012). How Predictable is the Indian Ocean Dipole? *Monthly Weather Review*, **140**(12), 3867–3884.

Singh, P., Chowdary, J., and Gnanaseelan, C. (2013). Impact of prolonged La Niña events on the Indian Ocean with a special emphasis on southwest Tropical Indian Ocean SST. *Global and Planetary Change*, **100**(2013), 28–37.

Smith, T. M., Reynolds, R. W., Peterson, T. C., and Lawrimore, J. (2008). Improvements to NOAAs Historical Merged LandOcean Surface Temperature Analysis (18802006). *Journal of Climate*, **21**(10), 2283–2296.

Tanaka, H., Ishizaki, N., and Kitoh, A. (2004). Trend and interannual variability of Walker, monsoon and Hadley circulations defined by velocity potential in the upper troposphere. *Tellus A*, pages 250–269.

Trenberth, K. E. (1997). The Definition of El Niño. (August).

Trenberth, K. E., Fasullo, J. T., and Mackaro, J. (2011). Atmospheric Moisture Transports from Ocean to Land and Global Energy Flows in Reanalyses. *Journal of Climate*, **24**(18), 4907–4924.

Vinayachandran, P., Francis, P. A., and Suryachandra Rao, A. (2009). Indian Ocean dipole: Processes and impacts. *Current trends in science*, pages 569–589.

Wang, B. (2006). *The Asian Monsoon*. Springer Praxis Books. Springer.

Wang, B. and Zhang, Q. (2002). Pacific-East Asian Teleconnection. Part II: How the Philippine Sea Anomalous Anticyclone is Established during El Niño Development*. *Journal of climate*, pages 3252–3265.

Wang, B., Wu, R., and Fu, X. (2000). Pacific-East Asian teleconnection: how does ENSO affect East Asian climate? *Journal of Climate*, pages 1517–1536.

Wang, C. (2002). Atmospheric Circulation Cells Associated with the El NiñoSouthern Oscillation. *Journal of Climate*, pages 399–419.

Wang, X. and Wang, C. (2013). Different impacts of various El Niño events on the Indian Ocean Dipole. *Climate Dynamics*, **42**(3-4), 991–1005.

Webster, B. P. J. and Yang, S. (1987). Monsoon and ENSO : Selectively interactive systems. (1992).

Webster, P. and Magana, V. (1998). Monsoons: Processes, predictability, and the prospects for prediction. *Journal of Geophysical Research: Oceans (19782012)*, **103**(C7), 14451.

Webster, P. J., Moore, A. M., Loschnigg, J. P., and Leben, R. R. (1999). Coupled ocean–atmosphere dynamics in the Indian Ocean during 1997–98. *Nature*, **401**(6751), 356–360.

Weller, E. and Cai, W. (2013). Asymmetry in the IOD and ENSO Teleconnection in a CMIP5 Model Ensemble and Its Relevance to Regional Rainfall. *Journal of Climate*, **26**(14), 5139–5149.

Wilks, D. S. (2006). Statistical Methods in the Atmospheric Sciences. *International Geophysics Series*, **102**, 380–380.

Xie, P. and Arkin, P. (1997). Global precipitation: A 17-year monthly analysis based on gauge observations, satellite estimates, and numerical model outputs. *Bulletin of the American Meteorological Society*, pages 2539–2558.

Xie, S., Annamalai, H., Schott, F., and Jr, J. M. (2002). Structure and mechanisms of South Indian Ocean climate variability. *Journal of Climate*, pages 864–878.

Yan, D. U., Kai, L. I. U., Wei, Z., and Wei-dong, Y. U. (2012). The Kelvin Wave Processes in the Equatorial Indian Ocean during the 2006 2008 IOD Events. **5**(4), 324–328.

Yule, G. (1907). On the theory of correlation for any number of variables, treated by a new system of notation. *Proceedings of the Royal Society of London*, (1), 182–193.